

2 mix

NASA CR-132842

SD 72-SA-0133-8

PART I FINAL REPORT

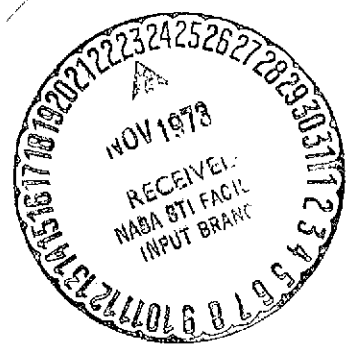
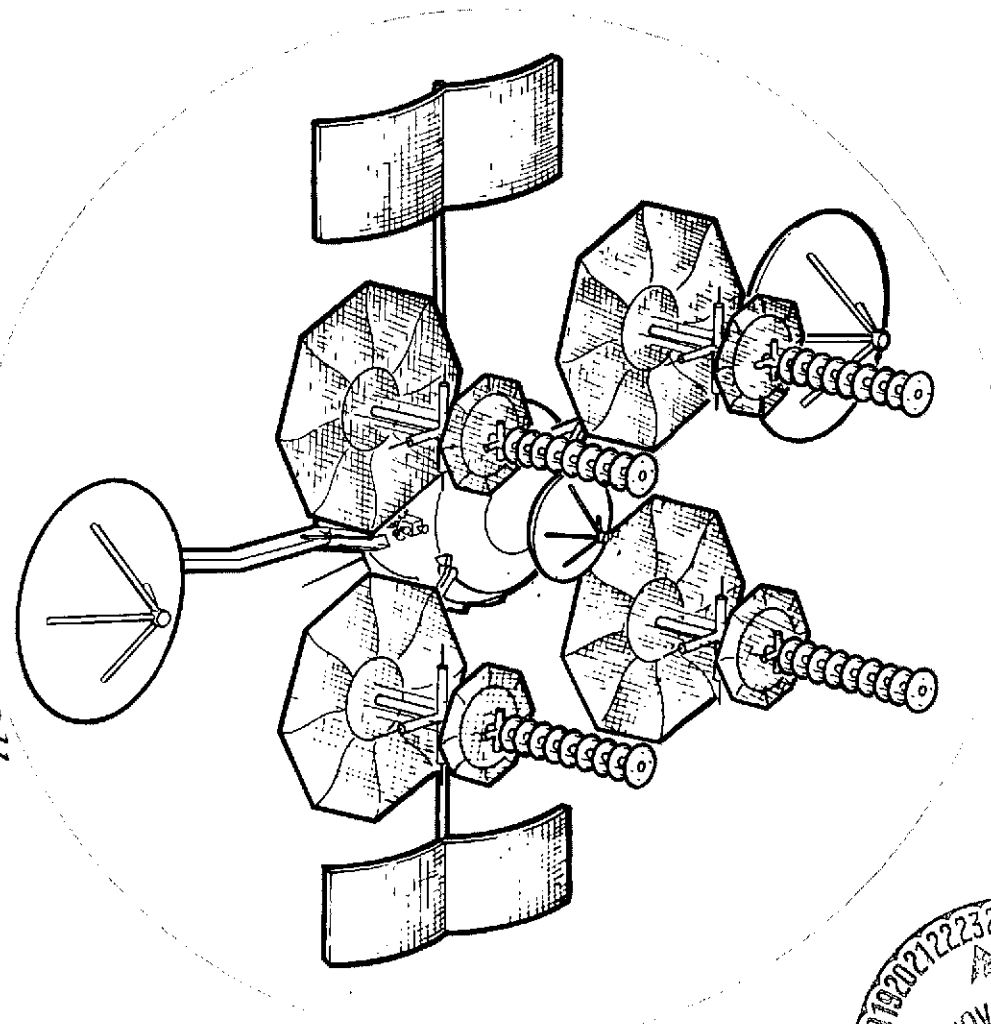
TRACKING & DATA RELAY SATELLITE SYSTEM CONFIGURATION & TRADEOFF STUDY

VOLUME VIII APPENDIXES

N74-10812

Unclas
21944

(NASA-CR-132842) TRACKING AND DATA RELAY
SATELLITE SYSTEM CONFIGURATION AND
TRADEOFF STUDY. VOLUME 8: APPENDIXES,
PART 1 Final Report (North American
Rockwell Corp.) 140 p HC \$9.00 CSCL 22B G3/31
112



OCTOBER 1972

SUBMITTED TO
GODDARD SPACE FLIGHT CENTER
NATIONAL AERONAUTICS & SPACE ADMINISTRATION

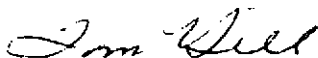


IN ACCORDANCE WITH
CONTRACT NAS5-21705

PART I FINAL REPORT

**TRACKING & DATA RELAY SATELLITE SYSTEM
CONFIGURATION & TRADEOFF STUDY**

APPENDIXES



T. E. Hill
TDRS STUDY MANAGER

OCTOBER 1972

SUBMITTED TO
GODDARD SPACE FLIGHT CENTER
NATIONAL AERONAUTICS & SPACE ADMINISTRATION



Space Division
North American Rockwell

;



Space Division
North American Rockwell

PRECEDING PAGE BLANK NOT FILMED

FOREWORD

This volume contains the appendixes to Report SD 72-SA-0133, Part 1, Final Report, Tracking and Data Relay Satellite System Configuration Trade-off Study. The study was conducted by the Space Division of North American Rockwell Corporation for the Goddard Space Flight Center of the National Aeronautics and Space Administration.

PRECEDING PAGE BLANK NOT FILMED

CONTENTS

Section	Page
2A	Orbit Orientation for Optimum Inclination Perturbation 2A-1
2B	Payload Increase Associated With Biased Synchronous Orbit I Injection
4A	EMC Program for the Spaceborne TDRS Telecommunication System 4A-1
4B	Material Backup List for the Spaceborne TDRS Telecommunication System 4B-1
4C	Summary of Telemetry and Command Input/ Output Requirements for TDRS 4C-1
5A	Alternate Concepts and Trade Studies of S/C Structure and Configuration 5A-1
5A.1	Spacecraft Structural Body Shapes 5A-1
5A.2	Solar Panel Configurations and Drive Systems 5A-1
5A.3	MDR Antenna Diameters and Construction 5A-9
5A.4	MDR Antenna Concept With S-Band Phased Array. 5A-17
5A.5	LDR Antenna Configurations 5A-17
5A.6	Summary 5A-37
6A	Solar Pressure Disturbance Torque Analysis 6A-1
6A.1	Solar Pressure Model 6A-1
6A.2	Spacecraft Representation 6A-2
6A.3	Discussion of Results 6A-5
6A.4	References 6A-23
6B	Effect of Propellant Motion on Nutation Stability During Spin 6B-1
6B.1	Slosh Model 6B-1

Section	Page
6B.2 Discussion of Results	6B-2
6B.3 Practical Considerations	6B-2
6B.4 Conclusions and Recommendations	6B-5
6B.5 References	6B-6
8A Energy Storage Assembly	8A-1
10A Reliability Definitions	10A-1
10B TDRS Reliability Design Practices	10B-1
10C Component Failure Rates	10C-1

ILLUSTRATIONS

Figure		Page
2A-1	Geometry for Optimum Inclination Perturbation	2A-2
2A-2	Ascending Node Versus Phase Angle	2A-2
2A-3	TDRS Orbit Inclination Versus Time	2A-3
5A-1	Trade Tree - Spacecraft Structural Body	5A-2
5A-2	Trade Study - Body Comparison	5A-2
5A-3	TDRS Configuration - Slab Sided Body	5A-3
5A-4	TDRS Configuration - Spheroidal Body	5A-3
5A-5	TDRS S/C Body - Non Jettisonable Apogee Motor	5A-4
5A-6	TDRS S/C Body - Non Jettisonable Apogee Motor	5A-5
5A-7	TDRS S/C Body - Jettisonable Apogee Motor	5A-5
5A-8	TDRS S/C Body - Four Element (AGIPA or FFOV) VHF Array	5A-6
5A-9	TDRS S/C Body - Sectional View	5A-6
5A-10	TDRS Configuration With Single Element VHF Array	5A-7
5A-11	TDRS Configuration With 10 Feet Diameter Furlable MDR Antennas	5A-11
5A-12	TDRS Configuration With 12 Feet Diameter Furlable MDR Antennas	5A-13
5A-13	MDR Antenna Offset	5A-15
5A-14	MDR Antenna Diameter Tradeoff	5A-16
5A-15	TDRS Configuration - One MDR S-Band Phased Array	5A-19
5A-16	TDRS Configuration - Spheroidal Body Shape	5A-21
5A-17	TDRS Configuration - Single Element VHF Array	5A-23
5A-18	TDRS Configuration - Four Element AGIPA Array	5A-25
5A-19	TDRS With Five Element AGIPA	5A-27
5A-20	Comparison of VHF (FFOV) Element & VHF (AGIPA) Element Dimensions	5A-28
5A-21	VHF Array Element (Frequency 117.55 MHz)	5A-29
5A-22	VHF Array Element (Frequency 117.55 Mhz)	5A-31
5A-23	TDRS Configuration - 12.5 Feet Diameter Furlable Antennas With 4-Element AGIPA VHF Array (Frequency 117.55 Mhz)	5A-33
5A-24	TDRS Configuration - 6.5 Feet Diameter MDR Antennas With VHF Array (Frequency 117.55 MHz)	5A-35
6A-1	Coordinate Frames and Angle Conventions	6A-3
6A-2	Surface Characteristics for Solar Torque Calculations	6A-3
6A-3	Solar Pressure Disturbance Torques on TDRS (Baseline S/C ZCG = 25", YCG = 0)	6A-6
6A-4	Solar Pressure Disturbance Torques on TDRS (ZCG = 19", YCG = 0)	6A-8
6A-5	Solar Pressure Disturbance Torques on TDRS (ZCG = 19", YCG = 0.6" (Design Condition)	6A-10
6A-6	Solar Pressure Disturbance Torques on TDRS Main Body ZCG = 19", YCG = 0.6" (Design Condition)	6A-12
6A-7	Solar Pressure Disturbance Torques on TDRS LDR Antenna	6A-14
6A-8	Solar Pressure Disturbance Torques on TDRS MDR Antenna	6A-16
6A-9	Solar Pressure Disturbance Torques on TDRS MDR Antenna (With Windmilling) (Baseline S/C)	6A-18



Figure		Page
6A-10	Solar Pressure Disturbance Torques on TDRS Solar Array . . .	6A-20
6B-1	Time Constant Versus Inertia Ratio	6B-4
6B-2	Time Constant Versus Fill Ratio	6B-4
6B-3	Propellant Weight and Fill Ratio Versus Fill Height . . .	6B-4
8A-1	Battery Cycle Life Versus Depth of Discharge	8A-2
8A-2	12 AH NiCd Battery Test at Synchronous Orbit Conditions . .	8A-2
8A-3	Parametric Battery Weights	8A-3
8A-4	Time Required to Charge 1 Battery	8A-5
10C-1	LDR Transponder Reliability	10C-2
10C-2	MDR Transponder Reliability	10C-3
10C-3	TDRS/GS Transponder Reliability	10C-4
10C-4	Frequency Source Reliability	10C-5
10C-5	Location Transponder	10C-5
10C-6	Beacon Reliability	10C-5



TABLES

Table		Page
4B-1	LDR Receiver Front End	4B-2
4B-2	LDR IF Summing Network	4B-3
4B-3	UHF Transmitter Divider Satellite Steered Beam	4B-4
4B-4	UHF Transmitter Satellite Steering	4B-5
4B-5	MDR Receiver	4B-6
4B-6	MDR #1 Transmitter	4B-7
4B-7	MDR #2 Transmitter	4B-8
4B-8	GS/TDRS Receiver	4B-9
4B-9	TDRS Transmitter	4B-10
4B-10	Frequency Source	4B-11
4B-11	S-Band Location and Order Wire System	4B-12
4B-12	Telemetry and Command	4B-13
4B-13	Ku-Band Beacon	4B-14
4C-1	Summary of TDRS Telemetry and Command Input/ Output Requirements	
6A-1	Projected Surface Characteristics	
6A-2	Momentum Requirements Due to Solar Pressure Torques (Ft Lb Sec)	
6B-1	Physical Data	6B-3
10C-1	Circuit Failure Rates	
10C-2	Reference Circuit Failure Rates	
10C-3	Part Failure Rates	
10C-4	Attitude Control	
10C-5	Auxiliary Propulsion	
10C-6	Electrical Power	

APPENDIX 2.A ORBIT ORIENTATION FOR OPTIMUM INCLINATION PERTURBATION

The geosynchronous orbit plane inclination is perturbed by the gravitational fields of the sun and moon, and by solar radiation pressure. The latter is considered negligible because of its size and the fact that its effect on inclination reverses itself every half day. The luni-solar perturbation must be considered, however. Its effect varies with the orientation of the TDRS orbit major axis with respect to the earth-moon geometry. The relationship between major axis orientation and the inclination variation is described below.

The major axis can be given an orientation in space by judicious selection of launch times such that the orbit inclination decreases to zero and then increases. This occurs when the intersection of the moon's orbit and the TDRS orbit lies 90 degrees from the intersection of the TDRS orbit with the equator. The angle is identified as ψ_m in Figure 2.A-1. This angle is related to the right ascension of the ascending node and to the inclination of the TDRS orbit by a series of equations which have been computer-programmed. The relation of Ω_0 to ψ_m is plotted in Figure 2.A-2 for a typical launch date, January 1, 1977.

The magnitude of the inclination perturbation is established when the Julian date and the inclination and node of the orbit are specified. The program computes the inclination of the TDRS orbit at regular time intervals after injection, given the initial orbit orientation, and the Julian date of injection. The instantaneous geographic location of the satellite does not enter into the computation. Figure 2.A-3 shows the variation in TDRS orbit inclination with time for an initial inclination $i_0 = 2.5$ degrees and a launch on January 5, 1977. Figure 2.A-3 shows the difference attributable to variations from the optimum initial ascending node location. The most favorable curve from the standpoint of keeping the inclination low corresponds to $\psi_m = 90$ degrees. This is true for any initial date and inclination, but the value of Ω_0 (right ascension of the ascending node) necessary to drive ψ_m to 90 degrees does vary with the initial conditions.

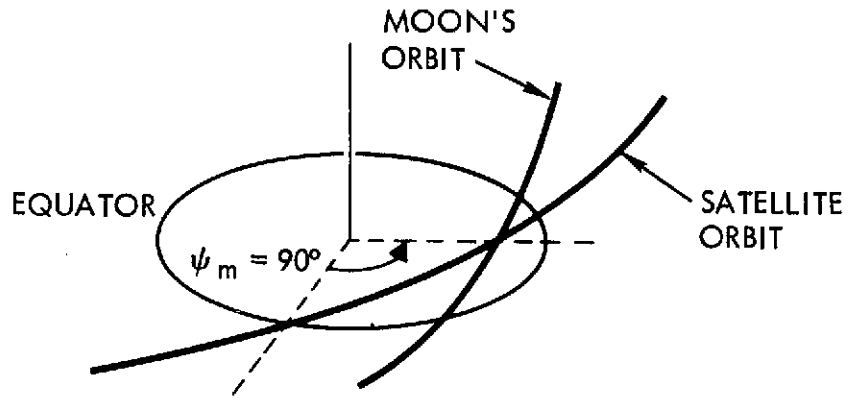


Figure 2.A-1. Geometry for Optimum Inclination Perturbation

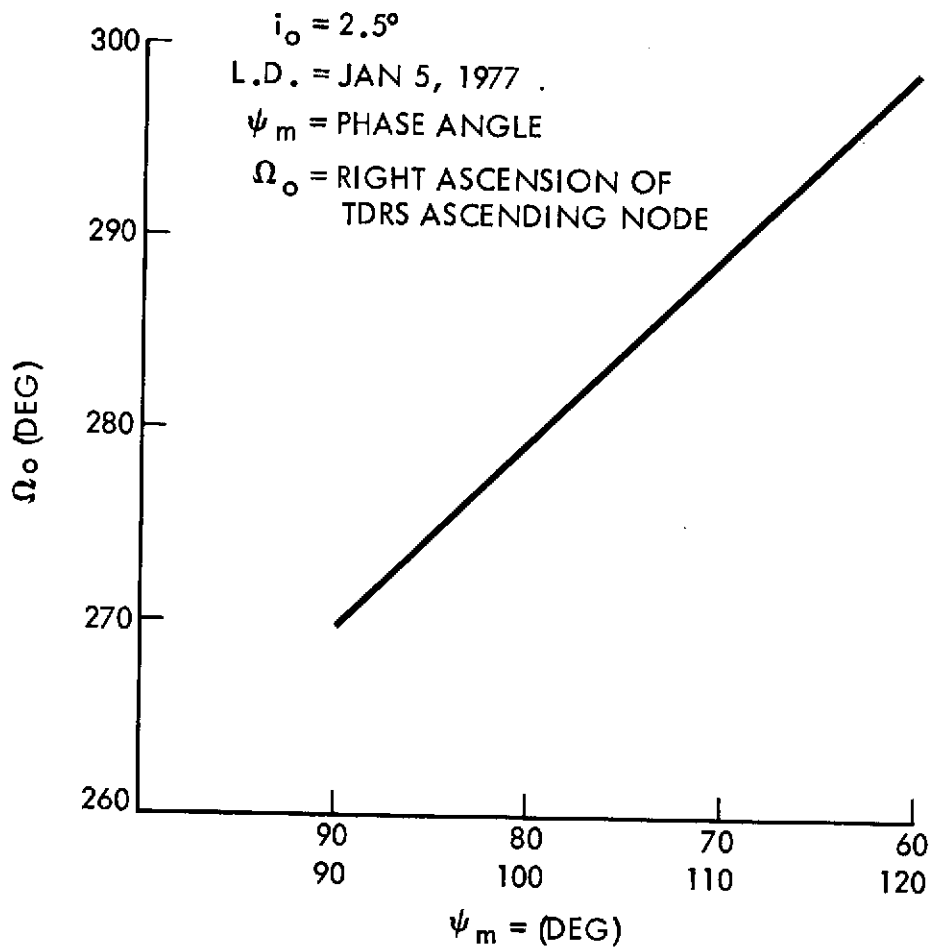


Figure 2.A-2. Ascending Node vs Phase Angle

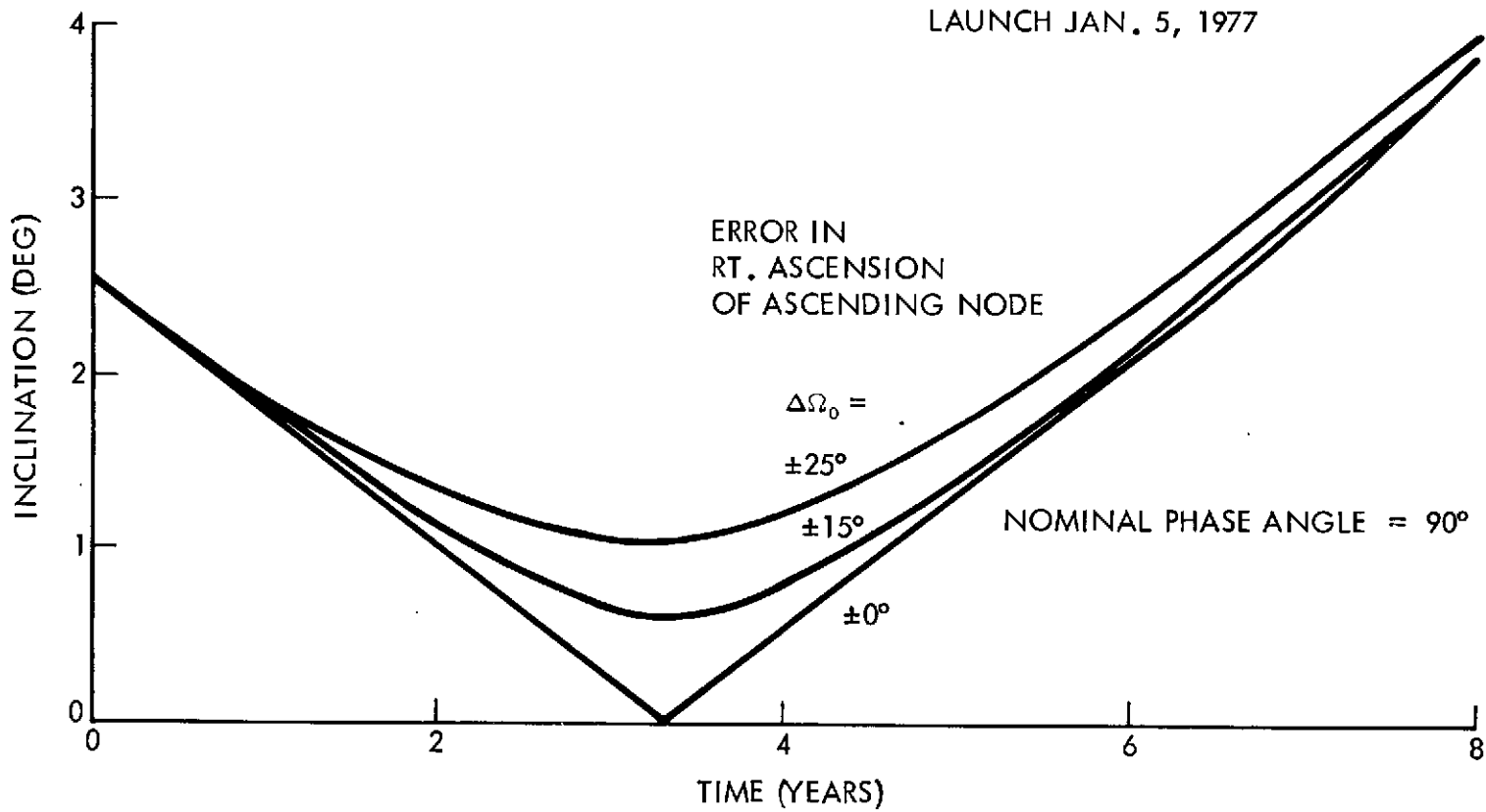


Figure 2.A-3. TDRS Orbit Inclination vs Time

2A-3

SD 72-SA-0133



Space Division
North American Rockwell

APPENDIX 2.B PAYLOAD INCREASE ASSOCIATED WITH
BIASED SYNCHRONOUS ORBIT INJECTION

A payload increase can be realized by injecting the TDRS into an orbit with a slightly shorter period than geosynchronous (drift bias mode) rather than injecting to geosynchronous velocity (start/stop mode) and allowing the on-board propulsion system to start and stop the drift.

If the velocity increment to initiate drift is visualized as a "unit," the start/stop mode requires the apogee motor to provide one unit (to get into synchronous orbit) and the on-board propulsion system to provide two units: one to start the drift and one to stop it. The drift bias mode removes the one-unit requirement of the apogee motor (since the achieved orbit is below synchronous) and reduces the on-board propulsion requirement to one unit (stopping the drift). The amount of apogee motor propellant thus conserved is

$$\partial W_{p_1} \text{ (lb)} = .0791N$$

where N is the number of fps per unit. The corresponding increase in payload capability is 1.145 times the propellant saving. The reduction in on-board propellant requirement is

$$\partial W_{p_2} \text{ (lb)} = .0979N$$

The propellant thus saved can be replaced almost directly with the payload. An analysis was made for a drift rate of 5 degrees/rev, which is equivalent to a drift rate of 47 feet/second.

The savings in propellant are 3.7 pounds in the apogee motor and 4.6 pounds in the on-board propulsion system. This results in a net payload improvement of 8.85 pounds or 1.765 pounds for each degree per day of drift employed. This net payload improvement will be reduced for higher drift rates. For the drift bias mode, the payload sensitivity to drift rate for the on-board propulsion system and the apogee motor is as shown below.

$$\begin{aligned} \frac{\partial W_{PL} \text{ (lb)}}{\partial \dot{\theta} \text{ (deg/rev)}} &= -.921 \text{ on-board propellant} \\ \frac{\partial W_{PL} \text{ (lb)}}{\partial \dot{\theta} \text{ (deg/rev)}} &= \frac{\partial W_{PL}}{\partial \Delta V} \cdot \frac{\partial \Delta V}{\partial \Delta V} \cdot \frac{\partial V}{\partial \dot{\theta}} \\ &= (-.0859)(.93)(-9.416) \\ &= .753 \text{ apogee motor} \end{aligned}$$

Thus, after the drift bias mode is selected, there is a net payload loss of approximately .168 pound for every degree/rev that the drift rate is increased. Increasing the drift rate reduces the delta-V requirement imposed on the apogee motor while increasing the requirement imposed on the on-board propulsion system. The apogee motor has a higher I_{sp} and combines the drift impulse with the "circularization" and plane change impulse. The on-board propulsion system, however, operates on a smaller mass.

Conclusion

The drift biased injection method of placing the TDRS satellites on station is preferable, but the payload increase varies inversely with drift rate. However, the sensitivity of payload increase to drift rate is low (-.168 lb/deg/rev); so the payload penalty in the drift rate range of interest (3 degrees/day to 10 degrees/day) is negligible (< 2 pounds).

APPENDIX 4A. EMC PROGRAM FOR SPACEBORNE TDRS
TELECOMMUNICATION SYSTEM

The Electromagnetic Compatibility (EMC) Section at AIL is staffed with specialists who conduct EMC programs for equipment and systems programs throughout the company. One of these specialists will be assigned to the TDRS hardware program. The TDRS shall meet the requirements of MIL-STD-461A, Notice 3 for Class A2 equipment.

The following are the applicable EMI requirements.

<u>Method</u>	<u>Description</u>
CE03	0.02 to 50 MHz, power leads
CE06, Tailored*	10 kHz to 12.4 GHz, antenna terminal
CS01	0.03 to 50 kHz, power leads
CS02	0.05 to 400 MHz, power leads
CS03, Tailored*	30 Hz to 10 GHz, intermodulation
CS04, Tailored*	30 Hz to 10 GHz, rejection of undesired signal
CS05, Tailored*	30 Hz to 10 GHz, cross-modulation
CS06	Spike, power leads
RE02	14 kHz to 10 GHz, electric field
RS02	Magnetic induction field
RS03	14 kHz to 10 GHz, electric field

The EMC program includes the following major steps:

1. Interference prediction
2. Design testing
3. Interference control design
4. Preparation of the interference control plan
5. Subcontractor and vendor EMC control
6. Electrical and mechanical design review
7. Interference testing of critical devices
8. Any necessary amendment of the interference control plan
9. In-process inspection during manufacture
10. Preparation of an interference test plan
11. Performance of interference control qualification tests
12. Re-engineering, where necessary
13. Preparation and submittal of the interference control test report

The Interference control plan is used as a working document by the engineers designing the equipment. Designs are based on interference prediction, design analysis, design tests and on good EMI design practice. Design includes

* See Appendix B, Phase I TDRS Final Report

controlling interference generation at the source and the use of interference control materials and components. Drawings incorporate all necessary details of interference control design. In-process inspection assures adherence to these details.

The project EMC engineer participates in all electrical and mechanical design reviews to assure adherence to the plan. In addition, he reviews designs for interference problems not anticipated by the plan and initiates necessary corrective action. He also reviews subcontractor designs and test results to insure compliance. On critical devices he witnesses subcontractor tests to insure conformance to the prescribed procedures.

Interference testing of critical devices is conducted to verify the interference design. The interference control plan is amended, if necessary, as a result of design reviews and interference testing.

The interference test plan specifies the detailed test setups and steps required to comply with the test requirements. Qualification tests are performed according to this plan at AIL's EMC test facilities. Any necessary reengineering revealed as a result of these tests is performed, the necessary fix incorporated in the equipment, and the applicable test repeated.

The interference test report is then prepared and submitted to the customer at the end of the program.



APPENDIX 4B. MATERIAL BACKUP LIST FOR THE SPACEBORNE
TDRS TELECOMMUNICATION SYSTEM

The following 13 tables provide a detailed backup to show what the weights and powers of the TDRS telecommunication system are based upon. An overall summary of these tables for the entire spaceborne TDRS telecommunication system is found in Section 3.0, Table 4-3.

Table 4B-5. MDR Receiver

ITEM	SIZE (LxWxH)	DESIGNATION *	QUANTITY	UNIT WT lbs.	TOTAL WT lbs.	TOTAL POWER Watts
S-Band Diplexer	6 x 2 x 1.5		1	1.22	1.22	
Ku-Band Diplexer	9 x 1.5 x .75		1	.44	.44	
RF Switch	1.7 x 1.3 x .5		4	.09	.36	
S Paramp	3 x 1 x 1.5		1	.53	.53	2.5
Ku Paramp	6 x 4 x 1		1	.56	.56	(2.5)
S Xistor Amp	1.25 x 2 x .75		1	.02	.02	0.2
Ku Mixer	.5 x .5 x .5		1	.05	.05	
S Mixer	1.5 x 2 x .75		1	.07	.07	
UHF Amp	1 x 1.5 x .75		2	.02	.04	0.2
BPF	3 x 1.5 x .75		1	.03	.03	
IF Amp	3 x 1.5 x .75		1	.03	.03	0.2
TO-5 Switch	.3D x .5		3	.01	.03	
Dir Coupler	2 x 1 x .25		4	.05	.20	
KuVCO	4 x 2 x 1		1	.66	.66	1.0
S VCO	3 x 4 x 1		1	.50	.50	.75
UHF VCO	2x2.5x1		1	.16	.16	.50
S Paramp			1	.53	.53	
Ku Paramp			1	.56	.56	
S Xistor Amp			1	.02	.02	
S Mixer			1	.07	.07	
Ku Mixer			1	.05	.05	
UHF Amp			2	.02	.04	
BPF			1	.03	.03	
IF Amp			1	.03	.03	
Ku VCO			1	.66	.66	
S VCO			1	.50	.50	
UHF VCO			1	.16	.16	
EMC Filters	.3 x .3 x .6	FL1-20	20	.01	.20	
Power Conditioning			2	.126	.25	0.81
Cables	5 x .1 x .1	W1	16	.015	.24	
Waveguide						
Chassis	12 x 9 x 3		1	.36	.36	
Connector (DC)	.5 x .5 x 1.0	J8	1	.03	.03	
Connector (RF)	.2 x .3 x .4	J1-7	7	.01	.07	
TOTAL	12x3x4				8.78	6.16

* Key: Amplifiers - A1
 Filters - F1
 Mixers - M1
 Power Dividers - PD1

Hybrid - H1
 Summer - PD1
 Diplexer - D1

APPENDIX 4C. SUMMARY OF TELEMETRY AND COMMAND
INPUT/OUTPUT REQUIREMENTS FOR THE TDRS SATELLITE

All of the telemetry and command input/output requirements for all of the subsystems on the TDRS satellite are tabulated in Table C-1. In this table, the following legend is used:

- "A" indicates analog data
- "D" indicates discrete bilevel data

Table 4C-1. Summary of TDRS Telemetry and Command Input/Output Requirements

Function	No. of I/O Channels	Format	
		Telemetry	Command
1. LDR Receiver			
• Switch main power on	4	D	D
• Preset PLL	2		
• Test PLL for Lock	2	D	
2. LDR Summing Unit			
• Switch main power	1	D	D
• Switch backup power on	1	D	D
• Select backup channel	1	D	D
• Preset PLL	1		
• Test PLL Lock	1	D	
3. LDR Transmitter Divider			
• Switch main power on	2	D	D
• Switch redundant power on	2	D	D
• Switch output to redundant amp	2	D	D
• Set Phase at Phase Shifter	2		8 bits
• Measure phase at shifters	8	4 bits	
• Test PLL Lock	4	D	
• Preset PLL	4		D
• Switch from 28V to 18V hr for power amplifiers	2	D	D
• Temperature measurement	2	A	
4. LDR Transmitter			
• Switch main power on	8	D	D
• Test output power	2	A	
• Temperature	2	A	
5. MDR Receivers			
• Switch main power on	4	D	D
• Switch redundant power on	4	D	D
• Switch to redundant Ku receiver	2	D	D

Table 4C-1. Summary of TDRS Telemetry and Command Input/Output Requirements
 (continued)

Function	No. of I/O Channels	Format	
		Telemetry	Command
• Switch to redundant S receiver	2	D	D
• Send count to Ku PLL	4	8 bits	8 bits
• Select PLL	6	D	D
• Preset PLL	6	D	D
• Test PLL Lock	6	D	D
• Select 500 MHz output	2	D	D
• Select baseband output	2	D	D
• Select 10 or 100 MHz bandwidth	2	D	D
• Select 6.5 ft dish for TDRS/GS link	1	D	D
• Send count to twenty step VCO	4	8 bits	8 bits
6. MDR Transmitters			
• Switch main power on	2	D	D
• Switch redundant power on	2	D	D
• Set programmable counter for Ku-Band PLL	4	8 bits	8 bits
• Send input to redundant unit	2	D	D
• Select S Band power amplifier unit	2	D	D
• Select Ku-Band power amplifier unit	2	D	D
• Ku-Band power out	2	A	
• S Band power out	2	A	
• Measure mixer L.O. power	8	A	
• Switch S Band to Ku-Band	4	D	D
• Turn on S-Band 6 db amp	2	D	D
• Switch to S-Band 6 db amp	4	D	D
• Preset Ku-Band PLL	4	D	
• Lock PLL(s) to center frequency	4		D
• Test Lock of PLL(s)	4	D	
• Select TDRS or MDR input	2	D	D
• Select IF Module	1	D	D
7. TDRS/GS Transmitter			
• Switch main power on	1	D	D
• Switch redundant power on	1	D	D
• Switch input to redundant unit	1	D	D
• Switch output to redundant unit	1	D	D

Table 4C-1. Summary of TDRS Telemetry and Command Input/Output Requirements
(continued)

Function	No. of I/O Channels	Format	
		Telemetry	Command
• Measure RF power out	1	A	
• Switch bandwidth of driver	2	D	D
• Change deviation of VCO	2	D	D
• Monitor VCO power	2	A	
• Monitor VCO frequency	2	A	
• Switch in 10 db additional Ku-band gain	2	D	
8. Ground Link Receiver			
• Switch main power on	1	D	D
• Switch backup power on	1	D	D
• Select redundant PLL	3	D	D
• Select redundant IF outputs	6	D	D
• Select MDR receiver input	1	D	D
• Select redundant 500 MHz input	2	D	D
• Measure baseplate temperature	1	A	
9. Frequency Source			
• Switch output to redundant channel	10	D	D
• Lock VCO to center frequency	4		D
• Switch input to redundant channel	1	D	D
• Main unit power On/Off	1	D	D
• Redundant unit power On/Off	1	D	D
• Switch main power on	1	D	D
• Switch redundant power on	1	D	D
10. VHF Transponder			
• Switch into ranging mode	1		D
• Switch telemetry data to Ku-band	1		D
• Transmitter power On/Off	1		D
• Switch data input to Ku-band	1	D	D
• Switch main power on	1	D	D
• Switch redundant power on	1	D	D

Table 4C-1. Summary of TDRS Telemetry and Command Input/Output Requirements
(continued)

Function	No. of I/O Channels	Format	
		Telemetry	Command
11. Tracking and Location Transceiver			
• Switch main power on	1	D	D
• Switch backup power on	1	D	D
• Send signal to redundant receiver	2	D	D
• Send signal to redundant transmitter	2	D	D
• Test lock of PLL	6	D	
• Lock VCXO	6		D
• Receiver AGC	2	A	
12. Ku Band Beacon			
• Switch main power on	1	D	D
• Switch backup power on	1	D	D
• Test PLL lock	1	D	
• Lock PLL	1		D
13. Electrical Power System			
• Battery connect	2	D	D
• Battery disconnect	4	D	D
• Circuit breakers	5	D	D
• Load contractors	8	D	D
<u>Solar Array</u>			
• Panel output voltage	2	A	
• Panel output current	2	A	
• Panel temperature	2	A	
• Orientation motor temperature	2	A	
• Orientation motor voltage	2	A	
• Orientation motor current	2	A	
<u>Battery/Power Conditioning</u>			
• Shunt regulator element voltage	2	A	
• Shunt regulator element current	2	A	
• Shunt regulator base plate temperature	2	A	
• Shunt regulator On/Off	2	D	D

Table 4C-1. Summary of TDRS Telemetry and Command Input/Output Requirements
 (continued)

Function	No. of I/O Channels	Format	
		Telemetry	Command
• Boost regulator voltage out	2	A	
• Boost regulator current out	2	A	
• Boost regulator base plate temperature	2	A	
• Boost regulator On/Off	2	D	D
• Inverter Output Voltage	2	A	
• Inverter output current	2	A	
• Inverter base plate temperature	2	A	
• Inverter On/Off	2	D	D
• Battery voltage	2	A	
• Battery current	2	A	
• Battery discharge current	2	A	
• Battery temperature	2	A	
• Battery state of charge	2	A	
• Amp hour counter On/Off	2	D	D
14. Altitude Stabilization and Control System			
<u>Spin Stabilized Phase</u>			
• Active mutation control enable	1	D	D
• Precession control enable	1	D	D
• Pitch solar acquisition mode	1	D	D
• Yaw solar acquisition mode	1	D	D
• Horizon acquisition mode	1	D	D
• Precession control pulse width	1	10 bits	10 bits
• Precession control phase angle	1	10 bits	10 bits
• Plus pitch jet torque command	1	D	D
• Minus pitch jet torque command	1	D	D
• Plus yaw jet torque command	1	D	D
• Minus yaw jet torque command	1	D	D
• ANC accelerometer	2	A	
• Spinning horizon sensor	2	A	
• Spinning sun sensor	2	12 bits	
<u>3-Axes Phase</u>			
• 3 Axes ASCS enable	1	D	D
• Reaction wheel power on	2	D	D
• Pitch altitude commands	1	10 bits	10 bits

Table 4C-1. Summary of TDRS Telemetry and Command Input/Output Requirements
 (continued)

Function	No. of I/O Channels	Format	
		Telemetry	Command
• Roll altitude commands	1		
• ΔV thrusting command	1	D	D
• ΔV thrusting duration	1	10 bits	10 bits
• ΔV thrusting exciter	1	D	D
• APS thruster enable	8	D	D
• Reaction weeel temperature	2	A	
• Reaction wheel speed	2	A	A
• Sun sensor pitch error	2	9 bits	
• Sun sensor yaw error	2	9 bits	
15. Propulsion			
• Hydrazine On/Off latching solenoid valve	1	D	D
• N/A propellent isolation valve activation	1	D	D
• N/A engine isolation valves	8	D	D
16. Structure and Mechanical System			
• Solar Panel Deployment	2	D	D
• 6-foot dish deployment	2	D	D
• VHF array deployment	4	D	D
• VHF control stem extension	4	D	D
• 6-foot dish gimbal power	2	D	D
• 6-foot dish azimuth pointing	2	A	A
• 6-foot dish elevation pointing	2	A	A
• 3-foot dish gimbal power	1	D	D
• 3-foot dish elevation pointing	1	A	A
• 3-foot dish azimuth pointing	1	A	A
• Solar panel drive power	2	D	D
• Solar panel drive rate	2	A	A
• Solar panel position	2	A	A
• Structural temperature	5	A	
17. Logic and Timing			
• Switch to alternate PROM	8	D	D
• Switch to redundant power supply	3	D	D
• Switch to redundant transponder	1	D	D

APPENDIX 5A
ALTERNATE CONCEPTS AND TRADE STUDIES
OF S/C STRUCTURE AND CONFIGURATION

During the preliminary design and baseline configuration determination, several approaches to many and varied problems were studied and evaluated. Some of the more pertinent and interesting studies are included in this Appendix.

5A.1 SPACECRAFT STRUCTURAL BODY SHAPES

Starting from an initial octagonal box structure as a baseline, various body shapes were investigated to reduce surface area and structural weight; to provide a minimum number of structural components that support the deployed antennas; and an equipment support shelf amenable to static and dynamic balancing with easy shift of equipment weights. With the several antennas filling most of the available volume within the Delta shroud, a short-coupled spacecraft body was required to maintain the structure ahead of the separation plane of the spacecraft attachment fitting. An analysis of spacecraft body shapes indicated a flattened spheroidal shape with reduced surface area and a transverse equipment shelf bulkhead would weigh less than the octagonal baseline. Figures 5A-1, 5A-2, 5A-3, 5A-4, 5A-5 and 5A-6 illustrate the progressive development of the spheroidal shaped structure. Further refinements and changes resulting from an investigation of jettisoning and non-jettisoning of the apogee motor is shown in Figure 5A-7 compared to Figure 5A-6. An analysis of weight, simplicity of structure, and number of parts indicated that the weight penalty of the jettison feature exceeds the fuel saved in subsequent maneuvers without the empty apogee motor case. Jettisoning of the apogee motor did not prove beneficial and it was retained after burnout.

Changes in LDR array deployment and packaging features resulted in a body shape with a flattened front face and later information on actual size and shape of the CTS apogee motor revised the internal structural cones as shown in Figure 5A-8. The baseline body configuration shown in Figure 5A-9 was the result of LDR antenna design finalization, equipment shelf, equipment installation studies, manufacturing considerations and weight control studies.

5A-2 SOLAR PANEL CONFIGURATIONS AND DRIVE SYSTEMS

Early in the program it was evident that if the solar panels were to be simple, with rigid substrate panels and deployable strut linkage, they would most conveniently be stowed above and below the spacecraft body and aft of the stowed VHF elements. Initial studies of flat panels generated typical arrangements shown in Figure 5A-10. The rectangular panels are limited in width by the curvature of the shroud envelope and the spacing between the

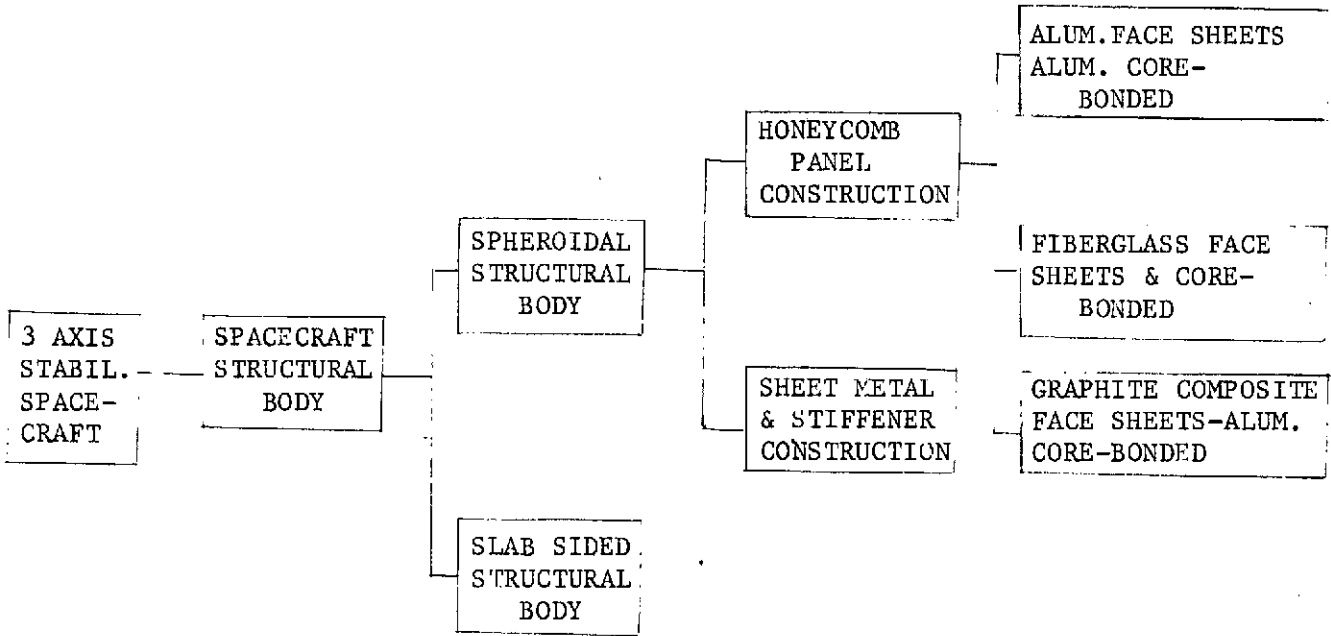
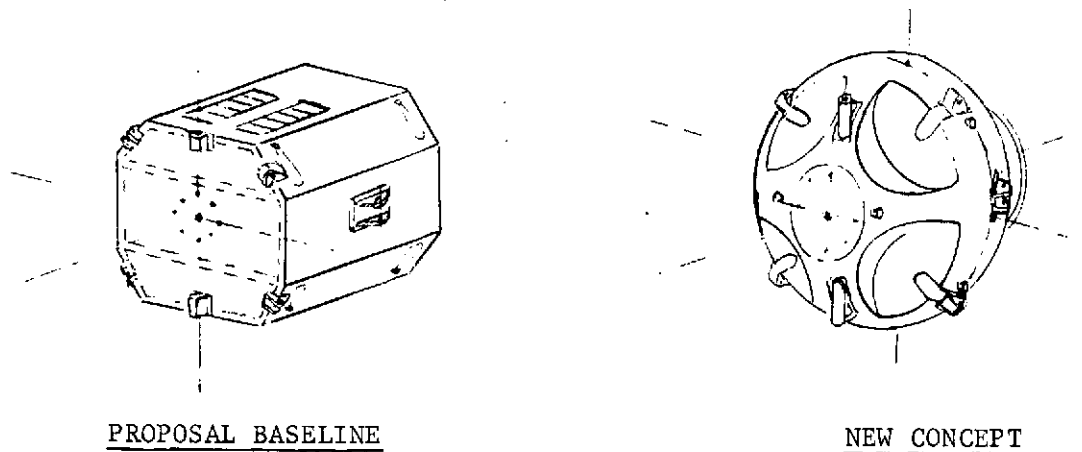


Figure 5A-1. Trade Tree - Spacecraft Structural Body



DESIGN FEATURES

- . ALUM. HONEYCOMB CONSTRUCTION
- . FLAT BODY PANELS
- . TWO FORF & AFT EQUIP. SHELVES
- . SURFACE AREA: 128.8 SQ. FT.
- . ESTIMATED WEIGHT: 96.03 LBS.

DESIGN FEATURES

- . ALUM. HONEYCOMB CONSTRUCTION
- . SPHEROIDAL OUTER SHELL
- . TRANSVERSE EQUIPMENT SHELF
- . SURFACE AREA: 83.1 SQ. FT.
- . ESTIMATED WEIGHT: 61.5 LBS.
- . WEIGHT SAVINGS: 34.53 LBS.

Figure 5A-2. Trade Study - Body Comparison

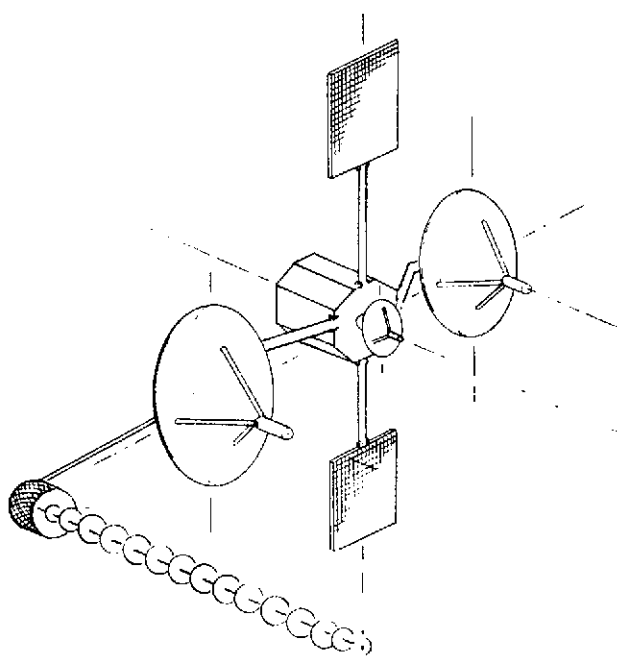


Figure 5A-3. TDRS Configuration-Slab Sided Body

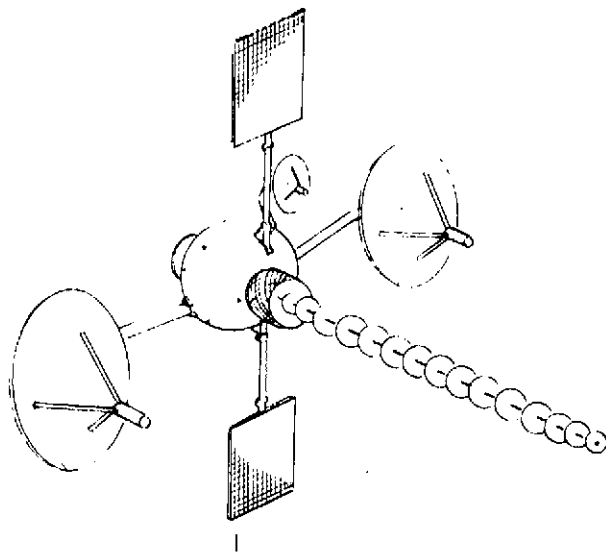


Figure 5A-4. TDRS Configuration-Spheroidal Body

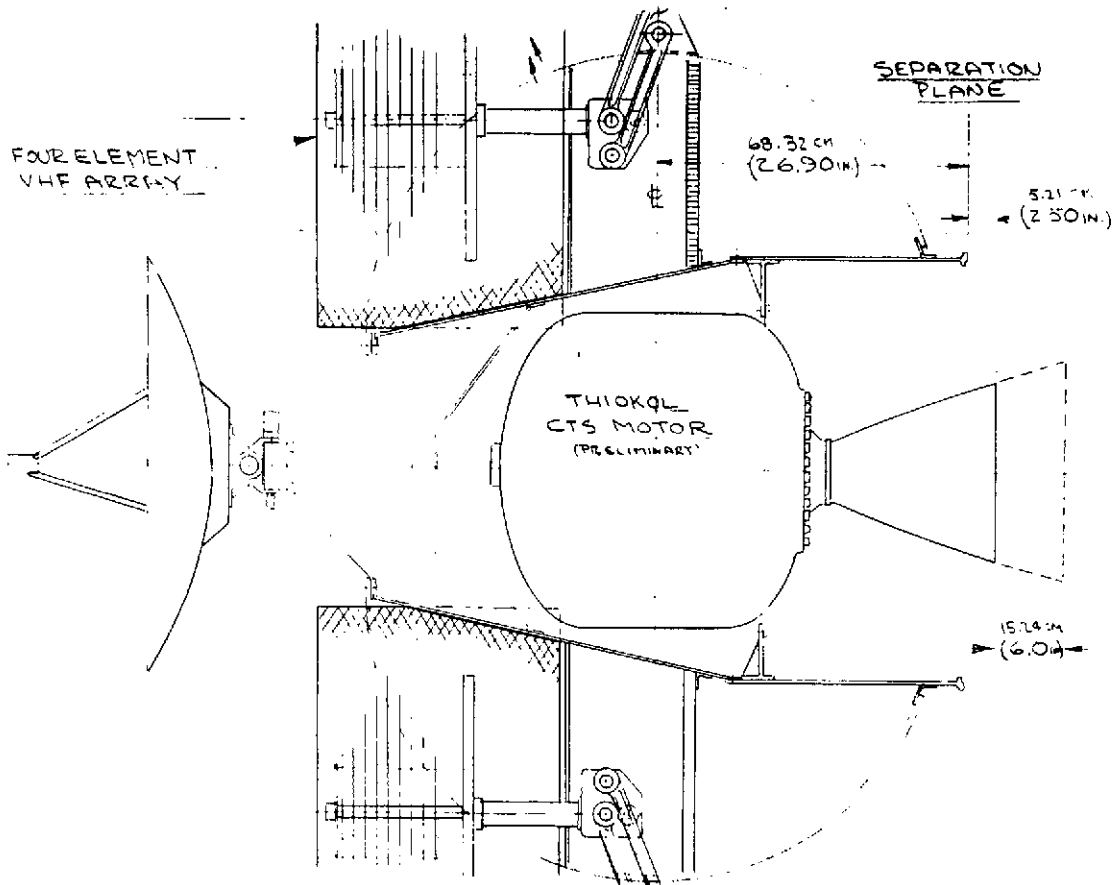


Figure 5A-5. TDRS S/C Body-Nonjettisonable Apogee Motor

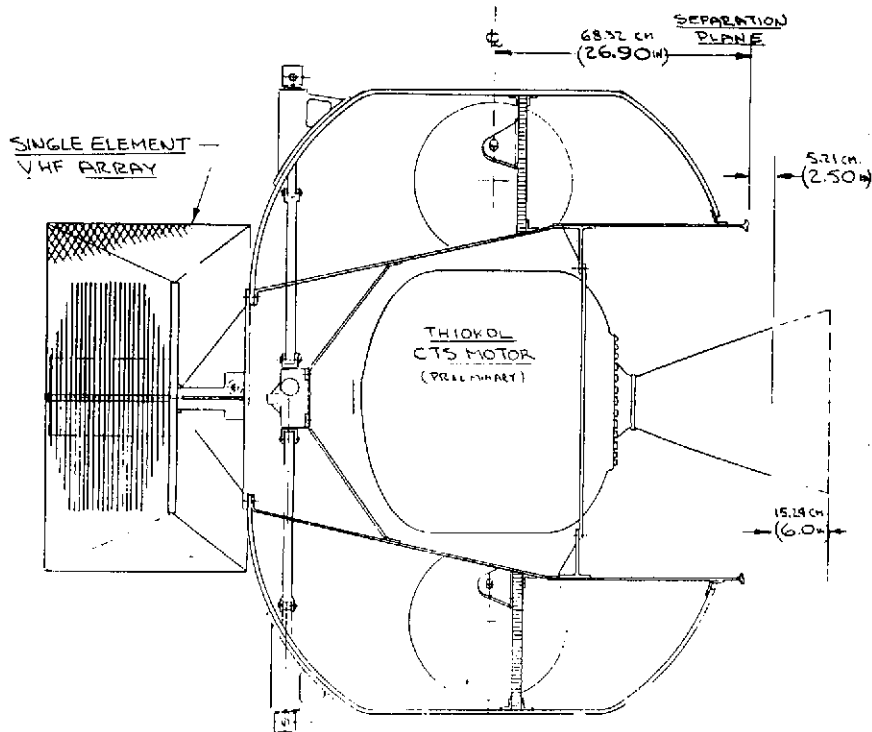


Figure 5A-6. TDRS S/C Body-Notjettisonable Apogee Motor

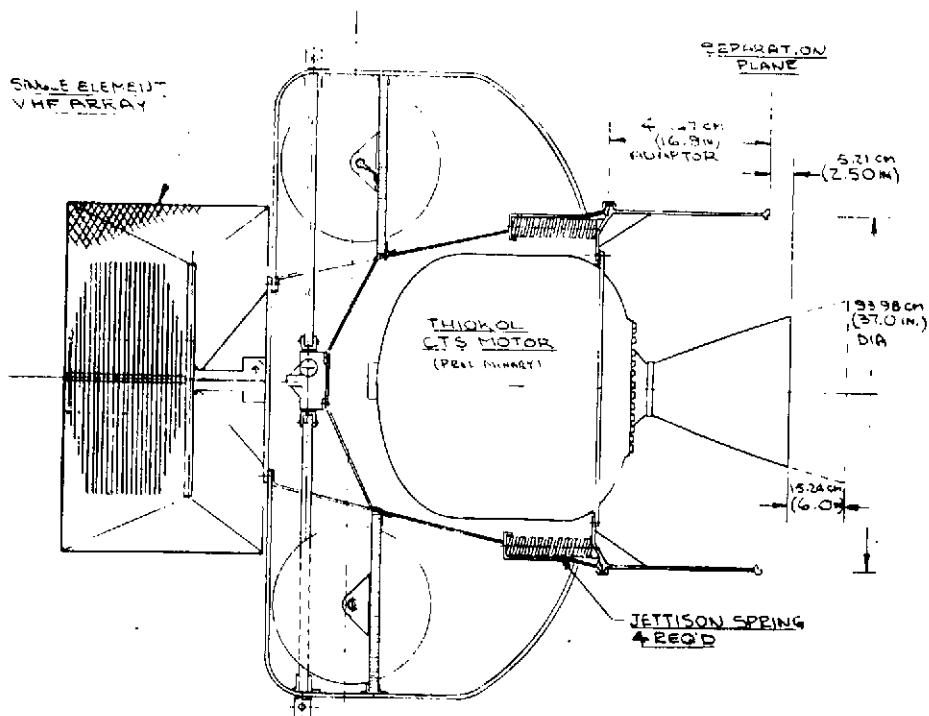


Figure 5A-7. TDRS S/C Body With Jettisonable Apogee Motor

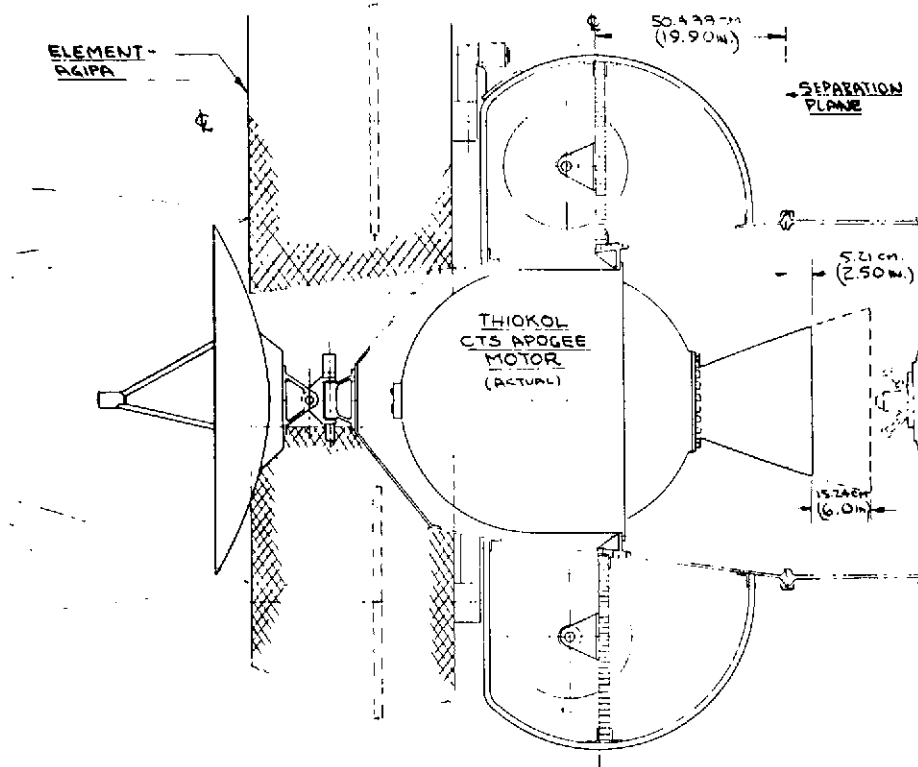


Figure 5A-8. TDRS S/C Body-Four Element (AGIPA or FFOV) VHF Array

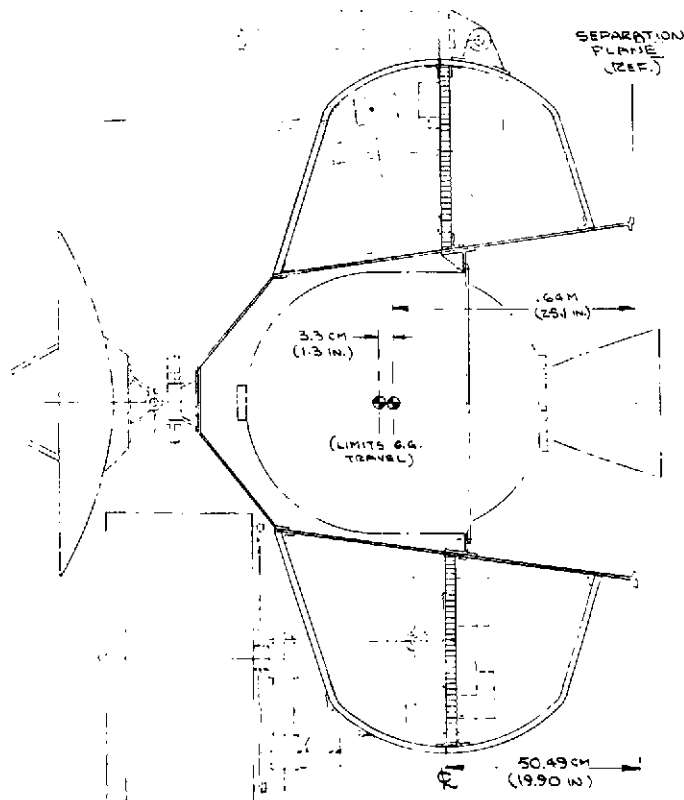


Figure 5A-9. TDRS S/C Body-Sectional View

Page intentionally left blank

Page intentionally left blank

stowed LDR array elements. An analysis of the electrical power generated by the solar cells on the stowed panels when spinning indicated cyclic interruptions and limited energy generation. To more closely approximate the cylindrical drum of the solar panels of a dual spin satellite, the panels were shortened in height and extended in a curve around the spacecraft. Limited gaps between panels at the sides provide clearance for the MDR antenna support booms and the operation of the ACS thrusters prior to deployment of the antennas and solar panels. This panel configuration provides more than adequate continuous electrical power during the spinning mode and was chosen as the baseline as shown in Figures 5-1 and 5-4. After deployment, the curved solar panels are slightly flattened by rotation of the two panel halves by spring loaded hinge fittings on the panel centerline for increased solar illumination efficiency.

The drive system and actuator necessary for the one rev/day rotation to maintain solar alignment with the solar panels initially had a common drive actuator at the spacecraft centerline with interconnected shafts to the solar panels as shown in Figure 5A-6. Later detail information on the CTS apogee motor increased the apogee motor length so that a clear through position for the solar panel interconnecting shafts was no longer available, and the drive system was divided into two separate and identical systems with the actuators mounted on the rear surface of the equipment shelf.

5A.3 MDR ANTENNA DIAMETERS AND CONSTRUCTION

Investigations were made to determine the maximum diameter for the MDR antennas with solid face parabolic reflectors and with various types of presently available furlable antennas suitable for S-Band and Ku-Band operation. Figures 5A-11, and 5A-12 illustrate maximum diameter furlable antennas of the folding panel design and Radiation, Inc. developed folding mesh-rib design. Several factors were involved in determining antenna offset from the spacecraft centerline. These include the clearance required to prevent antenna beam blockage, and reflective distortions caused by the tip elements of the LDR antenna when the MDR antennas are pointed at full gimbal limit toward the spacecraft centerline. Figure 5A-13 shows the MDR antenna spacing and offset required to place the tip of the LDR array element into position relative to the S-Band antenna beam halfway between the 1/2 power beam width and the first side lobe peak angle for the various antenna diameters considered. The variation in the offset dimension of the MDR antennas reflects in a change in the solar panel dimensional offsets because of the relative change in the solar shadow line caused by the MDR antennas. Figure 5A-14 illustrates configuration changes and antenna weight comparisons for the three antenna diameters studied.

The more complex deployment mechanisms required for the furlable antennas with longer support boom lengths, more stringent stowage space and launch load support restraints, and increased weight penalties, indicated that the solid face 6-1/2 foot diameter antennas was the logical choice for the baseline configuration.

Page intentionally left blank

Page intentionally left blank

Page intentionally left blank

Page intentionally left blank

Page intentionally left blank

MDR ANTENNA OFFSET
TO UHF - VHF ARRAY
(RF REFLECTION/BLOCKAGE MINIMIZED)

MDR (S-BAND)	ANT. DIA. (FEET)		
	6.5	10.0	12.5
1/2 POWER BW A DIM. (deg)	5.3	3.4	2.7
1 ST S.L. B DIM. (deg)	9	5.7	4.6
2 ND S.L. C DIM. (deg)	14	8.5	6.8
L DIM. (IN.)	102.4	118.5	132.7
D DIM. (IN.)	138.5	155.0	170.0

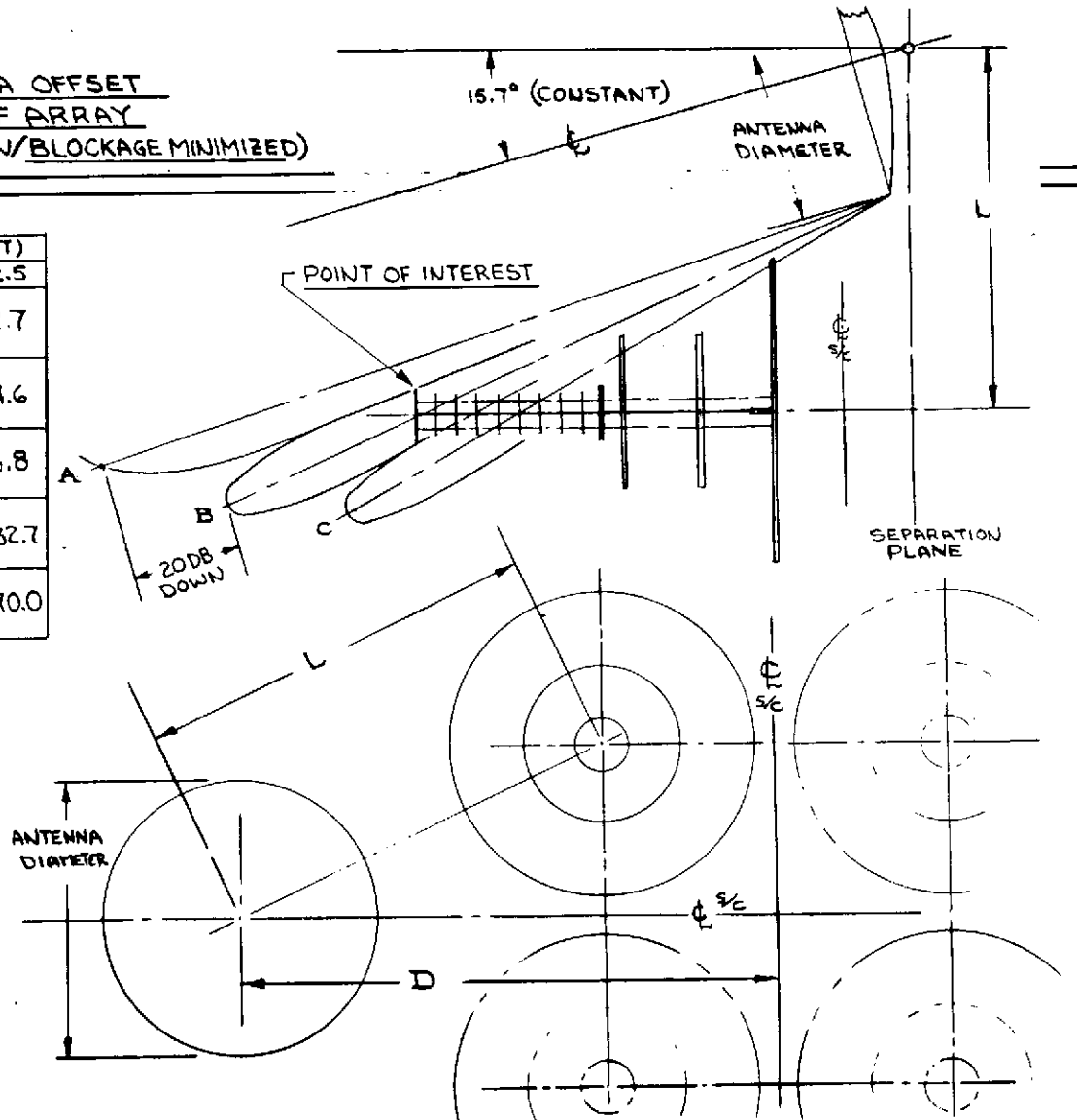
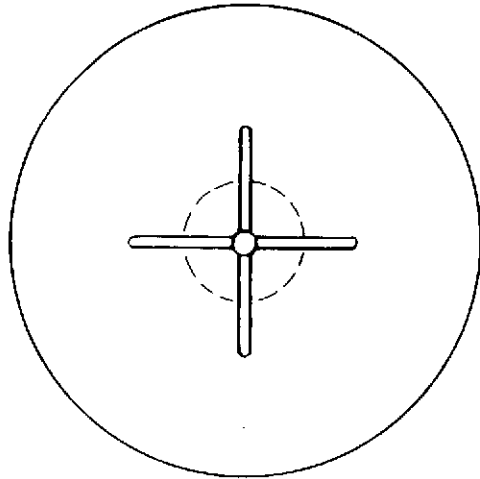


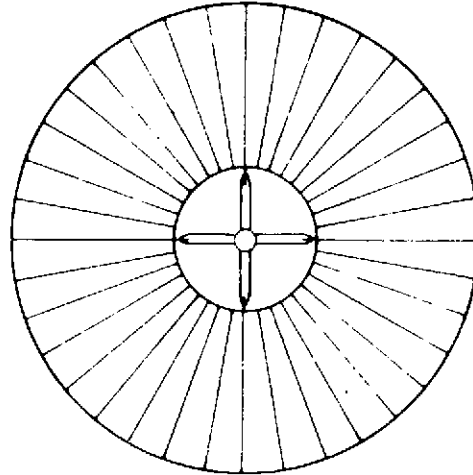
Figure 5A-13. MDR Antenna Offset

5A-15

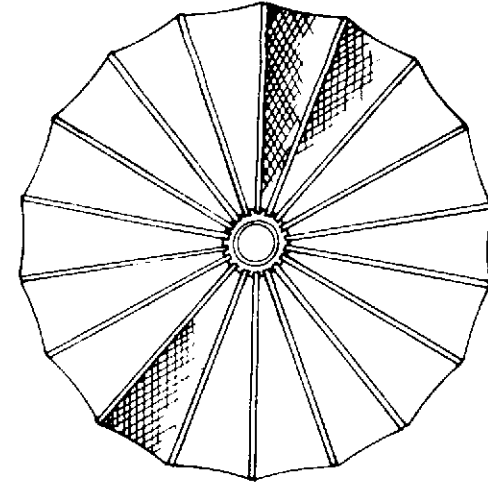
SD 72-SA-0133



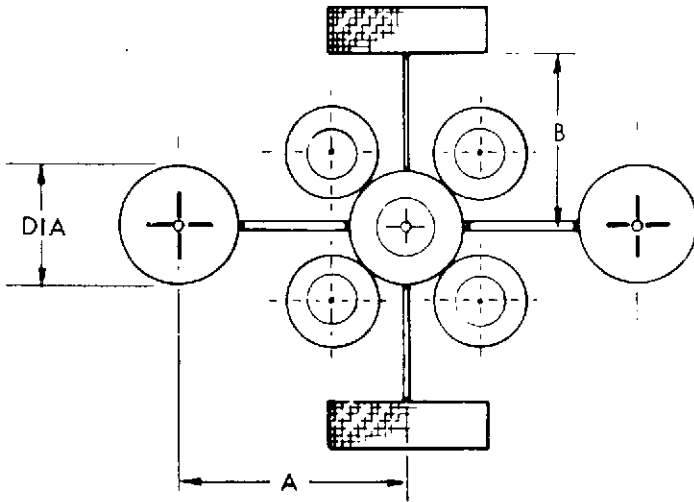
SOLID FACE
(6-1/2 FT MAX)



FOLDING PETALS



FOLDING RIB-MESH



DIA (FT)	A (IN.)	B (IN.)	ANTENNA WEIGHT (EACH) LB			
			DISH	GIMBAL	STRUT	TOTAL
6.5	138	108	15.6	3.3	5.7	24.6
10.0	155	133	17.5	4.0	6.6	28.1
12.5	170	154	27.3	5.3	8.5	41.1

Figure 5A-14. MDR Antenna Diameter Tradeoff

5A.4 MDR ANTENNA CONCEPT WITH S-BAND PHASED ARRAY

A variation of the MDR antenna with a S-Band phased array replacing one of the two 5.5 ft antennas was studied for feasibility of packaging and deployment. Figure 5A-15 illustrates the configuration generated from this study.

A slight rearrangement of the 5.5 ft antenna and the S-Band array in the stowed configuration was required for the S-Band phased array to clear the feed package of the 6.5 ft antenna. As shown in Figure 5A-15 the phased array is angled back closer to its support boom but since the beam is steered electronically and the array structure can be fixed to the boom this creates no problem. The array is so positioned that the boom rotates back and outward and in the deployed position the array centerline is parallel to the S/C centerline. The support boom length, fittings, pivot point and restraint latches are identical to those of 6-1/2 ft antenna. The replacement of the two-axis gimbal drive required on the 6-1/2 ft antenna by the fixed structural attachment of the array to the boom is the only basic change in structural detail.

5A.5 LDR ANTENNA CONFIGURATIONS

Various antenna designs were evaluated for the LDR antenna during the design program. Two designs submitted in the TDRS proposal, the VHF 4-element FFOV array and the VHF single element FFOV array, were integrated into preliminary configuration concepts as shown in Figure 5A-16 and 5A-17 with new structural bodies and antenna packaging. The solar pressure unbalance of the long single element VHF array outweighed the advantages of the simpler, body-mounted installation and the 4-element array was considered more acceptable.

Consideration of the AGIPA (adaptive ground implemented phased array) for the LDR VHF array required increased spacing between elements which changed element packaging and deployment methods, MDR antenna offset, spacecraft body shape, and solar panel packaging and configuration. Figure 5A-18 shows the new arrangement with these changes. The swing arm support link method for deploying the VHF array elements first employed in this configuration also became the baseline deployment method even though the LDR antenna design changed.

The AGIPA design with five array elements on a 11.0 foot dia. circle was studied and its effect on packaging, deployment and other antennas was evaluated (Figure 5A-19). The 5-element AGIPA design was less desirable than the 4-element design.

Optimization of VHF frequencies concentrated on the 117.55 MHz frequency for the forward LDR link and an electromagnetic design of an AGIPA element sized to 117.55 MHz increased the element in both length and diameter over a design based on 132 MHz. The comparison is shown in Figure 5A-20 and the larger element required completely new packaging to reduce length and diameter to stow the elements. If the element is packaged as shown in Figure 5A-21 stowage is similar to the previous design. An arrangement to package and

Page intentionally left blank

Page intentionally left blank

Page intentionally left blank

Page intentionally left blank

Page intentionally left blank

Page intentionally left blank

Page intentionally left blank

Page intentionally left blank

Page intentionally left blank

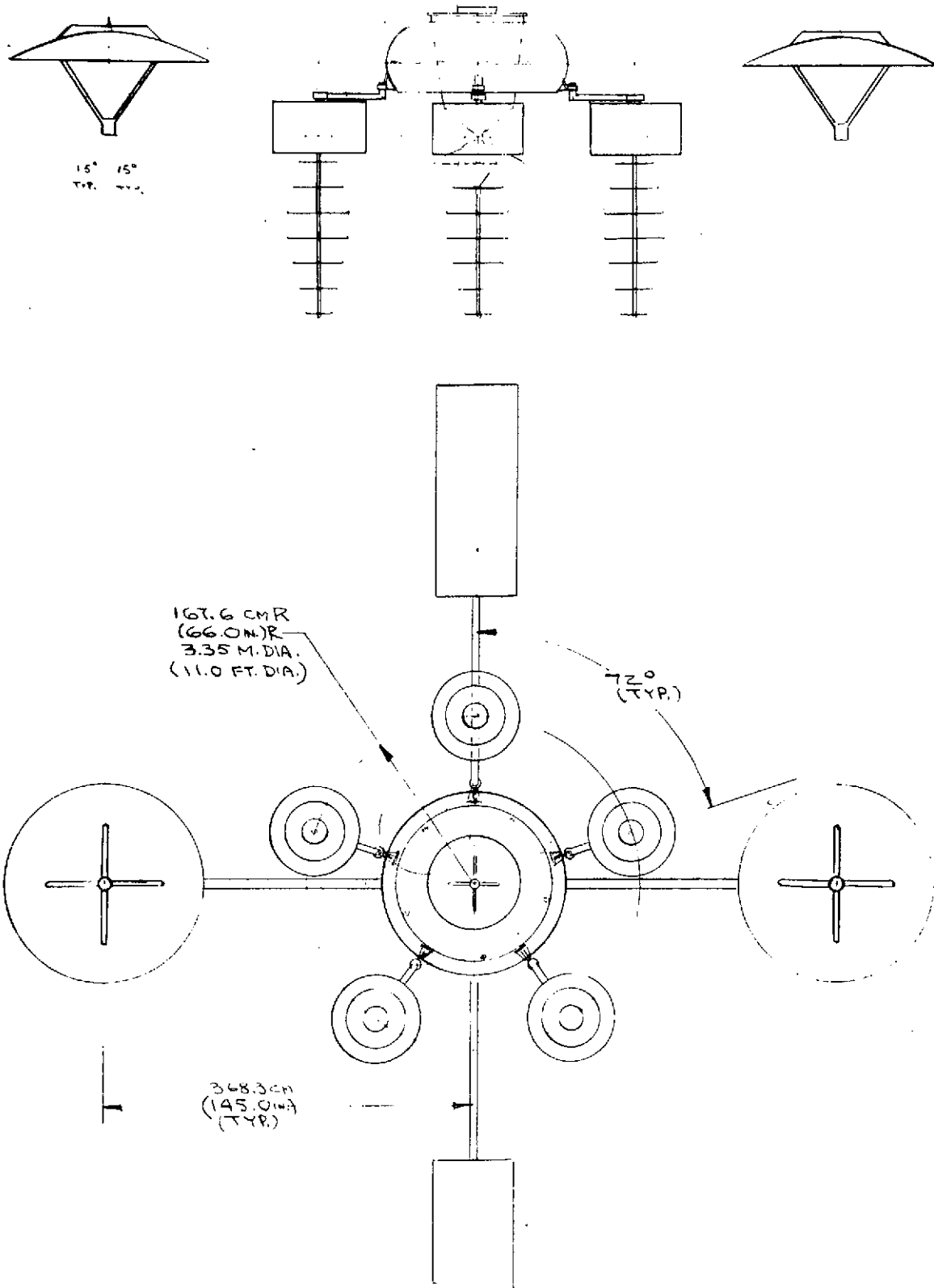
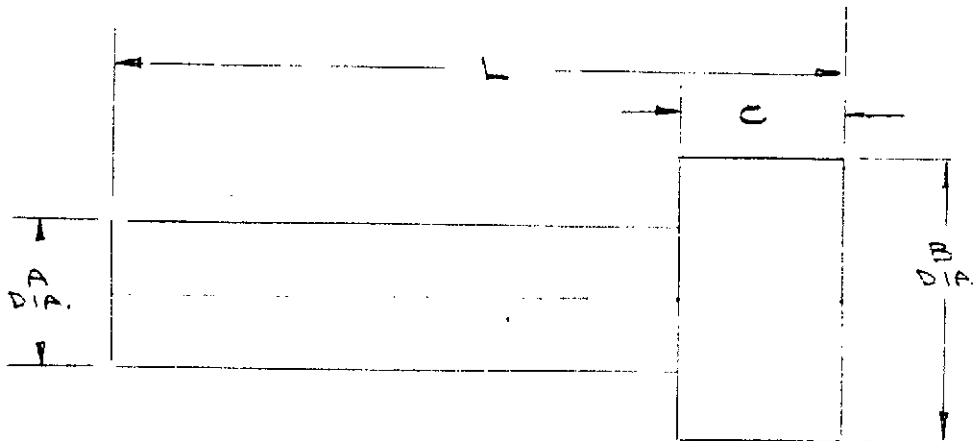


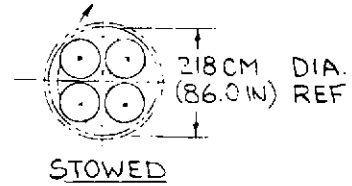
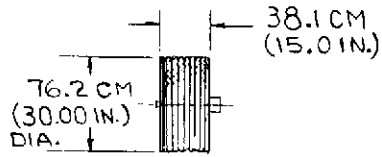
Figure 5A-19. TDRS With Five Element AGIPA



	L	A	B	C
VHF FFCV 132 MHz	96.0 in	24.0 in	36.0 in	21.0 in
VHF Jr. AGIPA COMMAND FREQ. 117.55 MHz	151.2 in	30.0 in	58.8 in	34.0 in

Figure 5A-20. Comparison of VHF (FFOV) Element & VHF (AGIPA) Element Dimensions

1. FOLDED & PACKAGED SIZE



2. DEPLOYED SIZE

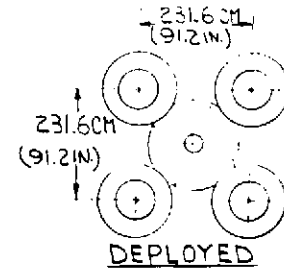
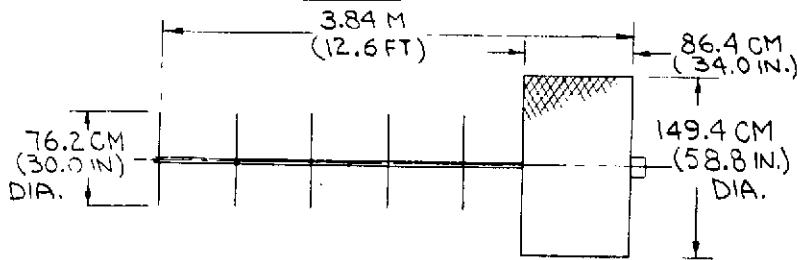


Figure 5A-21. VHF Array Element (Freq. 117.55 MHz)

deploy this new element was developed (Figure 5A-22) that provides light-weight, reliable and relatively simple means of restraint and deployment. Changes in TDRS configuration resulting from the larger VHF antenna are shown in Figures 5A-23 and 5A-24 as typical with different diameter MDR antennas.

A new design using UHF and VHF frequencies was developed to improve LDR capability and eliminate VHF frequency allocation problems in the forward link. This utilized a new antenna with four stacked UHF and VHF backfire elements (Figures 5-1 and 5-3). The packaging of these elements reduces the stowed diameter and length within the envelope of the UHF/VHF array element previously described.

Page intentionally left blank

Page intentionally left blank

Page intentionally left blank

Page intentionally left blank

Page intentionally left blank

Page intentionally left blank

Page intentionally left blank

5A.6 SUMMARY

The studies made during the design program led to the following recommendations:

- a) The spacecraft structural body shape and arrangement should be as shown in Figure 5-2. (Ref. Volume IV)
- b) The solar panel array configuration and deployment should be as shown in Figure 5-4.
- c) The MDR antennas should be 6-1/2 foot diameter, solid face parabolic reflector systems as shown in Figure 5-1.
- d) The LDR antenna should be the UHF VHF backfire array as shown in Figure 5-3.
- e) The TDRS/GS antenna should be a 3-foot diameter parabolic reflector system as shown in Figure 5-1.
- f) The baseline configuration based on the integration of the above components is as shown in Figure 5-1.

APPENDIX 6A SOLAR PRESSURE DISTURBANCE TORQUE ANALYSIS

The solar pressure disturbance torque analysis defines the momentum storage subsystem requirements and provides balancing information to the spacecraft design so the solar pressure torques and momentum storage requirements can be minimized. An existing NR digital program was utilized for the analysis. The program includes an improved solar pressure model received from GSFC during the study.

6A.1 SOLAR PRESSURE MODEL

Early formulations (References 1-3) utilized simple solar pressure models with specular reflections only. More recent work (References 4-6) also incorporate diffuse reflection. The model utilized herein was suggested by Carolyn Purvis and Marty Lidston of GSFC.

$$d\bar{F}_n = \left[\begin{array}{cccc} \text{Cos}^2\theta & + fR \text{Cos}^2\theta & + (1-f)R\frac{2}{3} \text{Cos}\theta & + a (1-R)\frac{2}{3} \text{Cos}\theta \end{array} \right] P_s dA \bar{n}$$

↑ (Absorbed)
↑ (Reflected specularly)
↑ (Reflected diffusely)
↑ (Absorbed & re-emitted diffusely)

$$d\bar{F}_t = P_s (1-fR) \text{Sin}\theta \text{Cos}\theta dA \bar{t}$$

↑ (Absorbed)
↑ (Reflected specularly)

This model provides a clearer and more intuitive definition of the coefficients and the origin of the terms. The basic terms are developed in Reference (6) with somewhat different coefficients. For convenience the equations may be written in vector form.

$$d\bar{F}_n = -P_s \left\{ (1+fR) |\bar{S} \cdot \bar{n}| (\bar{S} \cdot \bar{n}) + \frac{2}{3} [(1-f)R + a(1-R)] (\bar{S} \cdot \bar{n}) \right\} \bar{n} dA$$

$$d\bar{F}_t = -P_s (1-fR) \bar{S} \cdot \bar{n} (\bar{n} \times \bar{s} \times \bar{n}) dA$$

The radiation pressure due to absorbed and re-emitted energy (a term given in the solar pressure equations above) must be adjusted as a function of the thermodynamic state of the S/C element being analyzed. To simplify the analysis the following assumptions are made:

1. The time constants required for the surfaces to reach equilibrium temperature are small and may be neglected (i.e., steady state surface temperatures are assumed).
2. All thin walled elements (such as the solar panels and high gain antennas) are very conductive and have a negligible temperature drop from the front to the back of the surface. Thus the re-emitted radiation will be approximately equal from both sides of the element and the net pressure from this source may be neglected (a=0).

3. All well insulated surfaces (such as the main body) reach equilibrium temperatures rapidly such that all absorbed radiation on the illuminated side is re-radiated ($a=1$). The temperature of the non-illuminated side is assumed to drop rapidly to a very low value such that the re-emitted radiation can be neglected ($a=0$).

To obtain the solar pressure forces under the assumed thermal equilibrium conditions the coefficient (a) was inserted in the original force equation received from GSFC. The coordinate frames and angle definitions are shown in Figure 6A-1.

6A.2 SPACECRAFT REPRESENTATION

The program describes the spacecraft as a large number (i) of flat plate surfaces. Figure 6A-2 shows the surface characteristics of the various spacecraft components. The approximate component shapes and surface materials used in the digital program are:

- Main Body - right circular cylinder, covered with back silvered Teflon
- LDR Antenna Ground Planes - highly polished metallized screen, 50% porosity, represented as circular discs
- LDR Antenna Disks - projected area of rods is negligible, disks represented as a single circular disk at centroid of the disks, 5 disks per rod, 4 rods, 75% porosity, aluminized Kapton
- MDR Antennas - dishes are represented separately despite the symmetry about the S/C mass center to permit simulation of "windmilling"; right circular cylinders, aluminized paint thermal coating.
- Solar Arrays - two body-fixed projected areas to simulate the inertially oriented panels, N/P silicon cells with 12 mil quartz cover glass.

The areas, centers of pressure, and surface properties are summarized in Table 6A-1. The reflective properties and surface coatings are based on the thermodynamic analysis in Section IX.

Considerable shadowing of the various S/C elements by other elements is possible. The most significant shadowing occurs at S/C attitudes where the S/C symmetry results in negligible torques from those elements. The most outstanding example is with the VHF antennas illuminated on end. The total disk area can be shadowed to approximately one tenth but this occurs when the resulting torques are zero. Similarly the high gain antenna shadowing on the body (and vice versa) occurs when the torque contribution of these bodies is smallest. For these reasons and because of the complexity in mechanizing reasonably accurate shadowing of the various elements on each other, this type of shadowing is neglected producing slightly conservative results.

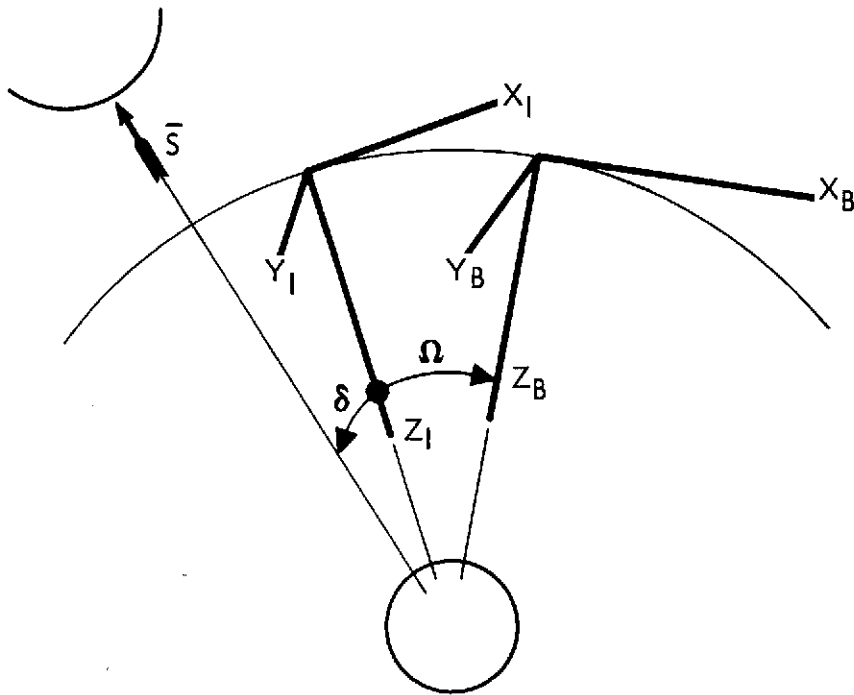


Figure 6A-1. Coordinate Frames and Angle Conventions

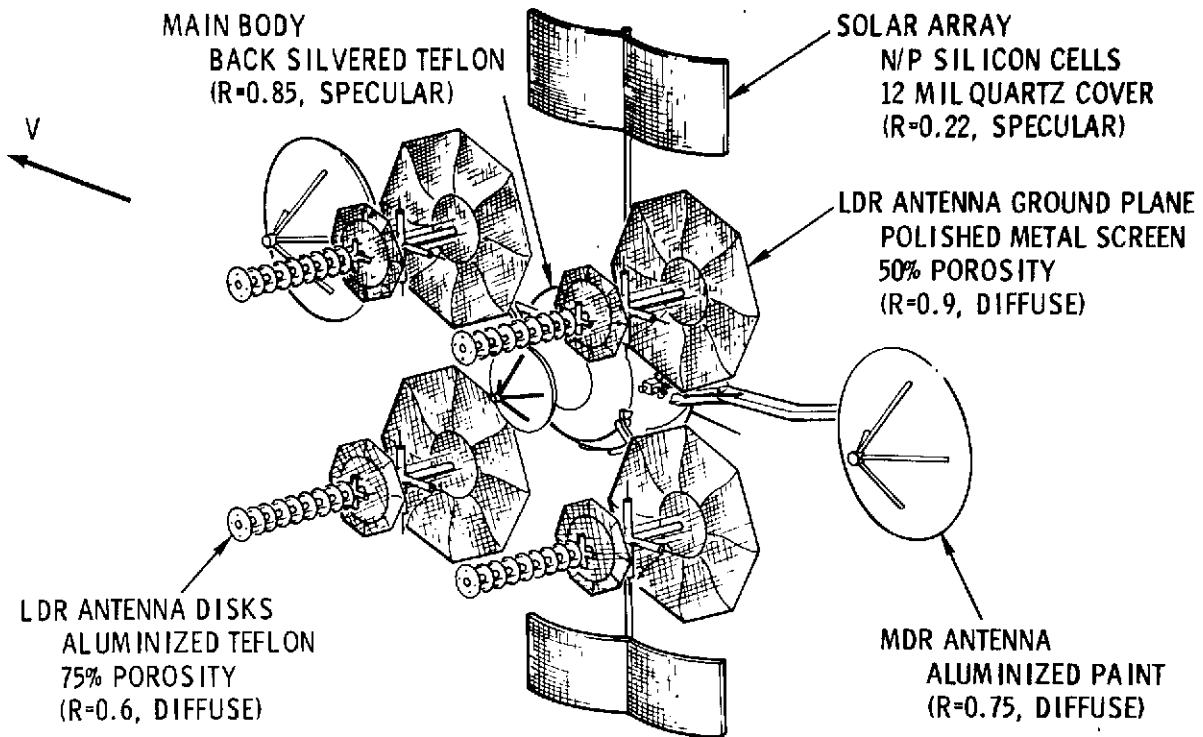


Figure 6A-2. Surface Characteristics for Solar Torque Calculations

CD

Table 6A-1. Projected Surface Characteristics

Element	Areas (Ft ²)			Center of Pressure ^{***} (Ft)			Surface Properties ^{**}		
	Ax	Ay	Az	Xcp	Ycp	Zcp	R	f	a
1. Main Body, Frontal	18.0			0	0	-.17	0.85	1	1
2. Main Body, Side		18.0		0	0	-.17	0.85	1	1
3. Main Body, Top			29.0(-)*	0	0	-2.0	0.85	1	1
4. Main Body, Bottom			29.0(+)	0	0	+1.7	0.85	1	1
5. LDR Antennas, Frontal	2.0			0	0	3.41	0.9	0	0
6. LDR Antennas, Side		2.0		0	0	3.41	0.9	0	0
7. LDR Antennas, Top & Bottom			54	0	0	3.02	0.9	0	0
8. MDR Dish (+X Axis)	6.0			11.5	0	-1.36	0.75	0	0
9. MDR Dish (+X Axis)		6.0		11.5	0	-1.36	0.75	0	0
10. MDR Dish (+X Axis)			33.2	11.5	0	-1.36	0.75	0	0
11. MDR Dish (-X Axis)	6.0			-11.5	0	-1.36	0.75	0	0
12. MDR Dish (-X Axis)		6.0		-11.5	0	-1.36	0.75	0	0
13. MDR Dish (-X Axis)			33.2	-11.5	0	-1.36	0.75	0	0
14. Solar Array	44.0			0	0	-.75	0.22	1	0
15. Solar Arry			44.0	0	0	-.75	0.22	1	0

* Plus and minus denotes illumination on one side of projected area only.

** R = Reflectivity, F = Fraction reflected specularly, a = Fraction of re-emitted radiation.

*** CP distance from nominal CG which is 2.1 ft. forward of separation plane.

6A-4

SD 72-SA-0133

6A.3 DISCUSSION OF RESULTS

Plots of the solar pressure moments (SUM()M) and angular momentum in body coordinates (H()B) were computed for the baseline TDRS and are presented in Figures 6A-3 through 6A-5. Figures 6A-6 through 6A-10 present data for each major spacecraft component. This latter data shows the relative contributions of these components and facilitates extrapolation for future design changes. A summary of the momentum storage and momentum dumping requirements for each of the spacecraft components is given in Table 6A-2.

Disturbance torque analyses of a preliminary spacecraft configuration (not the baseline) indicated the momentum storage requirements are a strong function of the Z location of the center of mass (CM). This configuration initially had a CM to average center of pressure (CP) offset of 1.5 feet in the Z direction. When approximately balanced the momentum storage requirements were reduced by an order of magnitude. With the present baseline configuration ($Z_{cg} = 25$ in.) the balance is near perfect with less than 0.3 inches between the Z_{cg} CM and average CP. This low value is less than the tolerance associated with the solar pressure analysis methods, assumptions and data and an unbalance of 6 inches was assumed in the analysis. The data for this case is denoted $Z_{cg} = 19$ inches in the curves and Table 6A-2 and is used for the momentum storage sizing.

Table 6A-2. Momentum Requirements
 Due to Solar Pressure Torques (~ Ft Lb Sec)

Maximum Cyclical Variation Per Orbit			Secular Growth Per Orbit*	Configuration
$\pm \Delta H_{XB}$	$\pm \Delta H_{YB}$	$\pm \Delta H_{ZB}$	ΔH_{XB}	
.020	.036	.015	-.012	Total S/C Nominal S/C ($Z_{cg}=25''$ & $Y_{cg}=0$) (Figure 6A-3) S/C with $Z_{cg} = 19''$ & $Y_{cg} = 0$ (Figure 6A-4) S/C with $Z_{cg} = 19''$, $Y_{cg} = 0.6''$ (Momentum Storage Design Condition, Figure 6A-5)
.041	.077	.031	-.012	
.076	.077	.058	-.092	
.009	.013	.0062	-.012	S/C Components Main Body (Figure 6A-6) LDR Antenna (Figure 6A-7) MDR Antenna (Figure 6A-8) Delta Due To MDR Ant. "Windmilling" (Figure 6A-9) Solar Arrays (Figure 6A-10) Design Values**
.068	.136	.052	0	
.026	.054	.022	0	
.050	.084	.052	0	
.0053	.019	.0052	0	
.126	.161	.110	-.092	

*Secular ΔH_{YB} and $\Delta H_{ZB} = 0$

**Sum of total S/C + delta due to "windmilling"

SOLAR PRESSURE DISTURBANCE TORQUES ON TDRS
(Baseline S/C, $Z_{CG} = 25''$, $Y_{CG} = 0$)

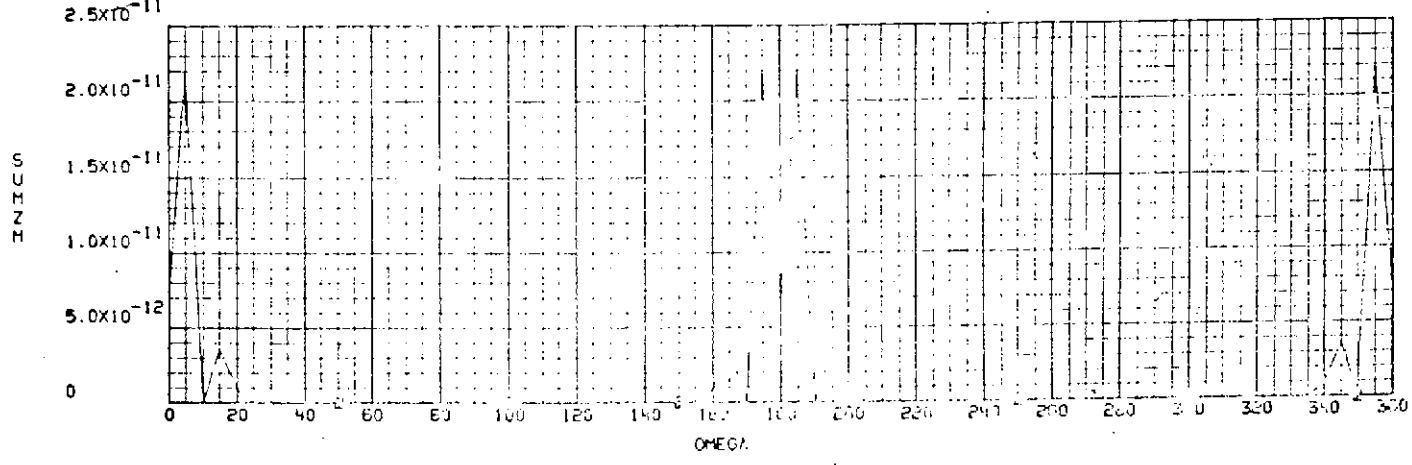
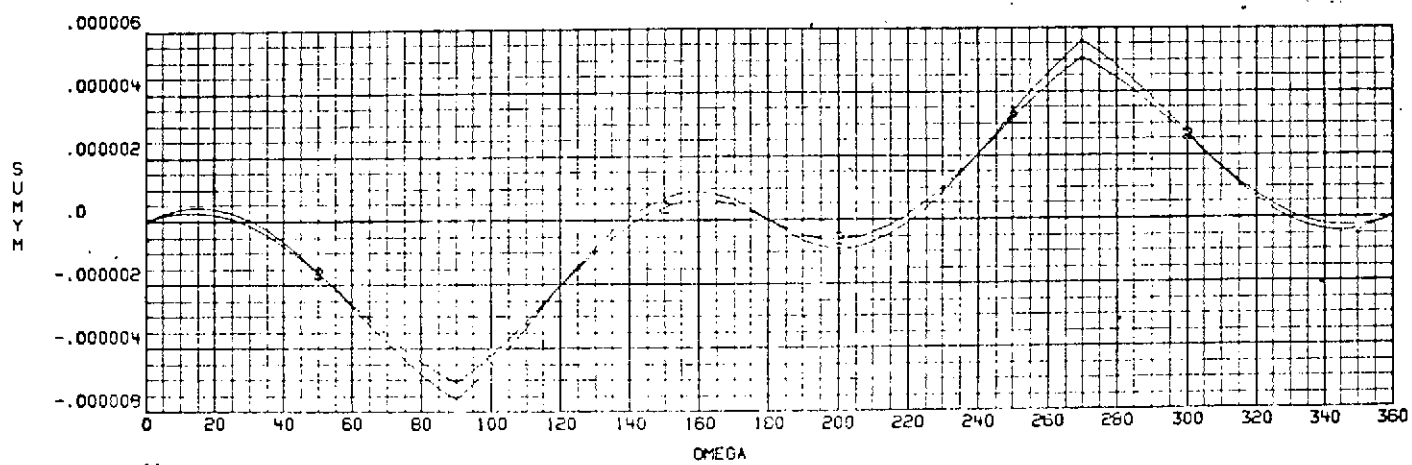
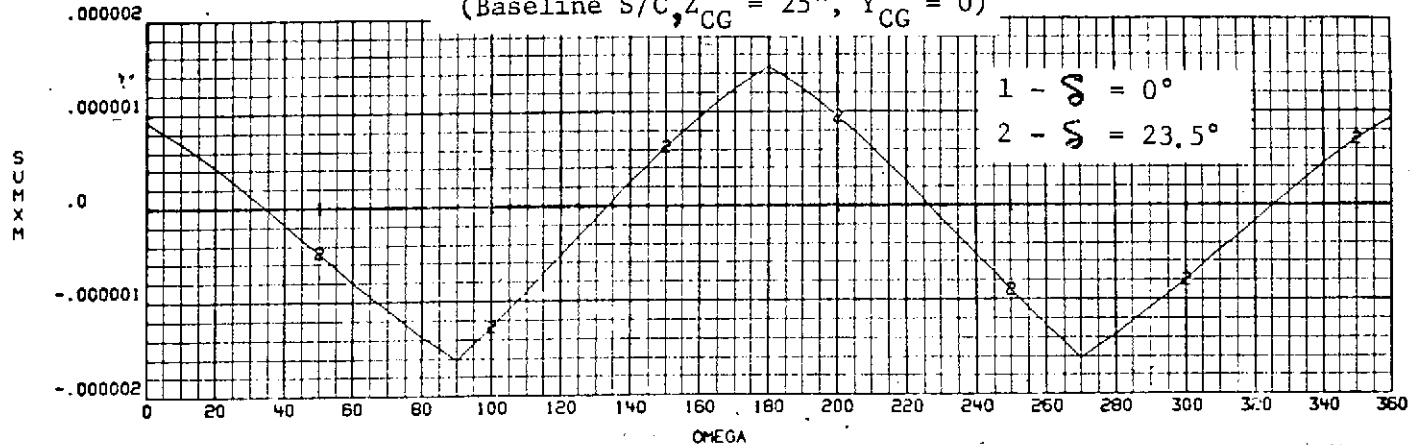


Figure 6A-3a. Solar Pressure Disturbance Torques on TDRS
(Baseline S/C $Z_{CG} = 25$ In., $Y_{CG} = 0$)

410237-03
062672-000

SOLAR PRESSURE DISTURBANCE TORQUES ON TDRS
(Baseline S/C, $Z_{CG} = 25''$, $Y_{CG} = 0$)

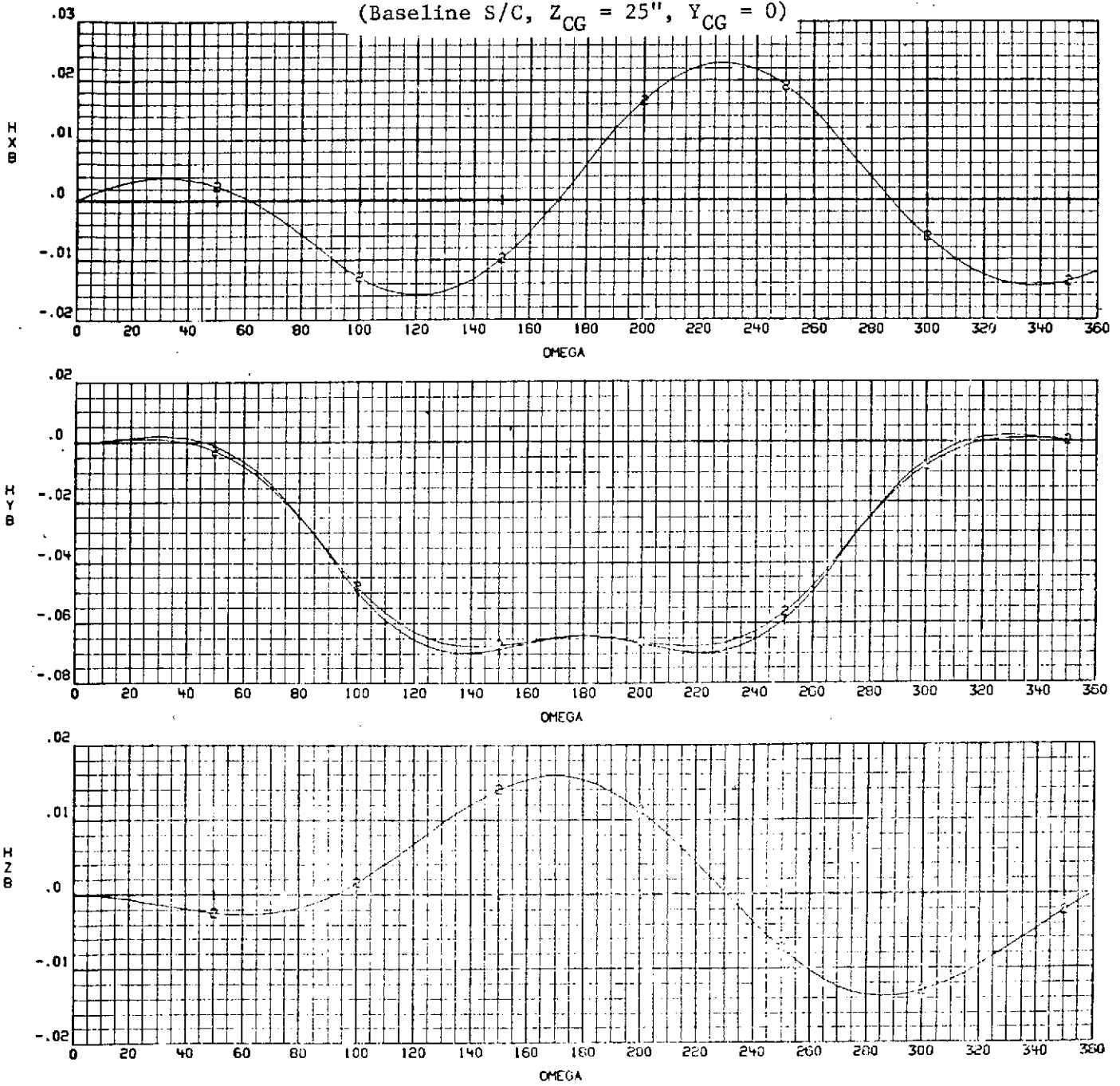


Figure 6A-3b. Solar Pressure Disturbance Torques on TDRS
(Baseline S/C $Z_{CG} = 25$ In., $Y_{CG} = 0$)

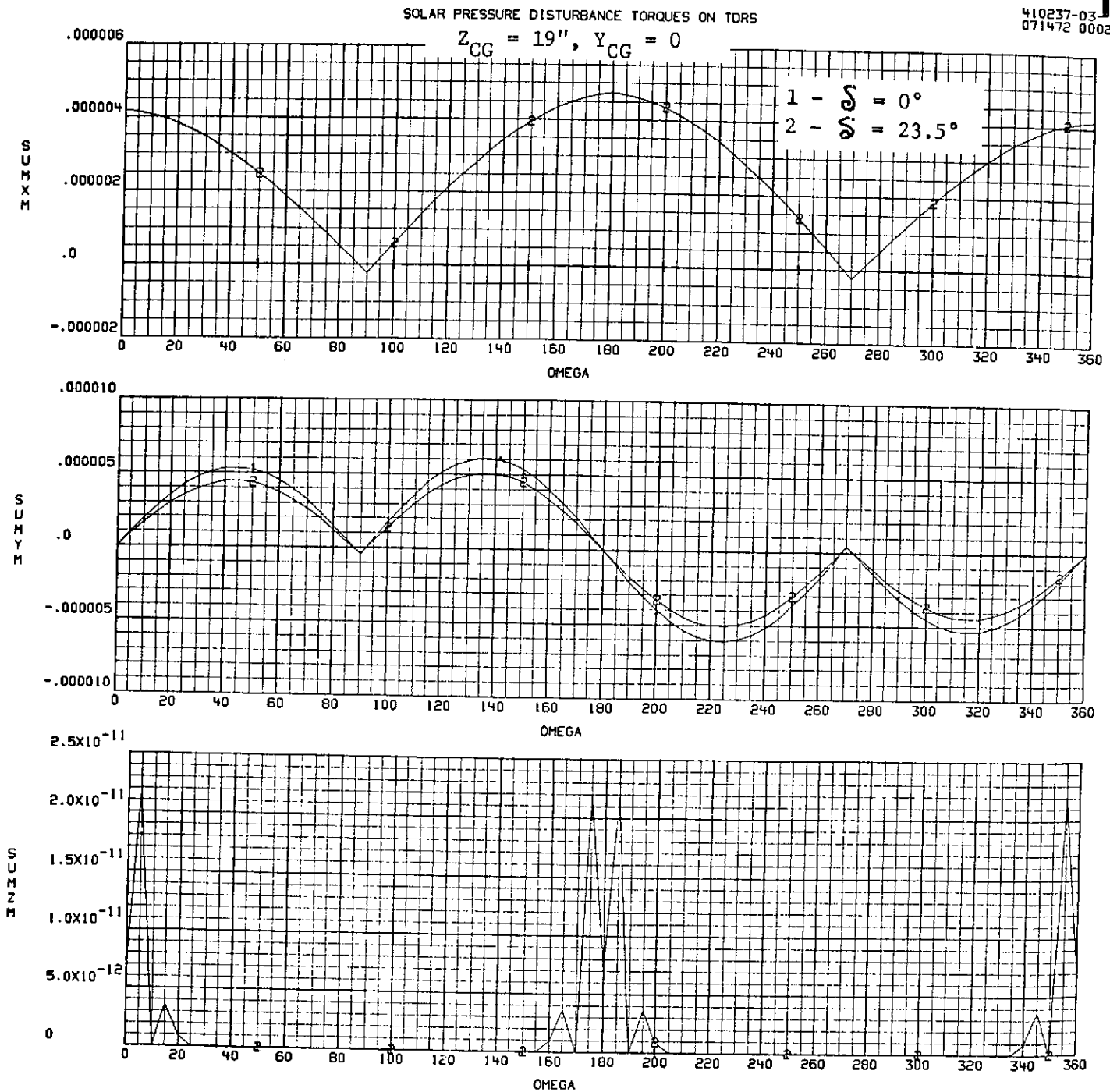


Figure 6A-4a. Solar Pressure Disturbance Torques on TDRS ($Z_{CG} = 19$ In., $Y_{CG} = 0$)

SOLAR PRESSURE DISTURBANCE TORQUES ON TDRS

$Z_{CG} = 19''$, $Y_{CG} = 0$

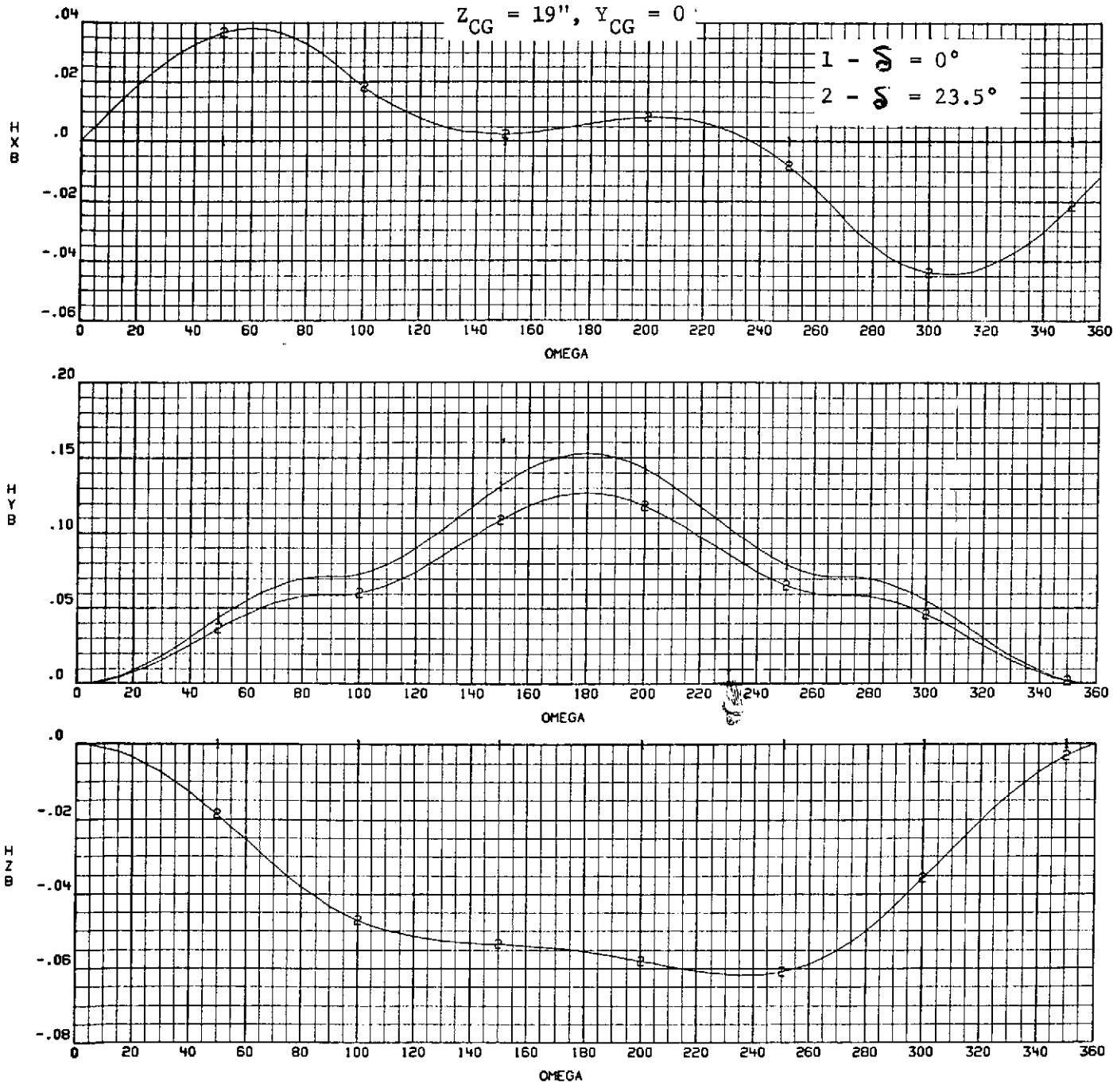


Figure 6A-4b. Solar Pressure Disturbance Torques on TDRS ($Z_{CG} = 19$ In., $Y_{CG} = 0$)

SOLAR PRESSURE DISTURBANCE TORQUES ON TDRS
 $Z_{CG} = 19''$, $Y_{CG} = 0.6''$ (Design Condition)

410237-03
 071472 0006

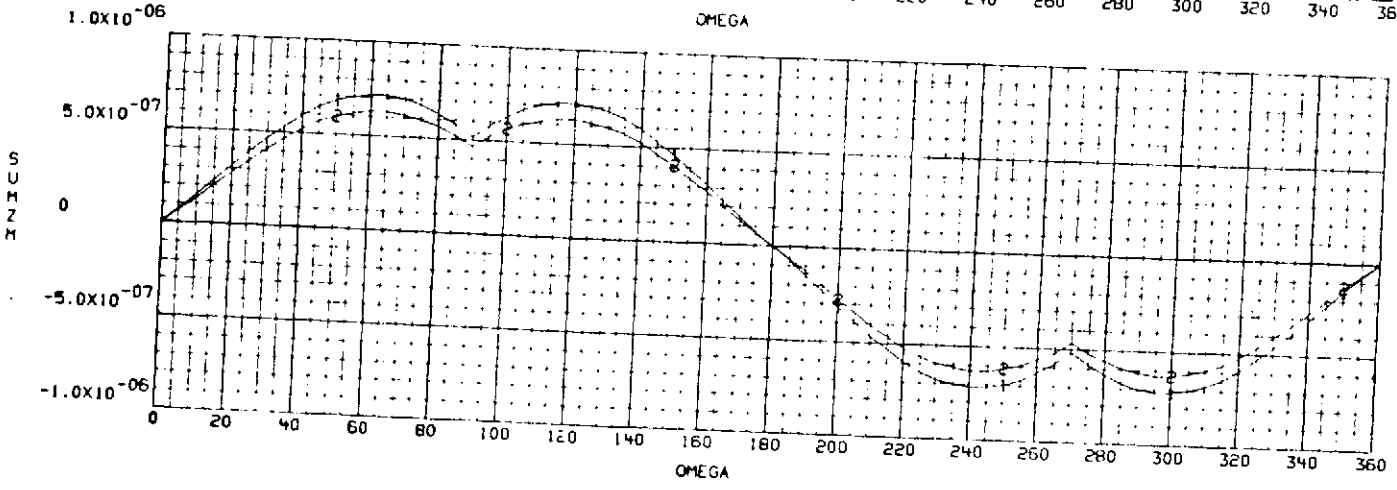
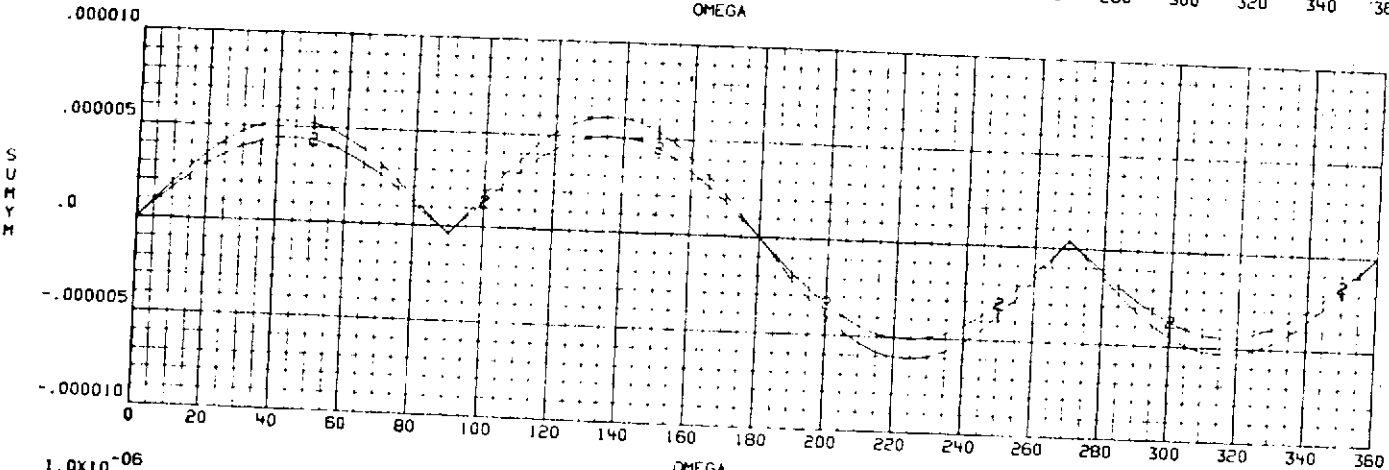
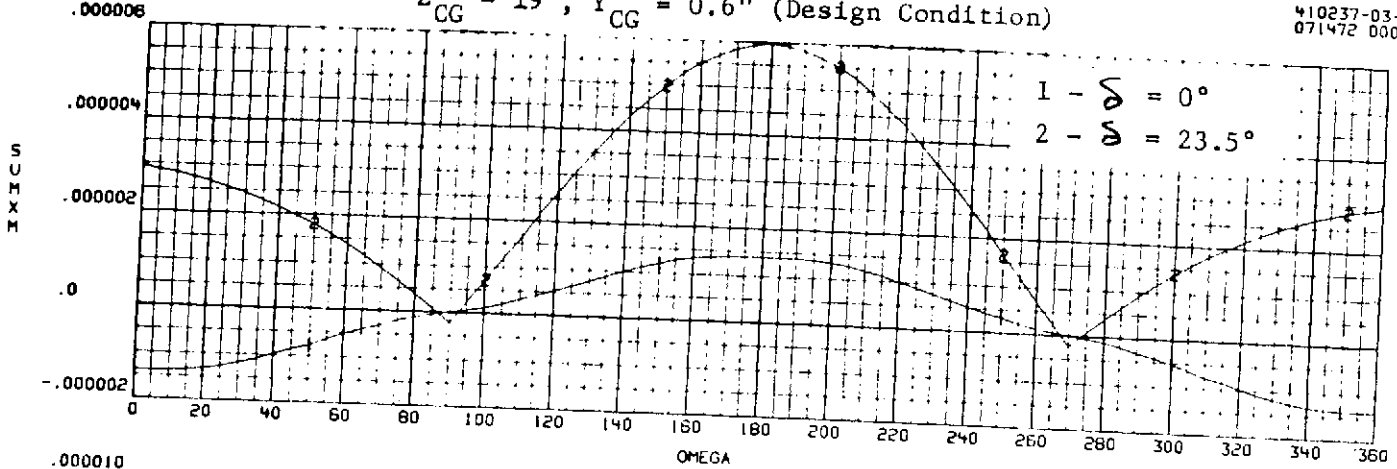


Figure 6A-5a. Solar Pressure Disturbance Torques on TDRS ($Z_{CG} = 19$ In., $Y_{CG} = 0.6$ In.) (Design Conditions)

SOLAR PRESSURE DISTURBANCE TORQUES ON TDRS

410237-03
071472 00

$Z_{CG} = 19''$, $Y_{CG} = 0.6''$ (Design Condition)

- 1 - $\delta = 0^\circ$
- 2 - $\delta = 23.5^\circ$

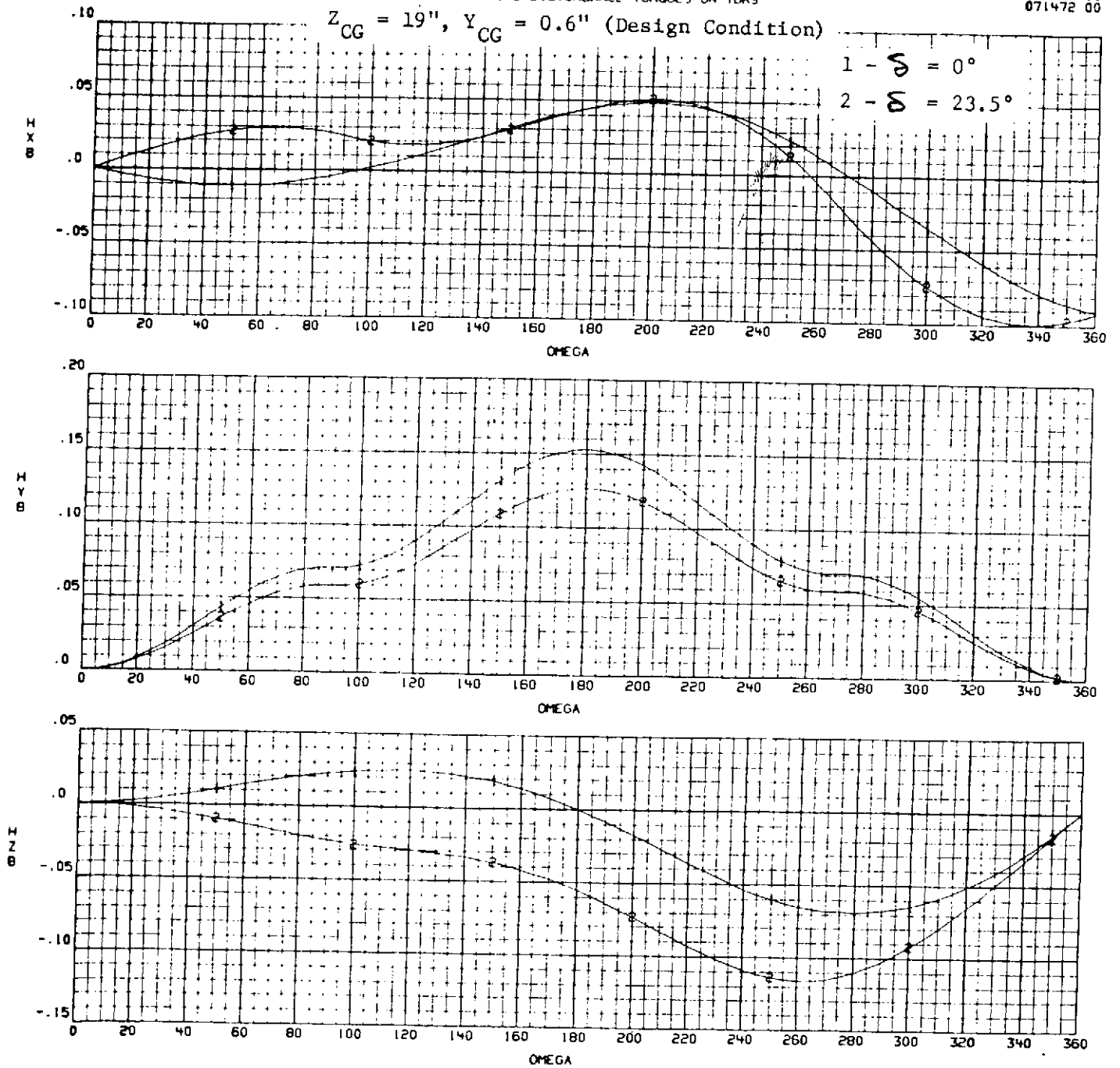


Figure 6A-5b. Solar Pressure Disturbance Torques on TDRS ($Z_{CG} = 19$ In., $Y_{CG} = 0.6$ In.) (Design Conditions)

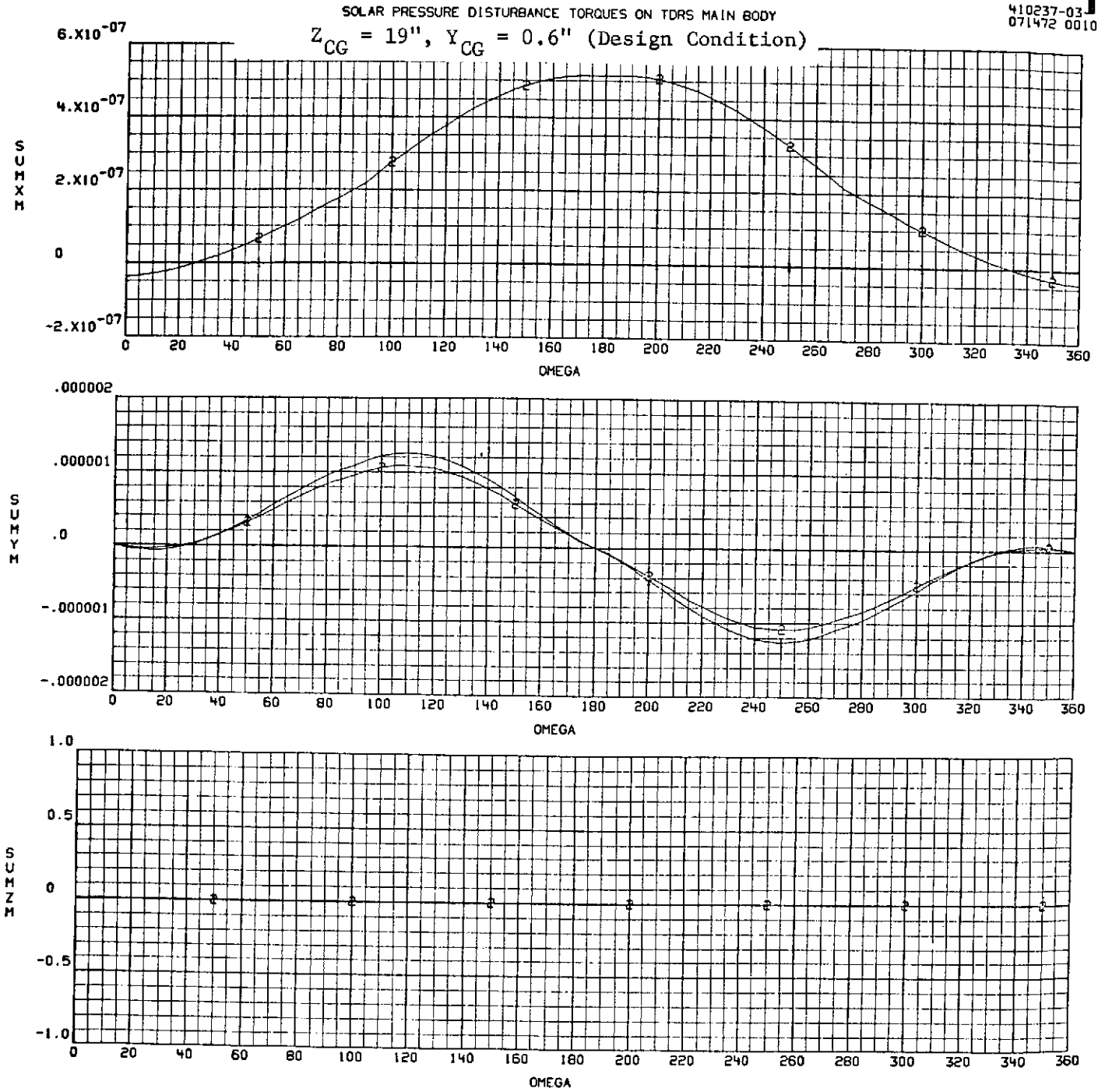


Figure 6A-6a. Solar Pressure Disturbance Torques on TDRS Main Body
 $Z_{CG} = 19$ In., $Y_{CG} = 0.6$ In. (Design Condition)

SOLAR PRESSURE DISTURBANCE TORQUES ON TDRS MAIN BODY

410237-03-
071472 0012

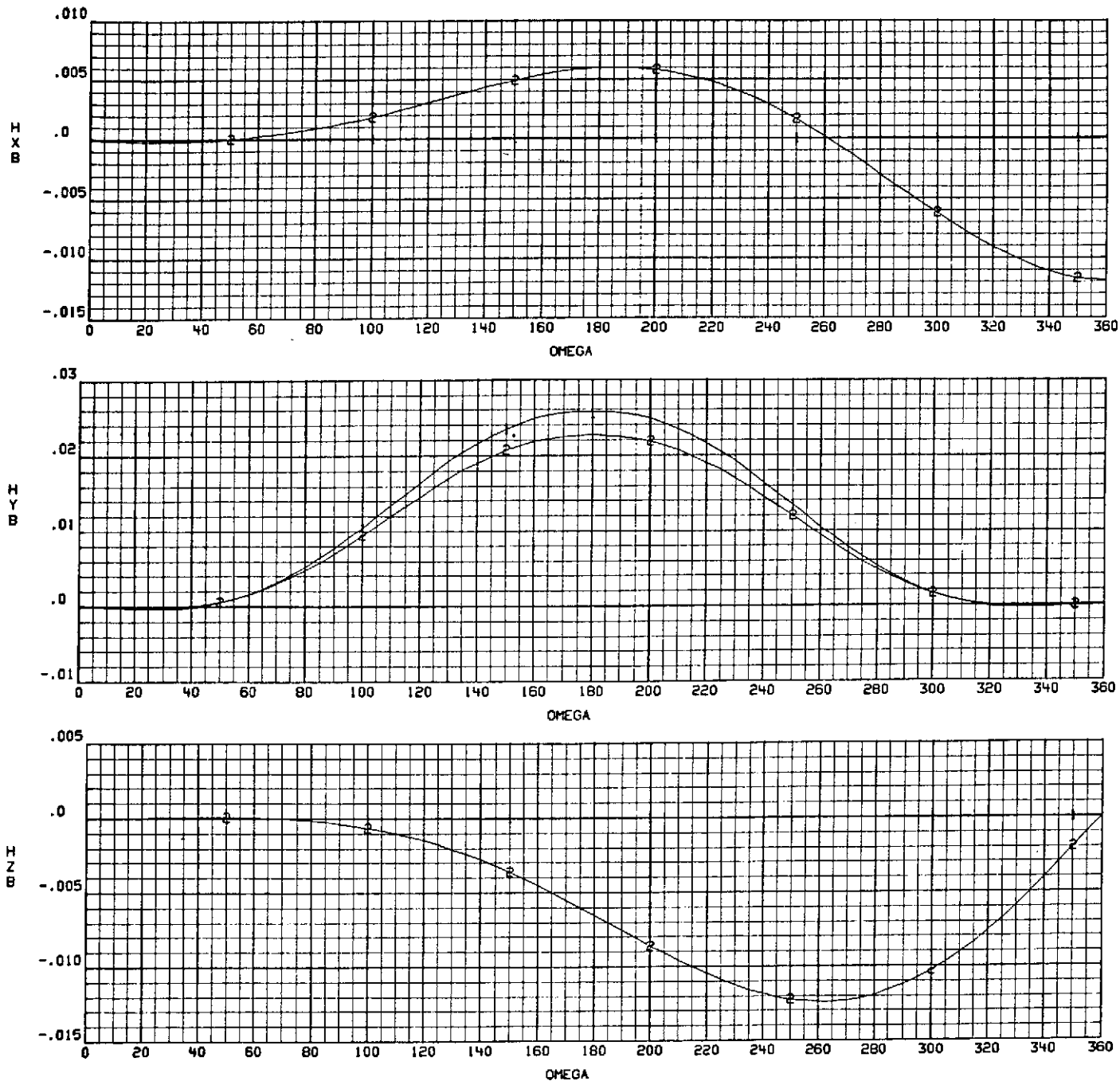


Figure 6A-6b. Solar Pressure Disturbance Torques on TDRS Main Body
 $Z_{CG} = 19$ In., $Y_{CG} = 0.6$ In. (Design Condition)

SOLAR PRESSURE DISTURBANCE TORQUES ON TDRS LDR ANTENNA

410237-03-
071472 0014

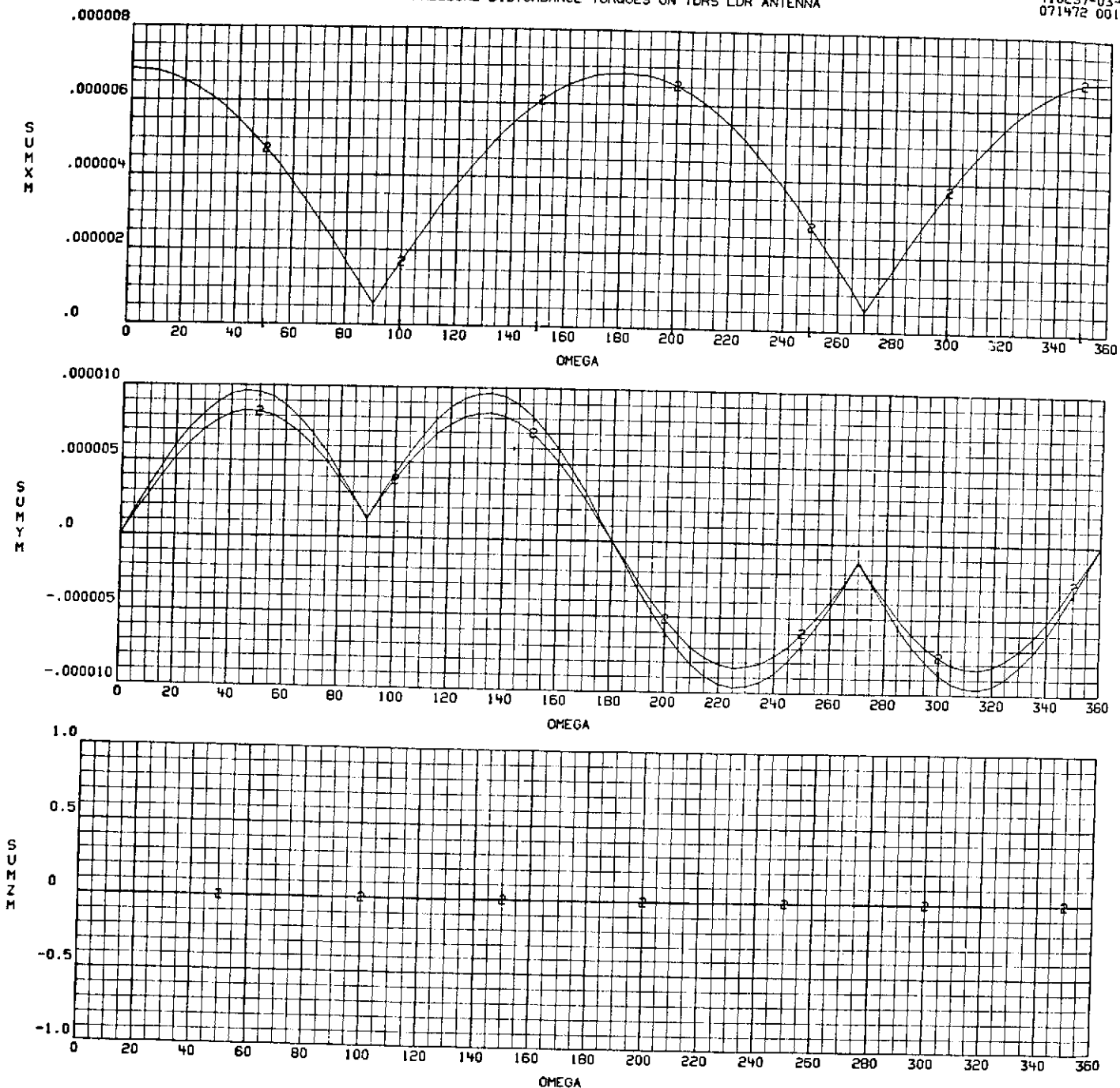


Figure 6A-7a. Solar Pressure Disturbance Torques on TDRS LDR Antenna

SOLAR PRESSURE DISTURBANCE TORQUES ON TDRS LDR ANTENNA

410237-03
071472 0016

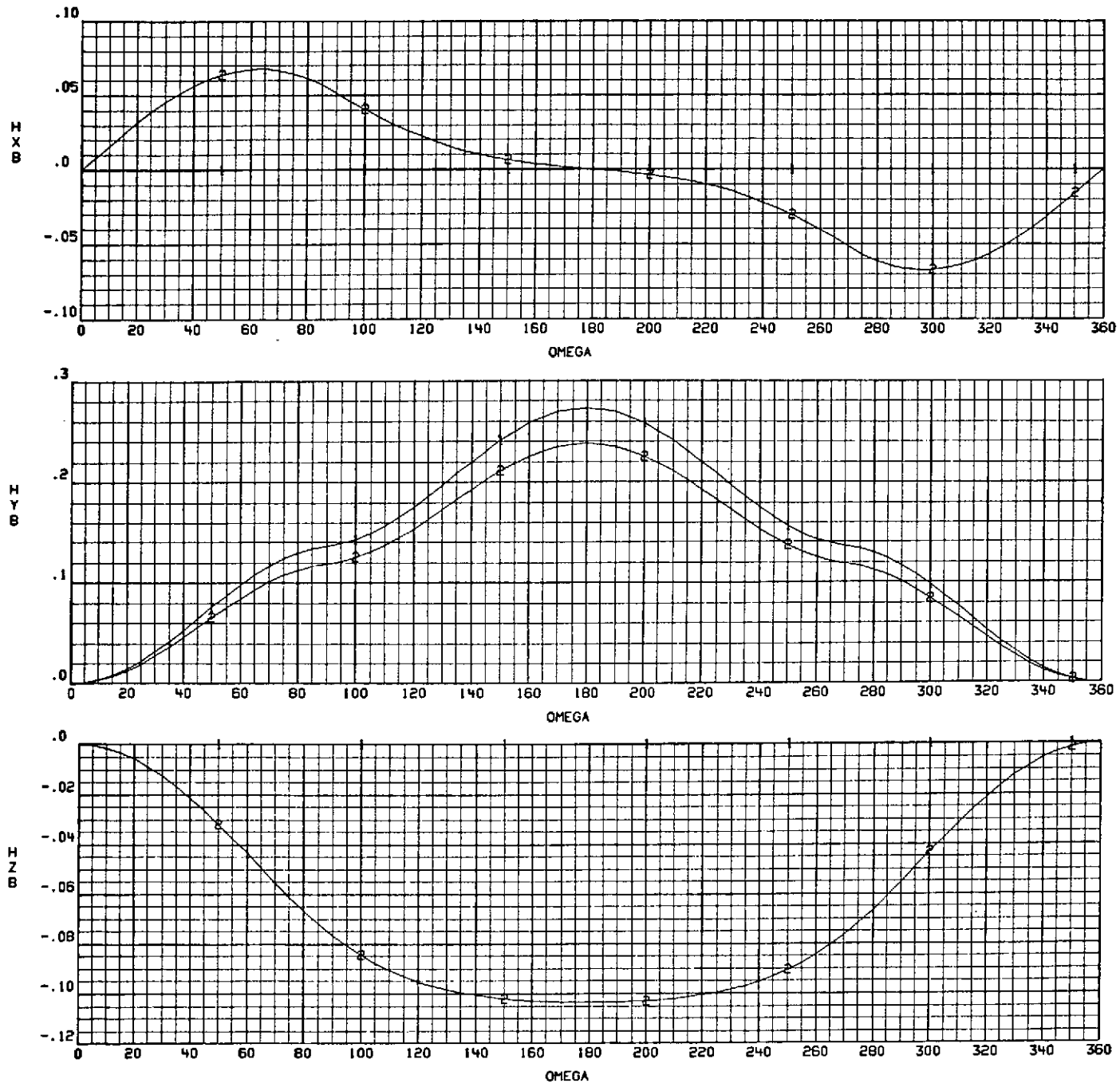


Figure 6A-7b. Solar Pressure Disturbance Torques on TDRS LDR Antenna

SD 72-SA-0133

SOLAR PRESSURE DISTURBANCE TORQUES ON TDRS MDR ANTENNAS

410237-03
071472 0022

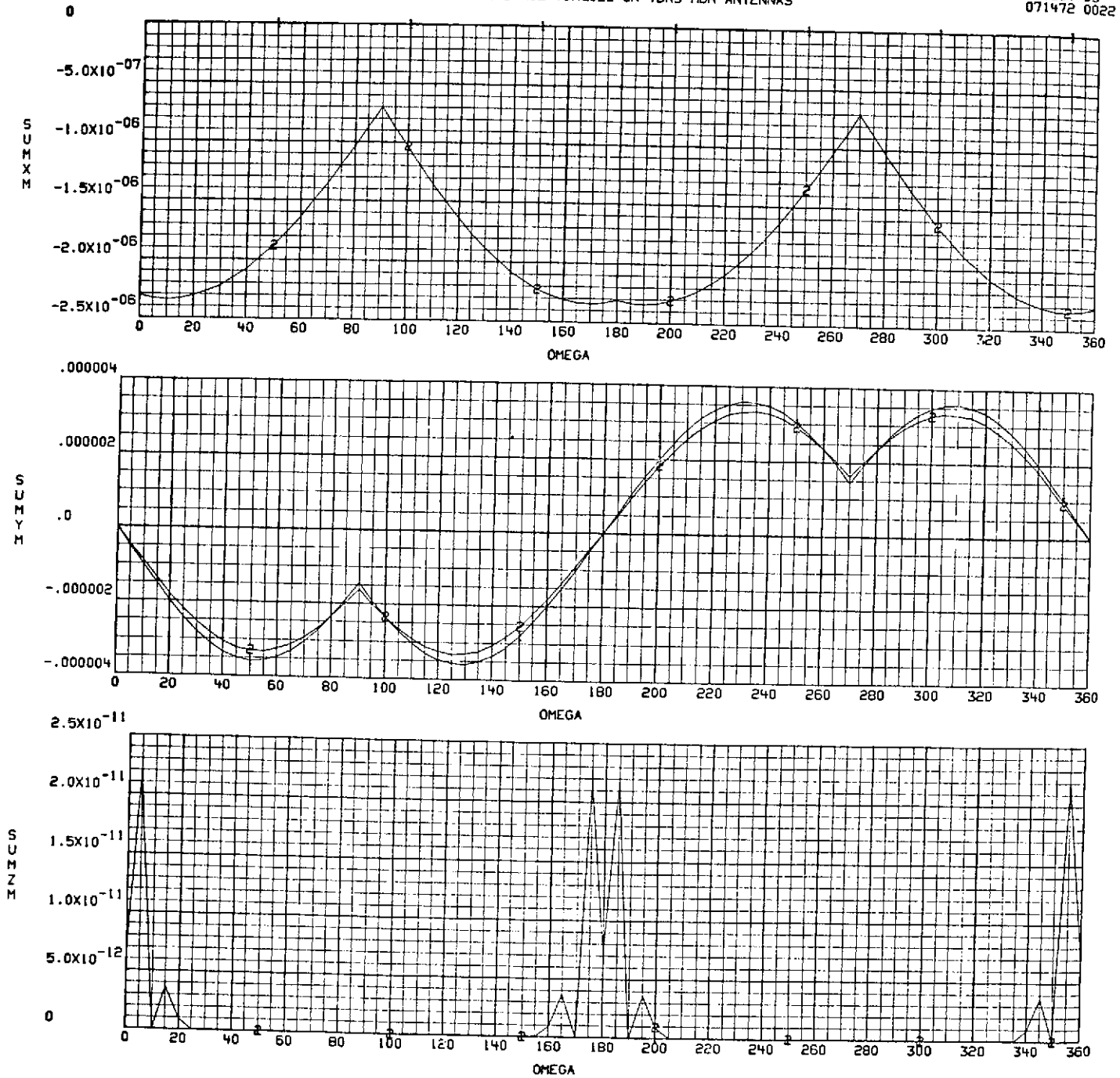


Figure 6A-8a. Solar Pressure Disturbance Torques on TDRS MDR Antenna

SOLAR PRESSURE DISTURBANCE TORQUES ON TDRS MDR ANTENNAS

410237-03
071472 0024

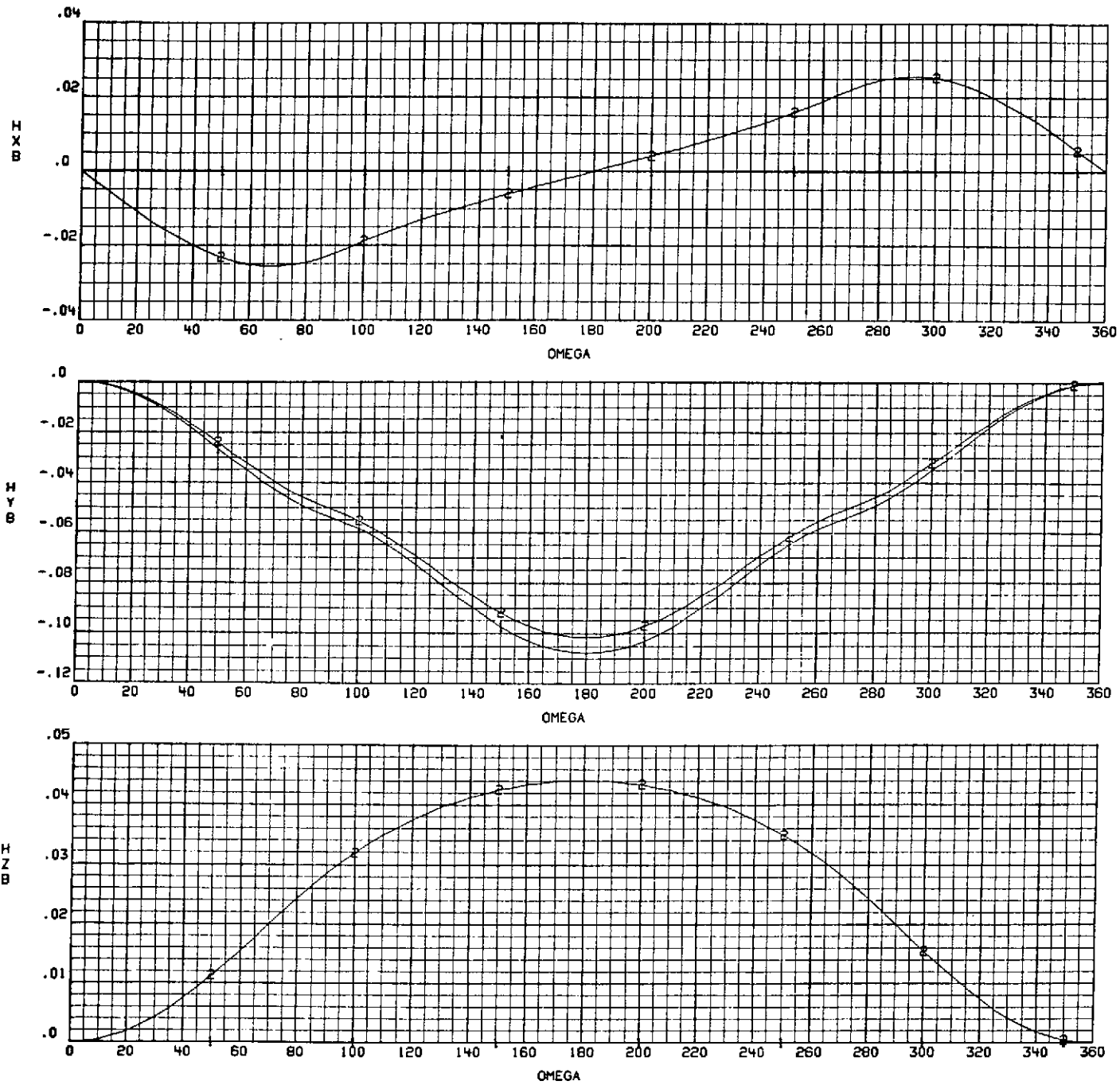


Figure 6A-8b. Solar Pressure Disturbance Torques on TDRS MDR Antenna

SOLAR PRESSURE DISTURBANCE TORQUES ON TDRS MDR ANTENNAS (WITH "WINDMILLING")
 (BASELINE S/C)

10237-03
 60272 0014

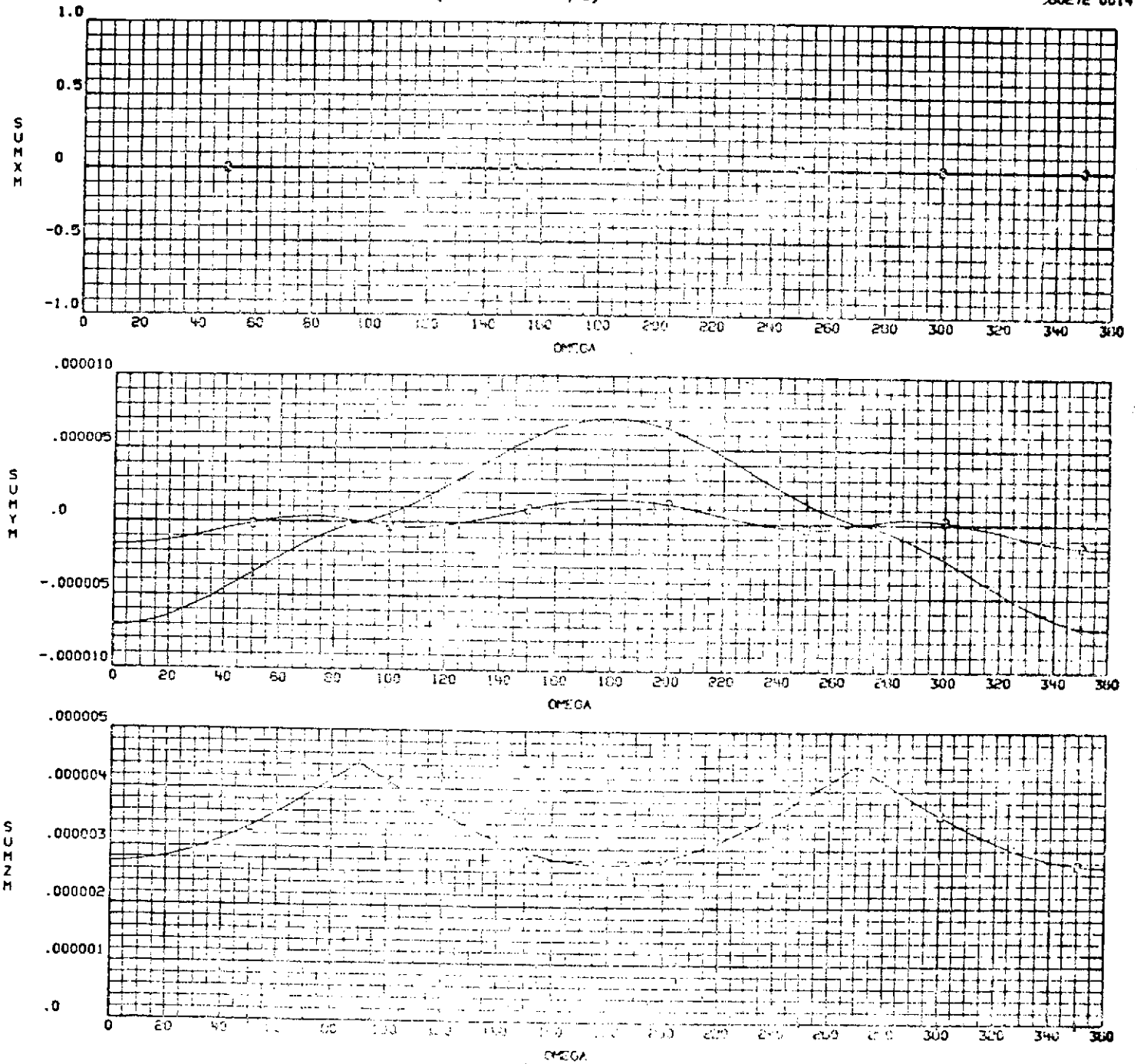


Figure 6A-9a. Solar Pressure Disturbance Torques on TDRS MDR Antenna (With Windmilling)
 (Baseline S/C)

SOLAR PRESSURE DISTURBANCE TORQUES ON TDRS MDR ANTENNAS (WITH "WINDMILLING")
 (BASELINE S/C)

77-93
72-0016

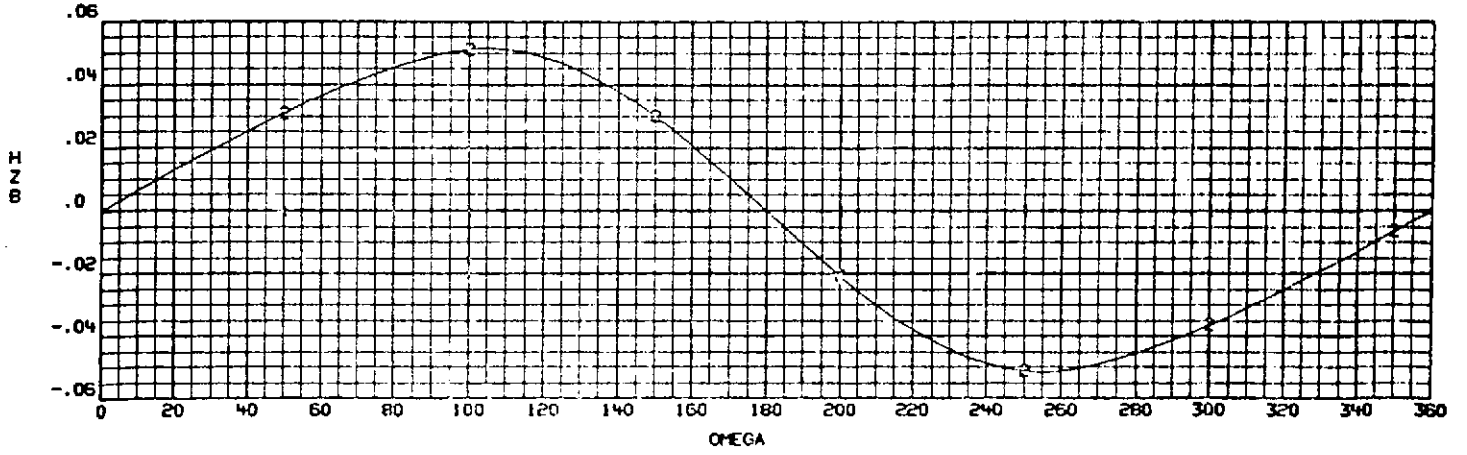
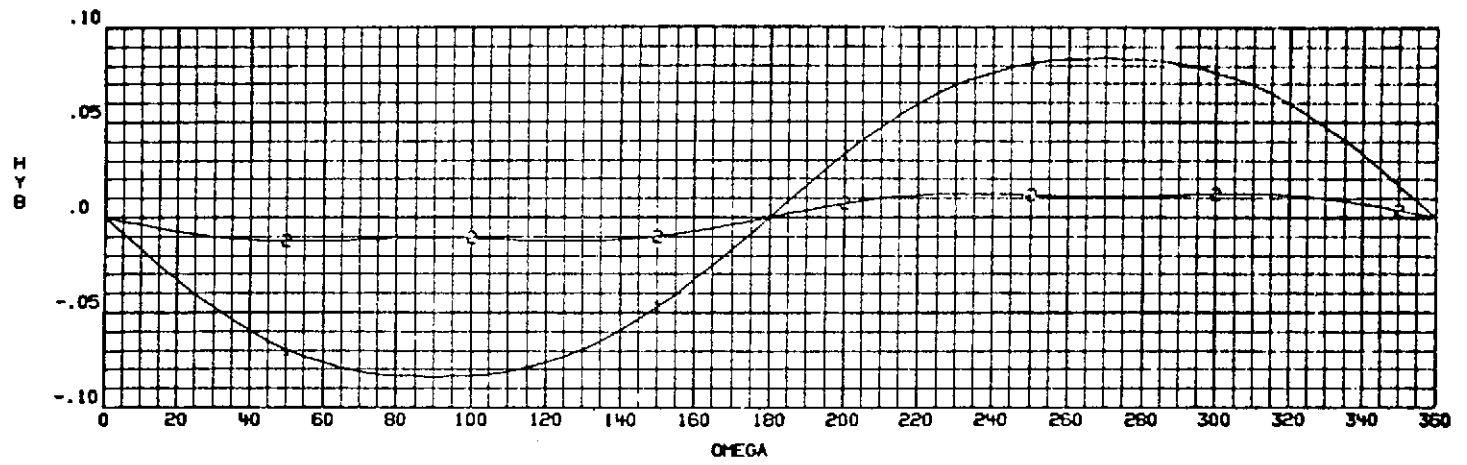
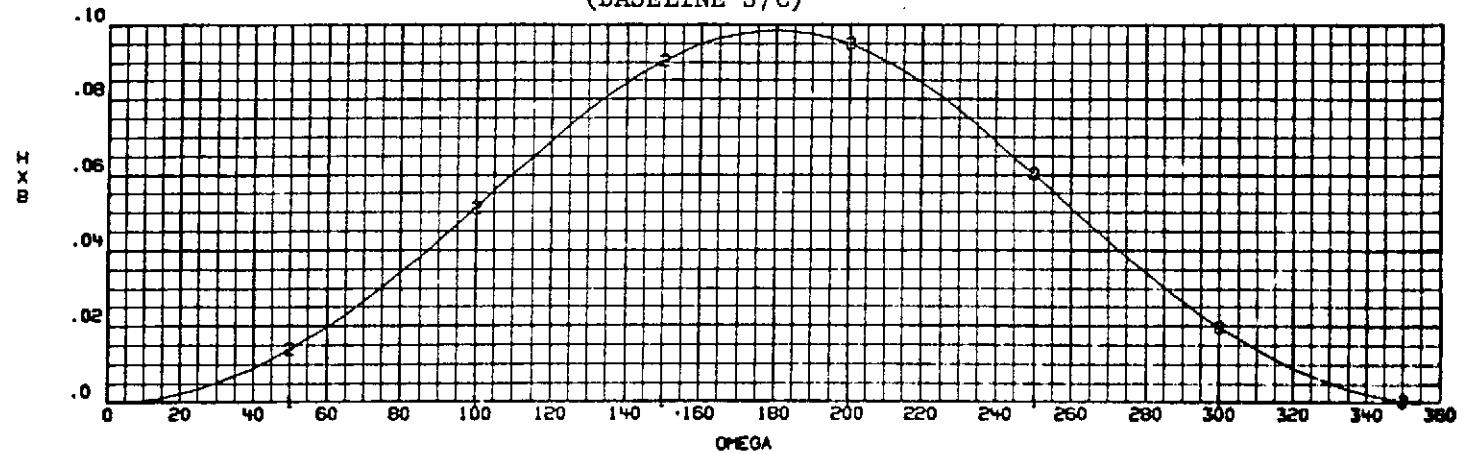


Figure 6A-9b. Solar Pressure Disturbance Torques on TDRS MDR Antenna (With Windmilling)
 (Baseline S/C)

SOLAR PRESSURE DISTURBANCE TORQUES ON TDRS SOLAR ARRAY

410237-03-
071472 0018

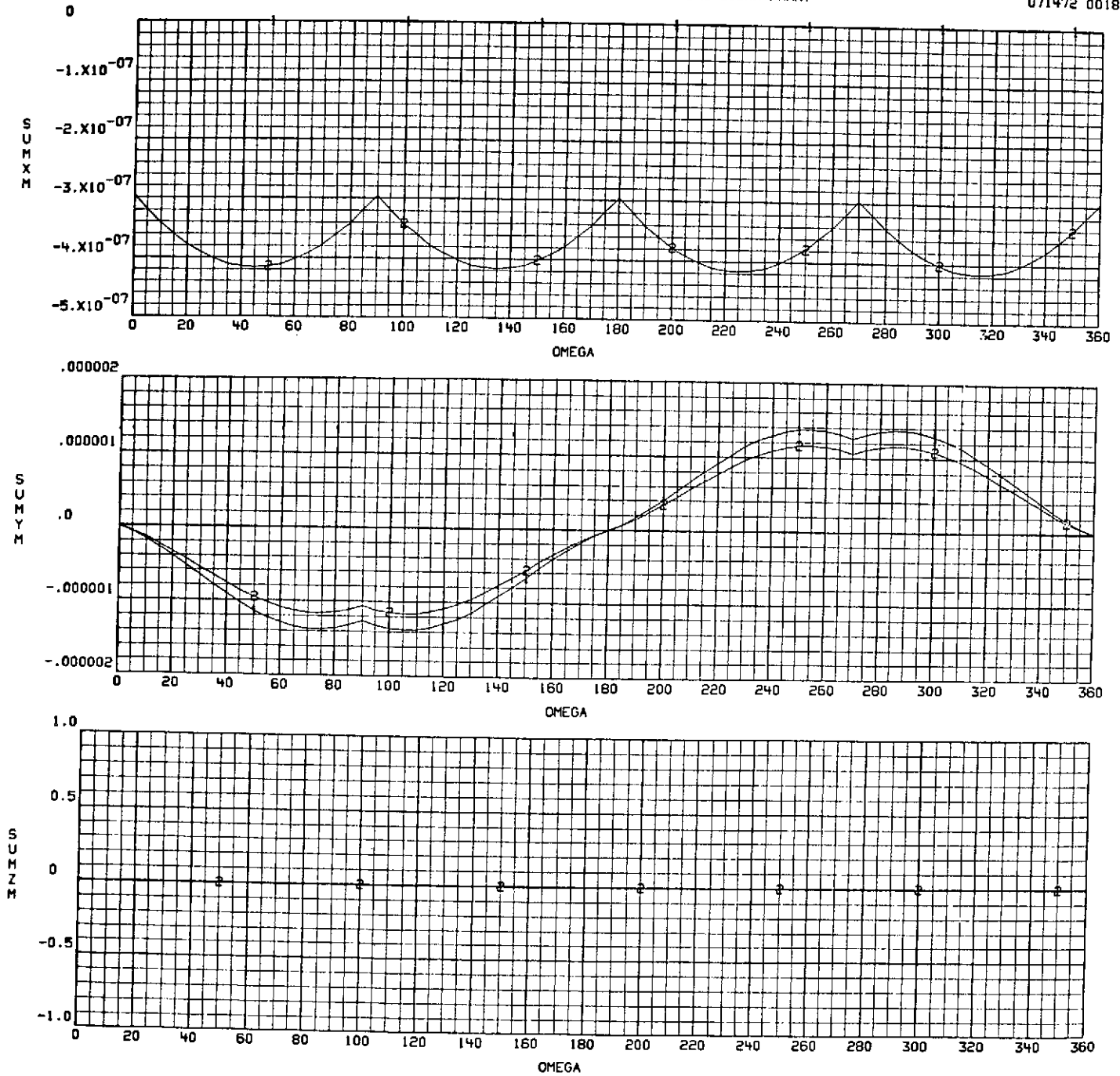


Figure 6A-10a. Solar Pressure Disturbance Torques on TDRS Solar Array

SD 72-SA-0133

SOLAR PRESSURE DISTURBANCE TORQUES ON TDRS SOLAR ARRAY

410237-03
071472 0020

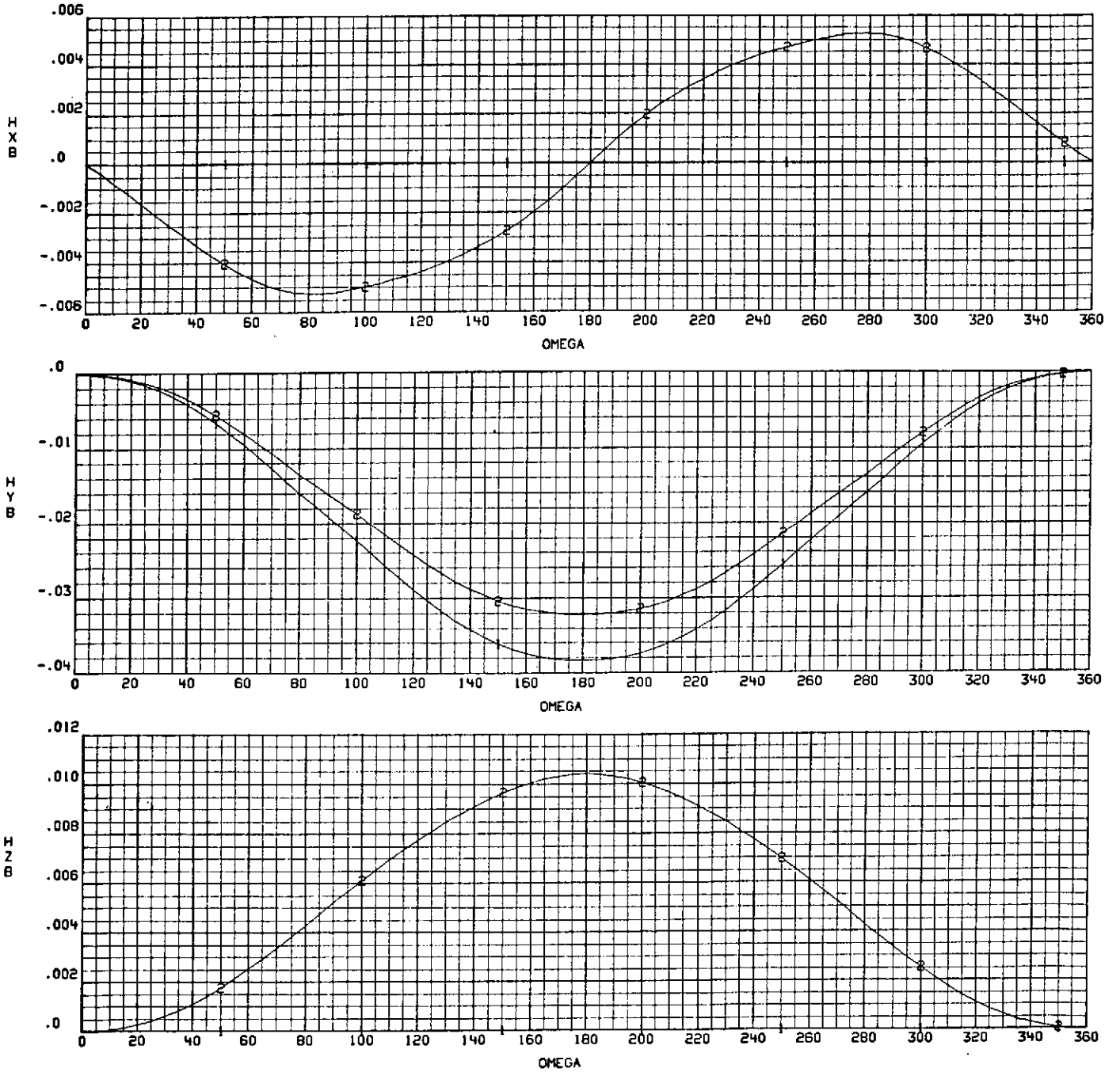


Figure 6A-10b. Solar Pressure Disturbance Torques on TDRS Solar Array

SD 72-SA-0133

To assess the effects of non-symmetrical MDR antenna gimbal deflections a "windmilling" configuration was devised. The run simulates one antenna with zero gimbal angles and the other with 28 degrees of roll gimbal deflection for an entire orbit. This is an extremely conservative assumption. The data in Figure 6A-9 and Table 6A-2 demonstrates that this windmilling effect is quite significant and must be considered in the momentum storage sizing.

To establish the momentum storage capacity necessary to accommodate the solar pressure torques the delta due to antenna "windmilling" is added to the momentum storage design case yielding:

$$\Delta H_x = 0.126 \text{ Ft. Lb. Sec.}$$

$$\Delta H_y = 0.161 \text{ Ft. Lb. Sec.}$$

$$\Delta H_z = 0.110 \text{ Ft. Lb. Sec.}$$

It is desirable to balance solar pressure effects as the S/C design progresses. A review of Table 6A-1 indicates that the Z axis CP location can be controlled very effectively by controlling the Z axis location of the solar arrays, the MDR antennas, and the LDR antennas. In addition, the porosity of the LDR antennas can be adjusted for effective CP control.

The data of Figures 6A-4 and 5 and Table 6A-2 indicate the CG to CP distance in the Y_B direction is the dominant factor in the secular momentum growth. In the momentum management it is operationally desirable to dump momentum as infrequently as possible. Therefore the $(Y_{cm} - Y_{cg})$ dimension should be minimized. This can be accomplished by:

1. Maintaining S/C Symmetry in the Y dimension
2. Tight CG control
3. Minimize misalignment and thermal deformation of the structure.

6A.4 REFERENCES

1. "Disturbance Analysis for the Aeronautical Satellite,"
IL 190-320-S&C-69-26, 30 April 1969, J. A. Hill
2. "Effects of Solar Radiation Pressure Upon Satellite
Attitude Control," R. J. McElvain, Paper 1918-61,
American Rocket Society Conference on Guidance,
Control and Navigation, Stanford Univ., 7-9 August 1961
3. "Angular Momentum Requirements for Spacecraft Control
Systems," E. J. Knobbe, Stabilization and Control
TN 67-5, 26 Dec. 1967
4. "Spacecraft Radiation Torques," NASA SP-8027,
Oct. 1969
5. "Mathematical Model of the Solar Radiation Force &
Torques Acting on the Components of a Spacecraft,"
R. M. Geogevic, Technical Memo 33-494, Jet Propulsion
Laboratory, Pasadena, Calif., 1 Oct. 1961
6. "Torques & Attitude Sensing in Earth Satellite,"
S. F. Singer, Academic Press, 1964. Chapter 5,
Radiation Disturbance Torques on Satellites Having
Complex Geometry, by W. J. Evans.
7. "Solar Pressure Disturbance Torque and Momentum Storage
Requirements Analysis Program", R. E. Oglevie, I.L.
192-506-72-027, 13 June 1972

APPENDIX 6B. EFFECT OF PROPELLANT MOTION ON NUTATION STABILITY DURING SPIN

Spin stabilization during transfer orbit and apogee motor firing is attractive for small spacecraft launched into synchronous orbit. The NR concept for the TDRS utilizes this technique. Booster packaging constraints require the spin axis to be a minor axis of inertia which causes an unstable divergence of the spin axis in the presence of energy dissipation (\dot{E}). The design approach taken is to minimize \dot{E} to keep the rate of divergence at an acceptable level. The unpredicted stability problem incurred during the ATS-V mission (see Reference i) motivated improved analysis techniques and a more thorough understanding of the mechanisms which produces \dot{E} .

Energy dissipation results from nutation induced mechanical vibration and propellant sloshing. Analyses such as those presented in Reference (a) show that careful engineering can reduce the \dot{E} from mechanical sources to negligible proportions causing propellant sloshing to be the dominant \dot{E} source. The analysis herein is based on a fluid "slug" propellant model. The validity of this model and its applicability to the specific TDRS problem are discussed.

6B.1 SLOSH MODEL

The fluid "slug" model was selected for the analysis of the sloshing in spherical tanks. The stability analysis is performed using the "energy sink" method. In this approach the fluid is represented as a rigid spherical segment with viscous interaction between the rigid body and the tank wall. The model was developed by Mr. V. Baddeley of NR (Reference b). Except for minor differences in the equation coefficients the model can be reduced to the full tank model developed by Vanyo (Reference c) and the half-filled Williams model (Reference a). For a full tank the model has been found to correlate well with test data (Reference d). The spherical tank test results of Reference (e) provide physical substantiation of the validity of the slug model for spherical tanks in the Intelsat IV nutation environment. Also the slug model correlates well with the classical modal model (particle model) (Reference b) which correlates well with test data (Reference f) for fill ratios from zero to half full. The model, therefore, appears to be valid for typical S/C if the remaining assumptions are made:

1. The membrane positive expulsion bladders used in the tanks impose no tangential or shear forces on the fluid such that the fluid motion still behaves as a slug.
2. The internal ridges about the circumference of the tanks are small and will not distort the fluid motion significantly.

Unfortunately no models or analyses are known which permit the analytical treatment of the problem without the above assumptions. The practical implications of the latter two assumptions and means of assessing their

impact are discussed in section 6B-3. Under the above assumptions the model appears well suited to the problem. The physical constraints employed in the calculations are presented in Table 6B-1.

6B.2 DISCUSSION OF RESULTS

The results of the analysis are presented in Figures 6B-1 and 6B-2. The propellant weight as a function of fill height (h) and fill ratio (f) is given in Figure 6B-3.

The effect of inertia ratio I_r/I_t on the nutation divergence time constant is presented in Figure 6B-1 which shows the time constant improves (gets larger) as I_r/I_t approaches one. This is due to the decreasing nutation (or excitation) frequency that also occurs as I_r/I_t approaches unity. Considerations such as mass balancing accuracies and control limit how close the unity inertia ratio may be approached in practice.

The effect of various fill ratios is presented in Figure 6B-2. The data is for an $I_r/I_t = 0.9$ which is at the low end of the expected value range of this parameter. The shortest time constant is for the full tank but this time constant is still very acceptable (13.5 hours). Also an anti-resonance occurs for a fill ratio of 0.88. Physically, this occurs when the translational forces on the fluid cause it to rotate exactly in phase with the spacecraft nutational motion. For the maximum nominal fill ratio currently utilized ($f_{Max} = 0.57$) the nutation divergence time constant is always greater than 89 hours. Thus the de-stabilizing influences of propellant sloshing are relatively small in the anticipated parameter region predicated on the above assumptions.

6B.3 PRACTICAL CONSIDERATIONS

The propellant slosh tests run for Intelsat IV (Reference e) demonstrate that minor changes from the basic spherical tank shape (sphere to cono-spheroid) produced an order of magnitude increase in E. The tanks selected for the TDRS are currently being developed for the Canadian Technology Satellite (CTS) and are spherical with positive expulsion diaphragms and have a small internal circumferential ridge between the two tank halves. The effect of the bladders and the ridges is assumed to be negligible in the analysis results presented above. These assumptions should be verified at some point. Although no previously flown minor axis spin stabilized spacecraft with positive expulsion bladders is known, the CTS falls in this category and will be tested and flown prior to the TDRS thereby providing the necessary verification. The Intelsat IV propellant slosh testing program (Reference e) and the flight test results (Reference g) indicate good agreement between flight and ground test slosh data for the cono-spheroid tanks. These results add credibility to the use of laboratory testing techniques to establish propellant slosh energy dissipation levels, even when analytical modeling becomes intractable.

Table 6B-1. Physical Data

Propellant viscosity - μ = 6.72×10^{-4} (lb_m/ft sec)
(80 F)

Propellant density - ρ = 62.8 (lb_m/ft³)
(70 F)

Tank radius - Q - 6.5 inches

Propellant nominally tanked - 47.62 lb (28.81 lb/tank)

. Fill ratio - f - 0.57

. Propellant height - h - 1.1Q

Tank location - Y = 2.00 ft, Z = 0, X = 0

Spin axis moment of inertial, I_T - 110 ft-lb-sec²

Transverse moment of inertia - varied from 110 to 220 ft-lb-sec²

Spin rate - 90 rpm = 9.42 rad/sec

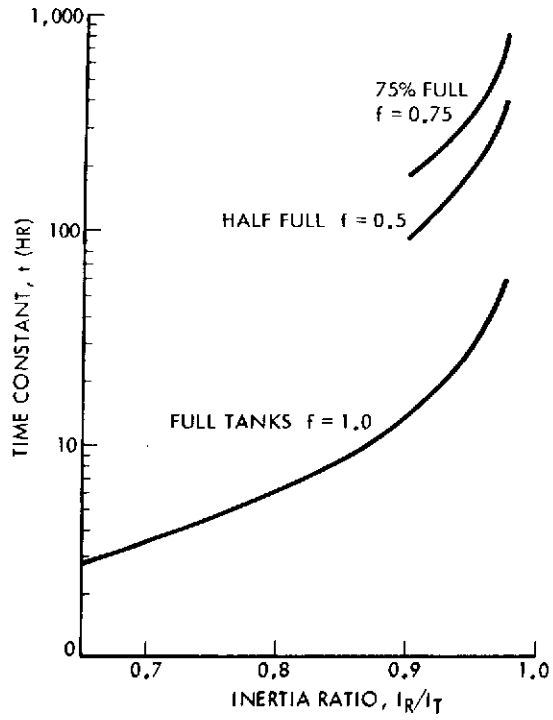


Figure 6B-1. Time Constant Versus Inertia Ratio

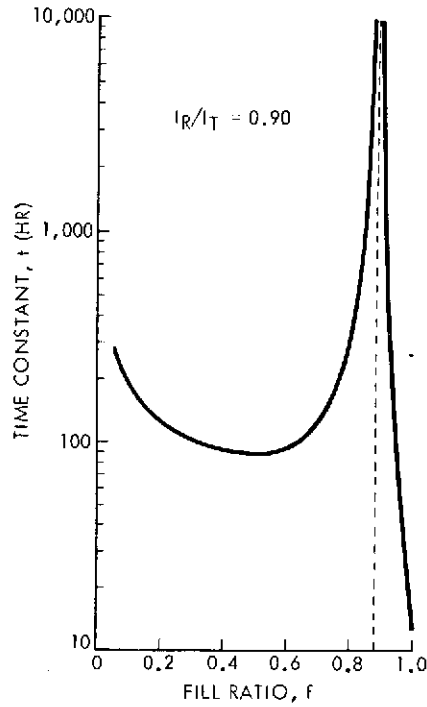


Figure 6B-2. Time Constant Versus Fill Ratio

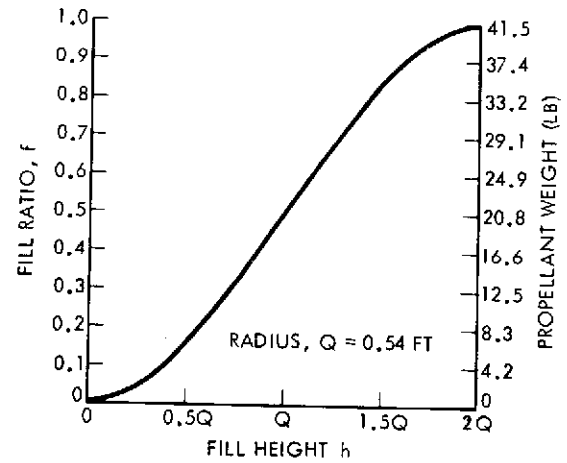


Figure 6B-3. Propellant Weight and Fill Ratio Versus Fill Height



Reference (h) also demonstrates good correlation between analytically predicted and observed flight data for the nutation divergence time constants. This analysis treats the fluid energy dissipation in heat pipes rather than propellant tanks and demonstrates that the energy dissipation inherent in the splashing of a high velocity fluid flow is a powerful mechanism for dissipating kinetic energy. Therefore, the tankage design should minimize any protuberances which result in localized high velocity flow patterns and splashing. In this regard, the positive expulsion bladders may actually tend to suppress splashing.

If the propellant tankage were to be designed and sized in such a way that the tanks could be essentially filled during the spin stabilized flight phases then the expulsion diaphragm would be pressed against the upper tank wall and the tank geometry (as seen by the propellant) would be rigid and spherical. This technique imposes design penalties (separate tank for pressurant and would probably require the development of new bladders and tankage) but will eliminate the requirements for slosh testing.

6B.4 CONCLUSIONS AND RECOMMENDATIONS

The analysis results using the fluid slug model and the "energy sink" stability analysis technique indicate that propellant slosh does not produce significant nutation control problems. The nutation divergence time constant is in excess of 89 hours in the parameter range anticipated for TDRS.

The use of positive expulsion diaphragms and internal ridges in the tanks were neglected in the analysis. The influence of these may have a substantial impact on S/C stability. No analytical techniques are presently known which adequately treat this problem. The validity of ground testing techniques to predict the propellant energy dissipation are established and should be employed to confirm TDRS nutation stability. Sufficient ground testing and flight test data may become available from the Canadian Technology Satellite program to qualify this approach without further testing. The CTS program is the first known S/C to employ propellant bladders in a minor axis spin stabilized mode.

6B.5 REFERENCES

- (a) "Analyses Related to the Hughes Gyrostat System," A. J. Iorillo, Hughes Aircraft Company Brochure, Dec. 1967, Section 4
- (b) "Energy Dissipation Due to Fuel Slosh in Spinning Spacecraft," V. Baddeley, Internal Letter 192-506-72-016, 19 May 1972
- (c) "Rigid Body Approximations to Turbulent Motion in a Liquid-Filled, Precessing, Spherical Cavity," J. P. Vanyo and P. W. Likins, ASME Paper No. 71-APM-Y, Transactions of the Journal of Applied Mechanics
- (d) "Measurement of Energy Dissipation in a Liquid-Filled, Precessing, Spherical Cavity," J. P. Vanyo and P. W. Likins, ASME Paper No. 71-APM-4, Transactions of the ASME Journal of Applied Mechanics, Presented at ASME Applied Mechanics Conference, Philadelphia, Pa., 23-25 June 1971
- (e) "Fuel Slosh and Dynamic Stability of Intelsat IV," Ernesto R. Martin, AIAA Paper #71-954, AIAA Guidance, Control and Flight Mechanics Conference, Hofstra University, Hempstead, New York, 16-18 August 1971
- (f) "The Dynamic Behavior of Liquids in Moving Containers," H. N. Abramson, NASA SP-106, 1966
- (g) "Intelsat IV Nutation Dynamics," J. T. Neer, Hughes A.C., AIAA Paper No. 72-537, AIAA 4th Communications Satellite Systems Conference, Washington, D.C., 24-26 April 1972
- (h) "Dynamic Analysis of Satellite Heat Pipe Fluid Energy Dissipation," E. A. O'Hern, V. Baddeley, J. E. Rakowski, North American Rockwell Corporation, to be Presented at the AIAA G&C Conference, Stanford University, California, 14-16 August 1972
- (i) "ATS V Post Launch Report," Goddard Space Flight Center Report, December 1969
- (j) "Communications Spacecraft Systems IR&D Project Directive," Internal Letter, dated 9 May 1972, from D. J. Shergalis, to Those Listed

APPENDIX 8A. ENERGY STORAGE ASSEMBLY

This Appendix presents data used to determine allowable battery depth of discharge, battery size, and charge times.

Figure 8A-1 shows battery cycle life as a function of depth of discharge for nickel cadmium batteries. The lines representing trend data limits are from reference 8A-1 and were derived from published industry data from many sources. The published data points are typical for a variety of test conditions and failure philosophies and, therefore, a least-square fit straight line is considered to be representative of state-of-the-art. Derating of the least square fit line to achieve high reliability is done by assuming that the design limit will confine random and wearout failures to the lower 3-sigma limit. Test data from reference 8A-2 and 8A-3 fall very closely to the least square fit line. Choice of a 60 percent maximum depth of discharge for the TDRS batteries results in a good performance margin. Additional data indicating a 60 percent depth of discharge to be obtainable for 450 cycles are shown by Figure 8A-2. The synchronous orbit tests were begun on six, 5-cell packs on 22 March 1969 at NAD, Crane, Indiana (Reference 8A-4). Each point shown represents 45 charge-discharge cycles typical of synchronous orbit conditions. In general, test results show:

1. Operating temperatures of -4 F and 104 F are very detrimental to cells in a synchronous orbit regime.
2. A temperature of 32 F gives the best capacity averaging 16.6 AH. Cells operating at 68 F have shown a tendency during the time on test thus far to drop in capacity at 80% depth of discharge.
3. At a temperature of 32 F, little difference in capacity is observed between 60 percent and 80 percent depth of discharge. The effect of DOD on battery capacity is more apparent at 68 F.
4. The test data show a total of 270 charge-discharge cycles and are still continuing. The trend of the data with time on test indicates that synchronous packs 7, 8, 9, and 10 have a high probability of going through a total of 450 charge-discharge cycles and still have a nominal 12 AH capacity.

Current TDRS thermal design will maintain the battery temperature in a range of 65 F to 75 F. For a very small weight penalty this temperature could be lowered to the 30 F to 40 F range, which appears to be optimum for battery operation in synchronous orbit.

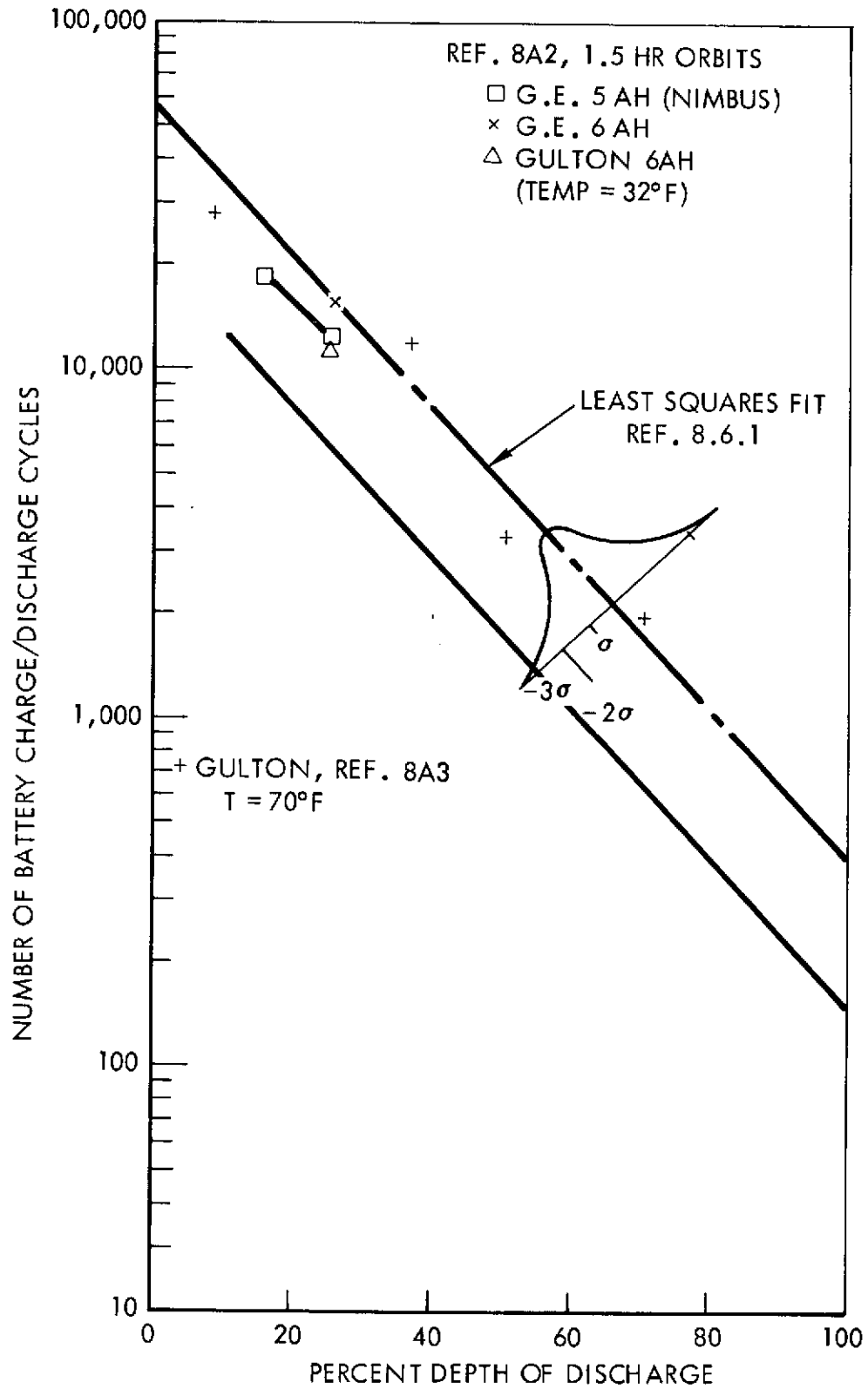


Figure 8A-1. Battery Cycle Life Versus Depth of Discharge

Battery capability and number of cells per battery results from eclipse period telecommunication considerations. Figure 8-13 (reference Volume IV) showed battery requirements as a function of data link operation.

Two LDR and two MDR forward links (one S and one Ku) operating require 300 watts total spacecraft power at the battery terminals. This capability is representative of that baselined for nominal operation during daylight (Table 8-3). Sixty pounds of batteries are required to deliver this power at 60 percent DOD during maximum eclipse period, i.e.,

$$\frac{291 \text{ watts} \times 1.2 \text{ hours}}{0.60 \text{ d.d.}} = 600 \text{ watt hours}$$

(see parametric battery weights in Figure 8A-3). One LDR forward link and one S-band operating require 230 watts of power. Reducing the telecommunication operations to this level allows a savings of 16 pounds in battery weight. In order to conserve weight the 12 AH--16 cell batteries are baselined.

Time required to charge batteries is primarily a function of solar array power available (and/or charge current) battery temperature, and state of charge. Figure 8A-4a shows time required to charge the baseline batteries for two different temperatures. It is possible to compute the state of charge Q as a function of time by means of the equation:

$$Q = Q_0 + \int_{t=0}^t (I) (n_{A-H}) \Delta t$$

$$n_{A-H} = \text{ampere hour efficiency}$$

The product of the current and the efficiency (which varies with Q and temperature) are integrated over the available charging period to determine state of charge. Amp hour efficiencies were taken from Reference 8A-4 to generate the charge times shown by Figure 8A-4b as a function of normalized current (charge current/ampere-hour capacity).

Figures 8A-4c and 8A-4d show time required to charge batteries as a function of solar array charge power available. Charging circuit losses of 17 percent are due to charges and ampere-hour meter losses. Charge voltages vary from 1.4 to 1.53 volts per cell depending on charge rate and state of charge. Figure 8A-4 indicates that charge rates less than C/10 (charge current = 1.2 amperes) will be marginal in returning the batteries to full charge (temperature = 78 F) during the 22.8 hours sunlight period. This sets the minimum solar array power for battery charging at approximately 30-33 watts and requires sequential battery charging. Lower charge rates at 78 F will result in amp-hour efficiencies so low at the higher states of charge that the battery would not return to full charge. At the lower battery temperature (59 F) parallel charging may be possible at solar array charging power of 35 - 40 watts.

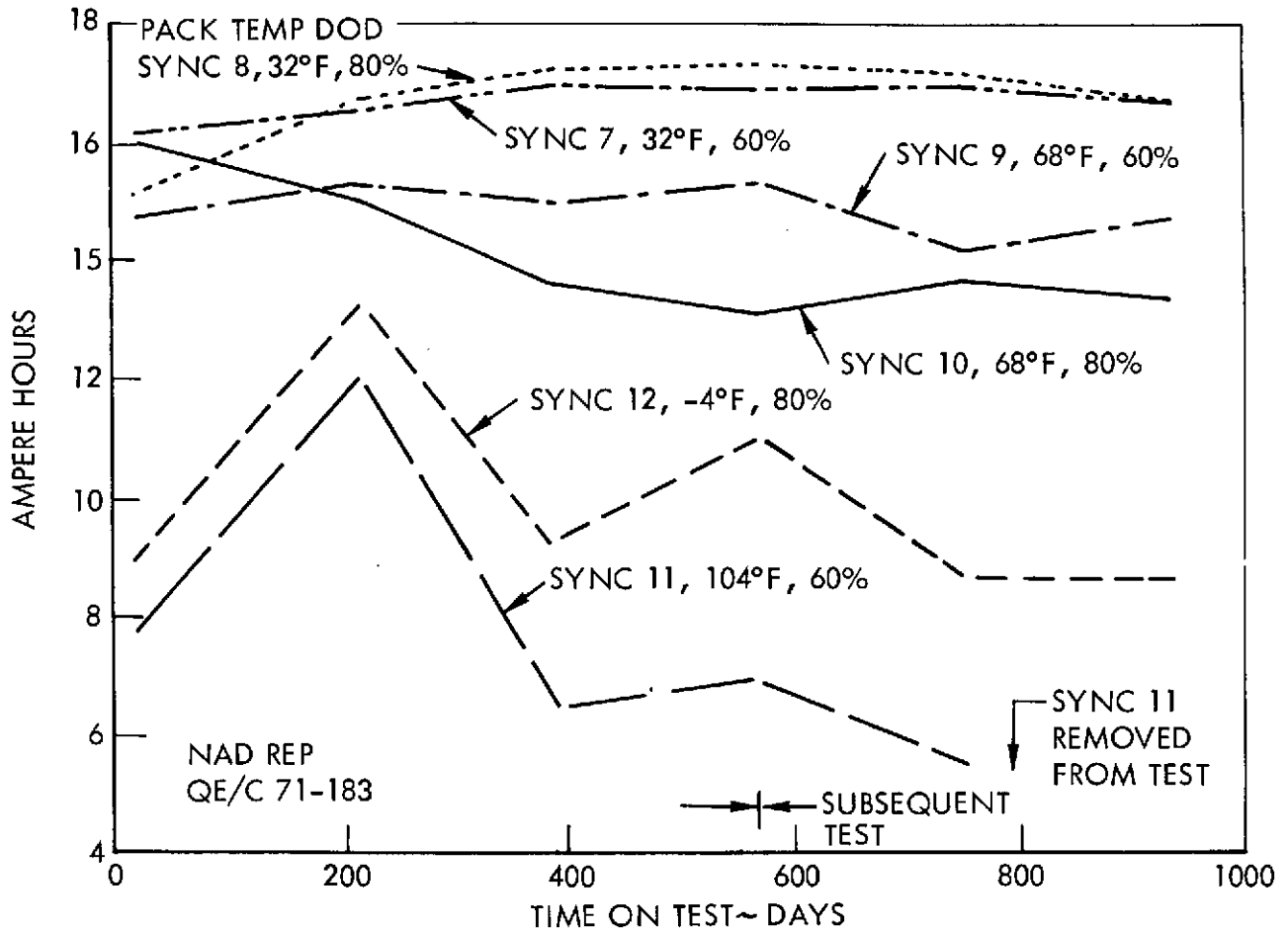


Figure 8A-2. 12 AH NiCd Battery Test at Synchronous Orbit Conditions

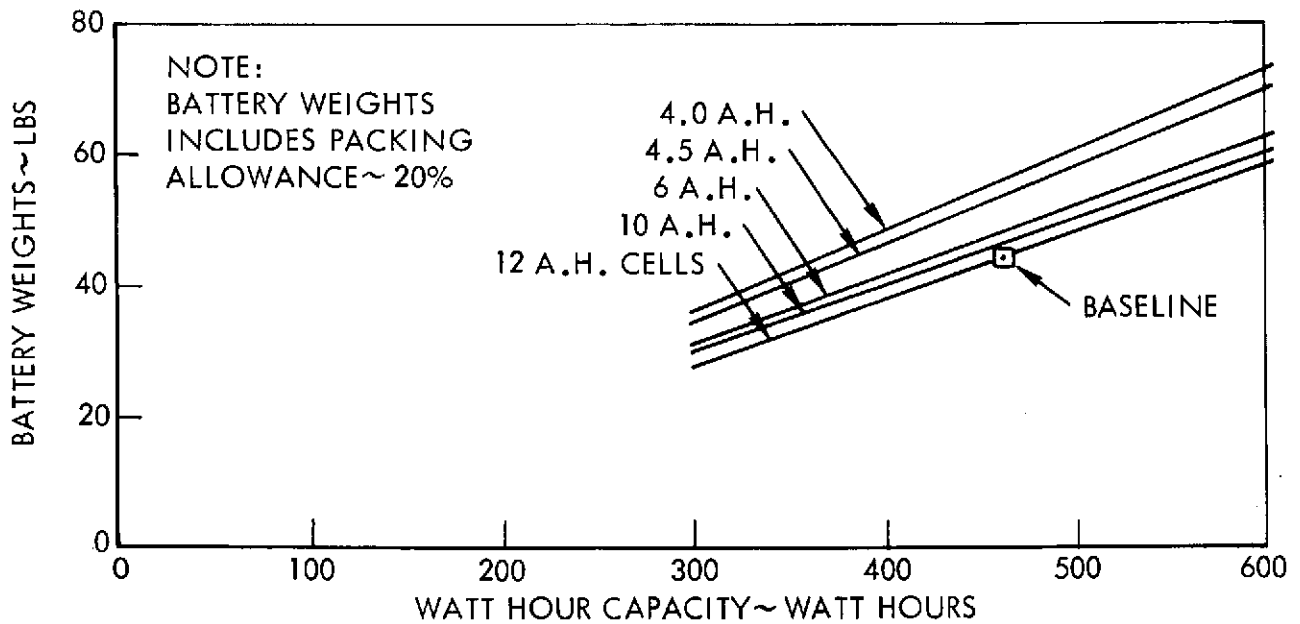


Figure 8A-3. Parametric Battery Weights

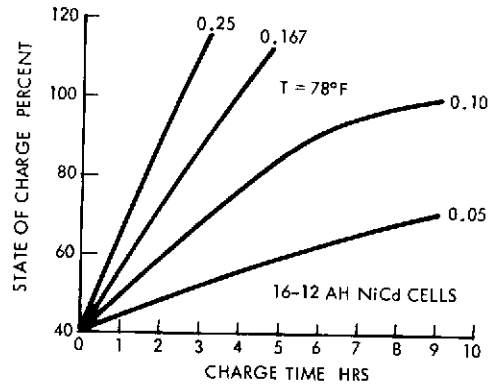
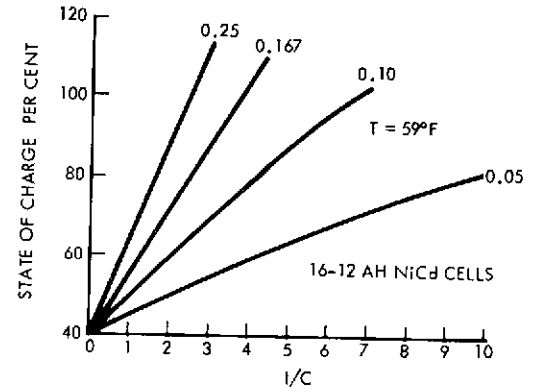
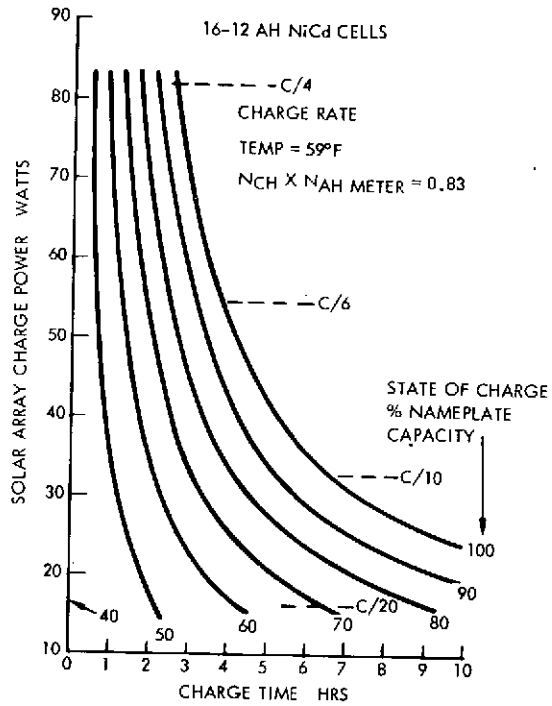
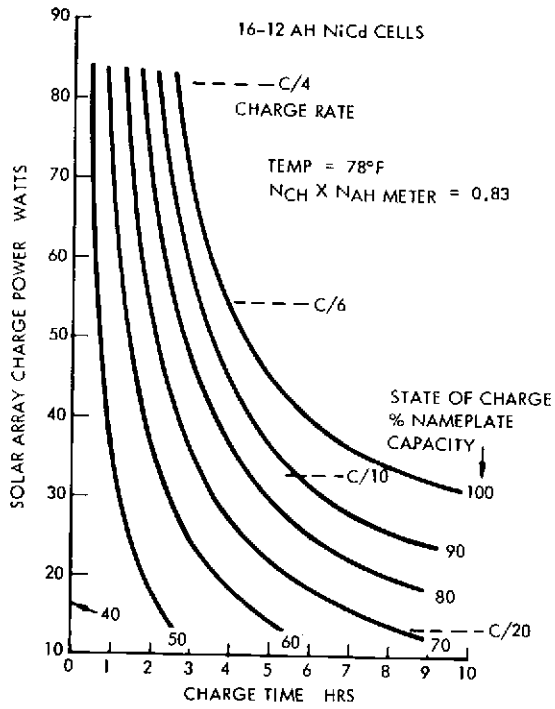


Figure 8A-4. Time Required to Charge Battery



REFERENCES

- 8A-1 "Design of a Multi-Kilowatt Photovoltaic Power System for Manned Space Station," 1967, Intersociety Energy Conversion Engineering Conference.
- 8A-2 "Evaluation Program for Secondary Spacecraft Cells, Eighth Annual Report of Cycle Life Test," Department of the Navy Naval Ammunition Depot Quality Evaluation and Engineering Laboratory Report No. QEEL/C72-1, 9 February 1972.
- 8A-3 "Reliability Assessment of Hemitically Sealed Nickel-Cadmium Cells," Gulton Industries, 1966.
- 8A-4 "Evaluation Program for Secondary Spacecraft Cells, Synchronous Orbit Testing of 12 Ampere-Hour Sealed Nickel-Cadmium Cells Manufactured by General Electric Company," Department of the Navy Naval Ammunition Depot Quality Evaluation and Engineering Laboratory Report No. QE/C71-183, 10 June 1971.
- 8A-5 "Batteries for Space Power Systems," NASA SP-172, 1968.

APPENDIX 10A. RELIABILITY DEFINITIONS

1. Mission Success - Ability to service 20 low data rate and 2 medium data rate users on the return link and two medium and 2 low data rate users simultaneously on the forward link for a period of five years. Reduced forward link capability is permitted during periods of eclipse.
2. TDRS Reliability - The probability of each satellite performing the required functions for a period of five years in orbit, given a successful launch and orbital injection.
3. Single Failure Points (SFP) - Failure of a single component which would preclude attainment of full mission success. (A single point failure is not necessarily of a mission critical nature which terminates the mission but in some instances only degrades the overall mission capabilities. It is to be noted that the definition of mission success is for capabilities in excess of the requirements in the SOW.)
4. Redundancy - The use of more than one means of accomplishing a given function where more than one must fail before the function cannot be performed. A program goal was established to eliminate all single-failure points by redundancy where feasible but not to protect against double failures except in some special cases where this can be done at little cost.
5. Component - A combination of parts, devices and structure, usually self-contained, which performs a distinctive function in the operation of the overall equipment. A "black box" (e.g., transmitter, encoder, cryogenic pump, star tracker).
6. Device - A combination of parts and structure, usually less complex than a component, which performs a specific function within a component or subsystem. Devices frequently are capable of disassembly, and may combine several types of functions such as electro-mechanical, electro-physical, or electro-chemical. The same type of article may be considered a device in one assembly and a component in another, depending on such factors as complexity and relative importance in the particular system. Some examples of devices are: valves, relays, small motors, bearings, gyros, batteries, thermocouples, strain gauges, and connectors.
7. Failure Mode and Effect Analysis (FMEA) - Study of a system and working inter-relationships of its elements to determine ways in which failures can occur (failure modes), effects of each potential failure on the system element in which it occurs and on other system elements, and the probable overall consequences (criticality) of each failure mode on the success of the system's mission. Criticalities are usually assigned by categories, each category being defined in terms of a specified degree of loss or degradation of mission objectives.
8. Part - One piece, or two or more pieces joined together which are not normally subject to disassembly without destruction of design use.
9. Reliability - A characteristic of a system, or any element thereof, expressed as a probability that it will perform its required functions at designated times for specified operating periods.

10. Reliability Apportionment - The assignment of reliability subgoals to subsystems and their elements which will result in meeting the overall reliability goals for the system if each of these subgoals is attained.
11. Reliability Assessment - An evaluation of reliability of a system or portion thereof. Such assessments usually employ mathematical modeling, directly applicable results of tests on system hardware, estimated reliability figures, and nonstatistical engineering estimates to insure that all known potential sources of unreliability have been evaluated.
12. Reliability Prediction - An analytical prediction of numerical reliability of a system or element thereof similar to a reliability assessment except that the prediction is always quantitative and is normally made in the earlier design stages where very little directly applicable test data is available.
13. System - One of the principal functioning entities comprising the project hardware, software, and related operational services within a project or flight mission. Ordinarily, a system is the first major subdivision of project work. Similarly, a subsystem is a major functioning entity within a system. (A system may also be an organized and disciplined approach to accomplish a task, e.g., a failure reporting system).



APPENDIX 10B. TDRS RELIABILITY DESIGN PRACTICES

The following design practices are proposed for use on the TDRS.

1. Alternate means of performing a necessary function shall be separated physically as much as practically possible such that redundancy of (two or more) functions will not be lost due to a single event.
2. Multiple redundancy system techniques that minimize or eliminate system transients caused by system component failures shall be adopted.
3. Redundant components susceptible to similar shock, vibration, acceleration and heat loads shall be physically oriented to reduce the chance of multiple failure from the same cause(s).
4. Servicing and test ports shall be designed to preclude leakage in flight. If caps are used, the material shall be compatible with the applicable spacecraft subsystem and environmental extremes.
5. Malfunction or inadvertent operation of vehicle fluid system equipment caused by exposure to debris or foreign material floating in a gravity free state shall be prevented by inclusion of strainers or traps in systems designs. In installations where flow reversal may occur, filters or strainers shall be installed on both sides of critical components.
6. Fluid systems shall have provisions to positively preclude vacuum and over-pressurization during fill and drain.
7. Sufficient fuel filters or strainers shall be provided in the thruster fuel feed lines (or GSE) to prevent contaminant buildup on the fuel nozzles.
8. Redundant electrical circuits shall not be routed through the same connector. Also, redundant connectors or paths for electrical wiring shall be so located that an event which damages one line is not likely to damage another.
9. Electrical circuits shall not be routed through adjacent pins of an electrical connector if a short circuit between them would constitute a single failure that would cause loss of mission. In addition, shorting springs or clips shall not be used in electrical/electronic connectors.
10. Malfunction or inadvertent operation of vehicle electrical or electronic equipment caused by exposure to conducting or nonconducting debris or foreign material floating in a gravity free state shall be prevented by design.
11. Derating of electrical/electronic piece-parts shall be utilized to ensure high inherent circuitry reliability.



APPENDIX 10C. COMPONENT FAILURE RATES

Appendix 10C shows the failure rates used in the predictive analyses for the individual components of the subsystems. The more detailed calculations used in attaining the overall reliability numbers are also shown.

Tables 10C-1 thru 10C-3 list the circuit and part failure rates used in the calculations for the telecommunication subsystem. Figures 10C-1 thru 10C-6 show the more detailed reliability logic diagrams for the basic components of the subsystem logic diagram of Figure 10-3. Since the VHF transceiver is used only during the initial phases of the mission, a 100 hour lifetime was used. Total operational time of the location transponder does not exceed 2,000 hours during the five year life of the mission. For the LDR transponder any one out of the four horizontal and vertical channels in the transceiver must be operational to meet mission requirements. The following operating times were used for the MDR transmitters and receivers: common 43,800 hours, S-band 32,800 hours, Ku-band 10,950 hours. This ratio was used because only one frequency at a time can be used for the MDR link and S-band was estimated to occupy about three times as much time.

Table 10C-4 shows the failure rates for the components used in the attitude control subsystem. In addition, the detailed calculations for nutation damping and momentum stiffness are described. The horizon scanners, reaction wheels and the gyro perform several functions. For momentum stiffness one scanner and one reaction wheel out of the two available are required. For nutation damping two out of the three available elements are required. The calculations for nutation damping are being utilized in the subsystem since they represent worst case conditions.

Table 10C-5 depicts the failure rates for the auxiliary propulsion subsystem. The same table also includes the basic calculations used for the thruster sub-assembly and the variation of reliability based on the number of expected use cycles during the five year period of the mission, e.g., ΔV , yaw and pitch attitude torque thrusters.

Table 10C-6 describes EPS component failure rates. A breakdown of the calculation for the solar array drive assembly is also shown.

The failure rates used in the reliability analysis were extracted from current literature. Even though the individual sources for each failure rate are not identified, careful selection was made to assure applicability to the hardware utilized in the design.

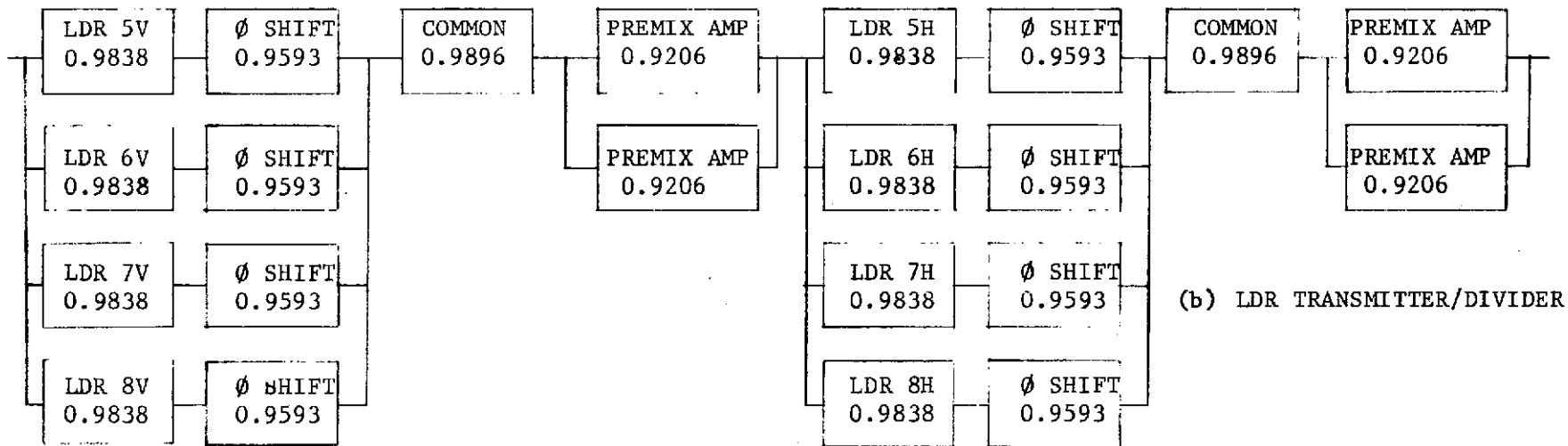
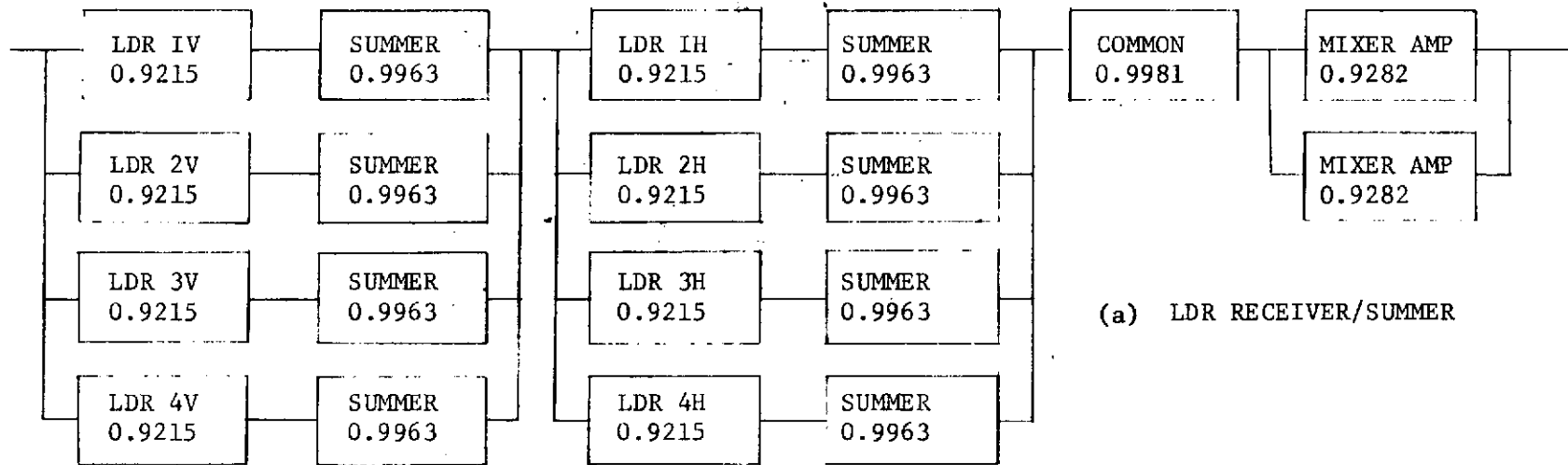


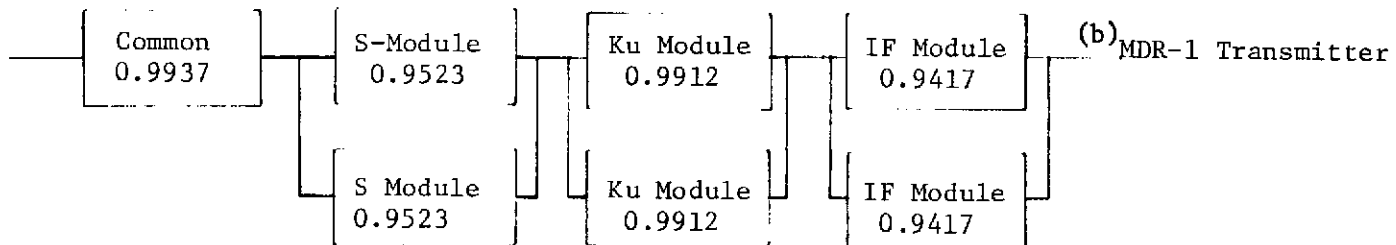
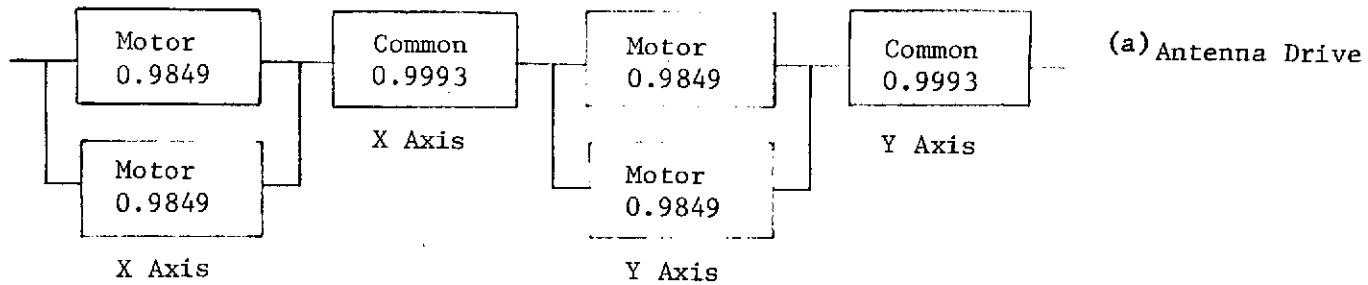
Figure 10C-1. LDR Transponder

10C-2

SD 72-SA-0133



Space Division
North American Rockwell



(Backup for TDRS Function)

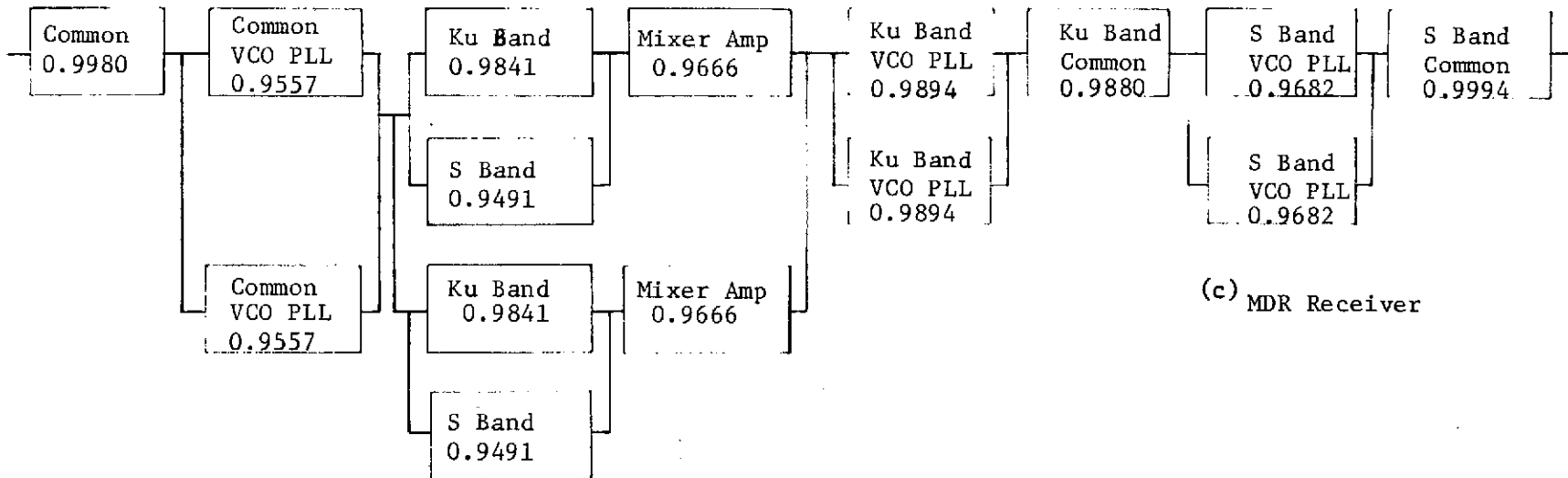


Figure 10C-2. MDR Transponder

10C-3

SD 72-SA-0133

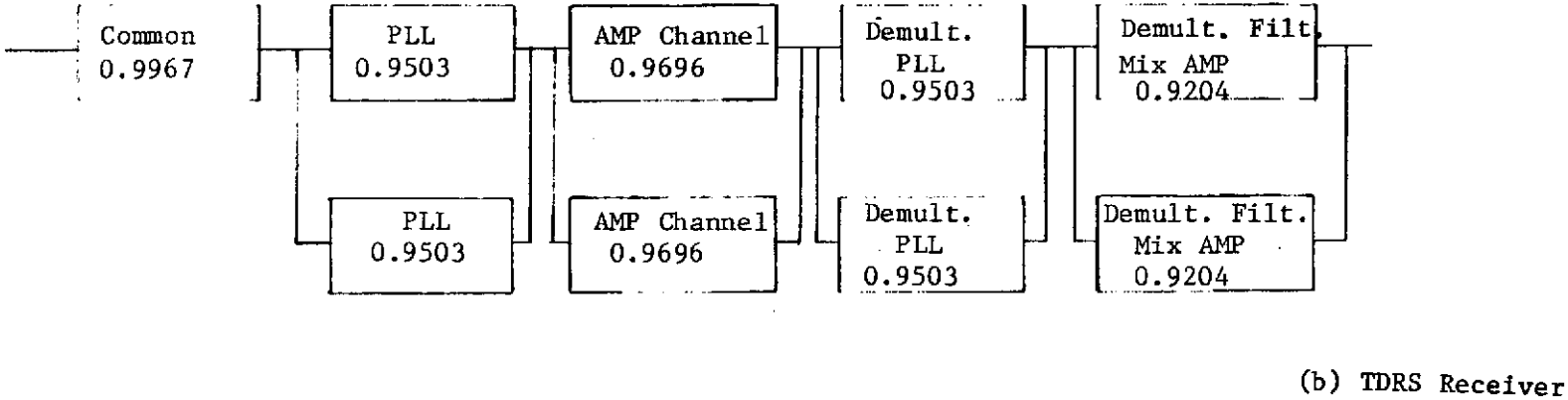
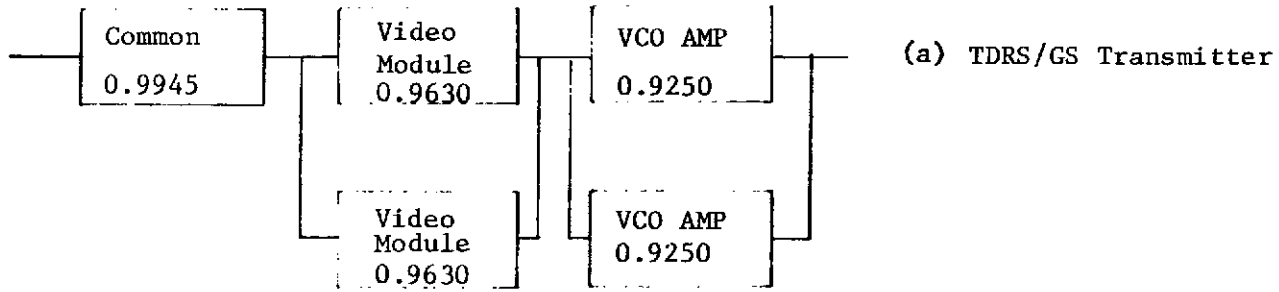


Figure 10C-3. TDRS/GS Transponder

10C-4

SD 72-SA-0133

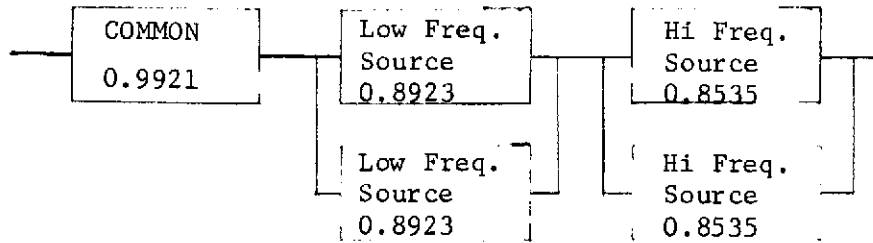


Figure 10C-4. Frequency Source

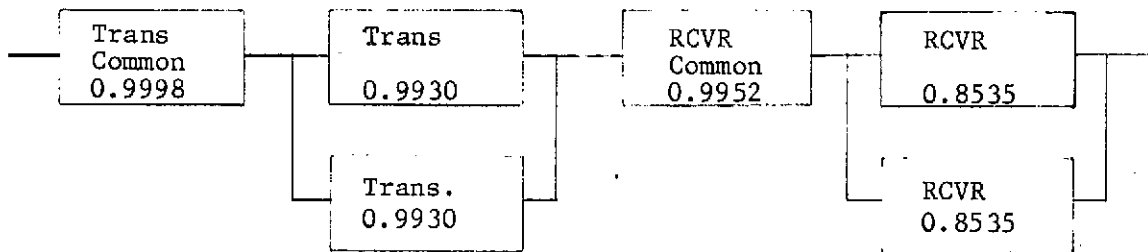


Figure 10C-5. Location Transponder

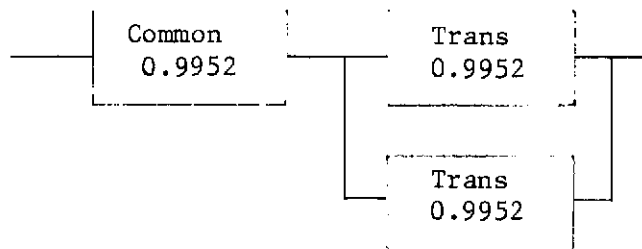


Figure 10C-6. Beacon

Table 10C-1. Circuit Failure Rates

Circuit	$f \times 10^{-9}$ hrs	Ref Ckt
Double balanced mixer	426	B
Balanced mixer	213	1/2 F.R. Ckt B
Filtercaps (Erie)	12	C
Hybrid amplifier (1 stage)	57	D
VCO	264	A
Ladder networks	2 x number of outputs	E
Summer, coupler	15	F
Divider stripline, passive	3N (N = divider)	G
Pole filter	17 x N (number of poles)	H
Multiplier Stage	205	I
Phase Lock Loop	632	J



Table 10C-2. Reference Circuit Failures Rates

Ref Ckt	Circuit Description	Quantity	f x 10 ⁻⁹
A	VCO		
	Varactor stage	1	126
	Amplifier stage	3	138
			<hr/> 264
	<u>Varactor Stage</u>		
	Coils RF	2	20
	Cap. Glass	2	6
	Varactor	1	100
			<hr/> 126
	<u>Amplifier Stage (RF)</u>		
	Transistor	1	15
	Capacitor-tantalum	1	3
	Coils	2	20
	Resistor	2	2
		<hr/> 40	
B	DOUBLE BALANCED MIXER		
	Coils RF	2	20
	Capacitor-Glass	2	6
	Diodes	4	400
		<hr/> 426	
C	FILTERCAPS		
	Coil RF	1	10
	Capacity-Ceramic	1	2
		<hr/> 12	
D	HYBRID AMPLIFIER		
	Transistor RF	2	40
	Resistor	1	1
	Capacitor-Ceramic	3	6
	Inducer	1	10
		<hr/> 57	
E	LADDER NETWORKS		2 x N (N = number of outputs)

Table 10C-2. Reference Circuit Failures Rate (Cont.)

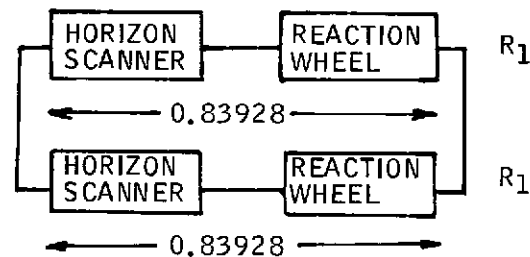
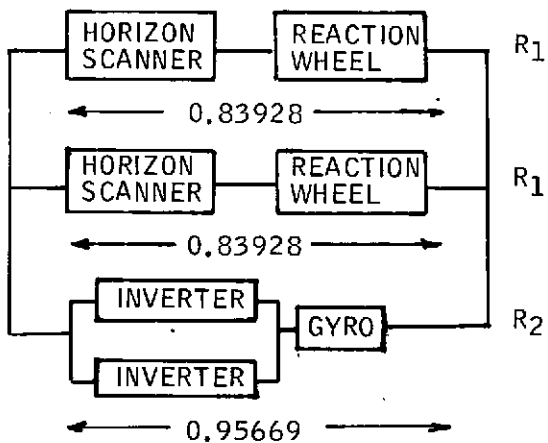
Ref Ck5	Circuit Description	Quantity	$f \times 10^{-9}$
	Equated to be made of film resistors at 2/output	2	2
F	SUMMER Assume complexity of torroid/ stripline also assumed	1	15
G	DIVIDE BY PASSIVE STRIPLINE Equate to 3 film resistor/ divide $3 \times 1 = 3 \times N$		$3 \times N$ $N = \div$ number
H	POLE FILTERS Fixed capacitor Coil Capacitor	2 10 3	4 10 <u>3</u> 17 x number of poles
I	MULTIPLIER STAGE Driver stage Step divide Capacitor Coils	1 1 3 2	46 130 9 <u>20</u> 205
J	PHASE LOGIC LOOP Single Balanced mixer Amp. stage Analog amp. ÷ assume 3 IC Phase detector	1 1 1 3 1	213 46 100 60 <u>213</u> 632

Table 10C-3. Part Failure Rates

Part	Failure per 10^{-9} hr
<u>Capacitors</u>	
Ceramic	2
Glass	3
Mica	3
Mylar	5
Polystyrene	20
Tant, solid	6
Tant, foil	20
Tant, wet	6
Variable, air	40
Variable, ceramic	120
Variable, piston	20
<u>Connectors</u>	
General	10 + 1 per active pin
Coaxial	20
<u>Diodes</u>	
General purpose	5
Pin	50
Microwave mixer	100
Microwave det	100
Power rect	50
Step recovery	130
Switching	2
Tunnel	100
Varactor	100
Zener	10
<u>Resistors</u>	
Composition	1
Film	1
(Wire wound) - power	25
- precision	15
- variable	130

Table I0C-4. Attitude Control

Item	Quantity	$\lambda \times 10^{-6}$ (Item)	λt	R (43,800 hours)
Inverter	2	0.5	0.0219	0.97833
Horizon scanner	2	2.0	0.0876	0.91612
Reaction wheel	2	2.0	0.0876	0.91612
Gyro	1	1.0	0.0438	0.95714
Spin electronics	-	0.5	0.0219	0.97833
R (30 hours)				
Accelerometer	2	20.0	0.0006	0.9994
Spinning horizon sensor	2	2.0	0.00006	0.99994
Spinning sun sensor	2	2.0	0.00006	0.99994
3-axis stabil. electronics	-	0.5	0.000015	0.999985
Solar aspect sensor	2	5.0	0.00015	0.99985



Momentum stiffness - redundant paths

$$R_{\text{MOMENTUM}} = 1 - (1 - R_1)^2 = 0.9741678$$

For nutation damping - any 2 of 3 paths required

$$R_{\text{NUT.DAMP}} = R_1^2 + 2R_1R_2 - 2R_1^2R_2 = 0.96248$$

$R_{\text{NUT.DAMP}}$ is being utilized in subsystem calculations since it represents worst case

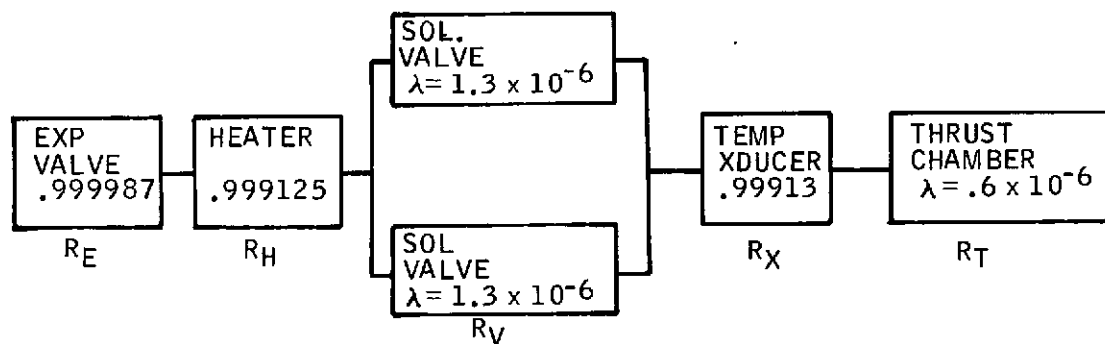
I0C-11

SD 72-SA-0133

Table IOC-5. Auxiliary Propulsion

Item	Quantity	$\lambda \times 10^{-6}$ (Item)	λt	R (5 years)
Propellant tank	2	0.0114	0.0005	0.99950
Propellant fill and drain valve	1	0.020	0.000875	0.99913
GN ₂ fill and drain valve	2	0.020	0.000875	0.99913
Pressure transducer	2	0.023	0.001	0.99900
Latching valve	1	0.2	0.00876	0.99124
Tank explosive valve	1	0.0003	0.000013	0.99999
Filter	1	0.0114	0.0005	0.99950
Thruster explosive valve	16	0.0003	0.000013	0.99999
Tank temp. transducer	2	0.02	0.000875	0.99913
Thruster assembly	16	(See Note 1 below)		
Thruster temp. transducer	16	0.02	0.000875	0.99913
Heater	16	0.02	0.000875	0.99913
Lines and fittings	-			0.99999

Note 1: Thruster analysis:



$$R_{ASSEMBLY} = [1 - (1 - R_V)^2] R_T R_R R_{HXR}$$

For pitch attitude torque thrusters, 2 of 4 required; 100,000 cycles
 $R_A = [1 - (1 - 0.87810)^2] (.94176)(.999987)(.999125)(.999125) = .92614$
 $R_{PITCH} = R_A^4 + 4R_A^3Q_A + 6R_A^2Q_A^2 = 0.99849$

For delta-V thrusters, 2 of 8 required; 10,000 cycles
 $R_A = [1 - (1 - 0.98708)^2] (.99402)(.999987)(.999125)(.999125) = 0.99210$
 $R_{\Delta V} = R_A^8 + 8R_A^7Q_A + 28R_A^6Q_A^2 = 0.99997$

For yaw attitude torque thrusters, 2 of 4 required; 50,000 cycles
 $R_A = [1 - (1 - 0.93707)^2] (.97045)(.999987)(.999125)(.999125) = .96489$
 $R_{YAW} = R_A^4 + 4R_A^3Q_A + 6R_A^2Q_A^2 = 0.99983$

IOC-12

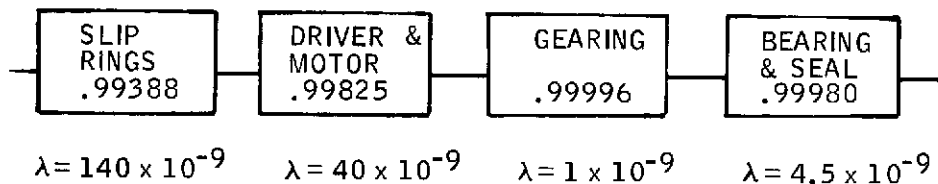
SD 72-SA-0133

Table IOC-6. Electrical Power

Item	Quantity	$\lambda \times 10^{-6}$ (Item)	λt	R (5 years)
Solar array assembly	2	(includes diode strings)		0.99900
Voltage sensor	3	0.129	0.00565	0.99436
Current sensor	2	0.043	0.0019	0.99810
Shunt dissipator	24	0.0057	0.00025	0.99975
Charge regulator	2	2.0	0.08760	0.91620
Discharge regulator	2	1.46	0.06395	0.93805
Battery	2	(See Note 1 below)		0.95000
Amp-hour meter	2	0.15	0.00657	0.99345
Battery isol. diode	4	0.014	0.00184	0.99816
Central power control	1	0.28	0.012264	0.98781
Solar array drive assembly	2	(See Note 2 below)		0.99190
Bus isolator	2	1 shot		0.99999

Note 1: Battery reliability taken from paper by M. Koslover of TRW entitled "Optimization of Battery Subsystems for Earth Satellite Lifetimes of Greater than Five Years," given at IECE Conference, September 1969.

Note 2: Solar array drive assembly analysis:



$R_{ASSY} = 0.99190$

10C-13

SD 72-SA-0133